NOTE TO USERS

Université d'Ottawa · University of Ottawa

Université d'Ottawa · University of Ottawa

FACULTÉ DES ÉTUDES SUPÉRIEURES ET POSTDOCTORALES

FACULTY OF GRADUATE AND POSTDOCTORAL STUDIES

Reid Alexander VAN BRABANT

AUTEUR DE LA THÈSE - AUTHOR OF THESIS

M. Sc. (Geography)

GRADE - DEGREE

Department of Geography

FACULTÉ, ÉCOLE, DÉPARTEMENT - FACULTY, SCHOOL, DEPARTMENT

TITRE DE LA THÈSE - TITLE OF THE THESIS

Lacustrine Sediment records of debris flow activity, northwestern British Columbia and southwestern Yukon Territory

A. Lewkowics

DIRECTEUR DE LA THÈSE - THESIS SUPERVISOR

CO-DIRECTEUR DE LA THÈSE - THESIS CO-SUPERVISOR

EXAMINATEURS DE LA THÈSE - THESIS EXAMINERS

L. Bernard

G. Konrad

J. Peter

J.-M. De Koninck, Ph.D.

LE DOYEN DE LA FACULTÉ DES ÉTUDES SUPÉRIEURES ET POSTDOCTORALES

DEAN OF THE FACULTY OF GRADUATE AND POSTDOCTORAL STUDIES

LACUSTRINE SEDIMENT RECORDS OF DEBRIS FLOW ACTIVITY, NORTHWESTERN BRITISH COLUMBIA AND SOUTHWESTERN YUKON TERRITORY

By
Reid Van Brabant

Master of Science Thesis
Submitted to the Faculty of Graduate and Postdoctoral Studies, University of Ottawa

Department of Geography
University of Ottawa
Ottawa, Ontario
Canada

Your file Votre référence
ISBN: 0-494-01626-4
Our file Notre référence
ISBN: 0-494-01626-4

ABSTRACT

Lacustrine sediment records were used to examine debris flow magnitude and frequency at two sites in northwestern Canada. A rod-driven piston corer was used to collect four lacustrine sediment cores from Mount Aramis Lake, Yukon Territory (YT) and five from Three Guardsmen Lake, British Columbia (BC).

Nine layers deposited in the lacustrine sediment of Mount Aramis Lake over an estimated 3400 to 3800 yrs and ten layers deposited in Three Guardsmen Lake over an estimated 3000 to 3500 yrs are inferred to be due to debris flows. However, these layers represent the minimum number of events because lacustrine sediments only contain a record of debris flows with sufficient energy to reach the lake. Variations in the sedimentary structure of the debris flow layers between the sites could not be attributed to differences in debris flow magnitude and frequency resulting from local variations in slope gradients, debris supply, or precipitation.

The lacustrine, terrestrial, and climatic evidence indicates that lower precipitation at Mount Aramis may result in higher magnitude, lower frequency debris flows. Conversely, higher precipitation at Three Guardsmen Mountain may cause lower magnitude, higher frequency debris flows. However, these are preliminary conclusions and further research regarding the relationship between precipitation regime, debris supply, and debris flow magnitude and frequency is required.

RÉSUMÉ

Des sédiments lacustres ont été utilisés pour examiner la magnitude et la fréquence des coulées de débris à deux sites le Nord-Ouest du Canada. Un carottier à piston a été utilisé pour échantillonner quatre carottes lacustres du lac Mount Aramis, Territoire du Yukon (T.Y.) et cinq du lac Three Guardsmen, Colombie-Britannique (C.B.).

Neuf couches, interprétées comme étant des coulées de débris, se sont déposées dans le lac Mount Aramis au cours des 3400 à 3800 ans et dix se sont déposées dans le lac Three Guardsmen au cours des 3000 à 3500 ans. Ces couches ne représentent qu'un minimum d'évènements attendu que seulement certaines coulées ont l'énergie nécessaire pour atteindre le lac. Des variations dans les structures sédimentaires observées entre les sites ne peuvent être attribuées aux différences dans la magnitude et fréquence des coulées de débris causées par des variations locales dans l'angle d'inclinaison de la pente et par l'alimentation en débris ou précipitations.

Les observations lacustres, terrestres et climatiques indiquent que les précipitations moins abondantes au lac Mount Aramis favorisent des coulées rares mais de forte magnitude. Les précipitations plus élevées au lac Three Guardsmen favorisent des coulées fréquentes mais de faible magnitude. Ces conclusions sont préliminaires et soulignent le besoin d'études approfondies de la relation entre le régime de précipitation et la magnitude et la fréquence des coulées de débris.

ACKNOWLEDGEMENTS

First and foremost thanks to Dr. Antoni Lewkowicz who undertook the strenuous task of supervising my studies at the University of Ottawa. His support and guidance were greatly appreciated, as was his tolerance of my tendency towards inflexibility. Matt Thompson proved to be an excellent assistant in the field and without his hard work and dedication this thesis could not have been completed.

The National Science and Engineering Research Council (NSERC), the Government of Ontario, and the University of Ottawa provided much needed financial support during the course of this thesis through a Post-Graduate Scholarship A (PGS A), an Ontario Graduate Scholarship (OGS), and an Excellence Scholarship respectively. An NSERC Research Grant to Dr. Lewkowicz and a Northern Science and Training Program (NSTP) Grant to the author supported field work and laboratory expenses.

Bruce Saunders (DiagnostiCare Inc.) and Isabelle Girard (Geological Survey of Canada) were instrumental during x-ray radiography and laser particle size analyses respectively. Thanks to Dr. Konrad Gajewski, Dr. Peter Johnson, and Dr. Bernard Lauriol (University of Ottawa) who took the time to answer my questions and Jim McGrath (University of Ottawa) who averted several near computer disasters. Particular thanks are owed to Jean Bjornson (University of Ottawa) who provided excellent support during the laboratory work and was always willing to play devil's advocate.

Most of all thanks to my family (both the Van Brabants and the Aumonts) without whose support I could have not completed my undergraduate degree let alone a graduate program. And, finally, to my wife Amy, without your encouragement and kindness none of this would have been possible. Thank you.

TABLE OF CONTENTS

Abstract ii
Résumé iii
Acknowledgements iv
Table of Contents v
List of Figures vii
List of Tables viii
1. Introduction 1
2. Literature Review 3
2.1 Debris Flows 3
2.2 Debris Flows in Southwestern Yukon Territory and Northwestern British Columbia 7
2.3 Debris Flow Signatures in Lacustrine Sediment 9
3. Study Area 12
3.1 Site Selection 12
3.2 Mount Aramis, Yukon Territory 14
3.2.1 Mount Aramis Site Description 14
3.2.2 Mount Aramis Climate 14
3.2.3 Mount Aramis Debris Flow Map and Profile 16
3.2.4 Mount Aramis Lake Bathymetry 19
3.3 Three Guardsmen Mountain, British Columbia 20
3.3.1 Three Guardsmen Mountain Site Description 20
3.3.2 Three Guardsmen Mountain Climate 20
3.3.3 Three Guardsmen Mountain Debris Flow Map and Profile 22
3.3.4 Three Guardsmen Lake Bathymetry 25
3.4 Comparison of the Mount Aramis and Three Guardsmen Mountain Sites 25
4. Methods 27
4.1 Terrestrial Methods 27
4.1.1 Mapping and Profiling of Debris Flows 27
4.1.2 Excavation of Levees 27
4.2 Lacustrine Methods 28
4.2.1 Bathymetric Mapping 28
4.2.2 Collection of Lacustrine Sediment Cores 28
4.3 Laboratory Analyses 30
4.3.1 Magnetic Susceptibility 30
4.3.2 X-Ray Radiography 31
4.3.3 Sketching 32
4.3.4 Loss on Ignition 32
4.3.5 Grain-size Analyses 34
4.3.6 Accelerator Mass Spectrometry Dating 36
5. Results 38
5.1 Core MA1 38
5.2 Core MA2 41
5.3 Core MA3 43
5.4 Core MA4 45
5.5 Correlation of Mount Aramis Lake Cores 50

5.6 Core TG1 54
5.7 Core TG2 54
5.8 Core TG3 58
5.9 Core TG4 62
5.10 Core TG5 62
5.11 Correlation of Three Guardsmen Lake Cores 65
5.12 Interpretation of Results 68
5.12.1 Interpretation of Mount Aramis Lake Cores 71
5.12.2 Interpretation of Three Guardsmen Lake Cores 78
6. Discussion 81
7. Conclusions 91
8. References 93
Appendix A: Core Data 100
Core MA1 100
Core MA2 103
Core MA3 106
Core MA4 110
Core TG1 113
Core TG2 115
Core TG3 118
Core TG4 120
Core TG5 123
Appendix B: Grain-Size Data for Cores TG3 and MA4 125
Core MA4 125
Core TG3 128

LIST OF FIGURES

Figure 3.1: Study area map 13
Figure 3.2: Map of Mount Aramis, Yukon Territory 15
Figure 3.3: Photographs of Mount Aramis. 15
Figure 3.4: Aerial photograph of Mount Aramis 17
Figure 3.5: Mount Aramis debris flow map and profile 18
Figure 3.6: Bathymetric map of Mount Aramis Lake 19
Figure 3.7: Map of Three Guardsmen Mountain, British Columbia 21
Figure 3.8: Photographs of Three Guardsmen Mountain. 21
Figure 3.9: Aerial photograph of Three Guardsmen Mountain. 23
Figure 3.10: Three Guardsmen Mountain debris flow map and profile 24
Figure 3.11: Bathymetric map of Three Guardsmen Lake 26
Figure 5.1: Diagrams and x-rays for Mount Aramis Lake cores 39
Figure 5.2: Diagram, x-ray, magnetic susceptibility, and LOI graphs for MA1 40
Figure 5.3: Diagram, x-ray, magnetic susceptibility, and LOI graphs for MA2 42
Figure 5.4: Diagram, x-ray, magnetic susceptibility, and LOI graphs for MA3 44
Figure 5.5: Diagram, x-ray, magnetic susceptibility, LOI, and LPSA graphs for MA4 46
Figure 5.6: Ternary plot of median grain-sizes for MA4 49
Figure 5.7: Bivariate plot of sediment sorting *versus* skewness for MA4 49
Figure 5.8: Correlation of Mount Aramis Lake cores 51
Figure 5.9: Diagrams and x-rays for Three Guardsmen Lake cores 55
Figure 5.10: Diagram, x-ray, and magnetic susceptibility graph for TG1 56
Figure 5.11: Diagram, x-ray, and magnetic susceptibility graph for TG2 57
Figure 5.12: Diagram, x-ray, magnetic susceptibility, LOI, and LPSA graphs for TG3 59
Figure 5.13: Ternary plot of median grain-sizes for TG3. 61
Figure 5.14: Bivariate plot of sediment sorting *versus* skewness for TG3 61
Figure 5.15: Diagram, x-ray, and magnetic susceptibility graph for TG4 63
Figure 5.16: Diagram, x-ray, magnetic susceptibility, and LOI graphs for TG5 64
Figure 5.17: Correlation of Three Guardsmen Lake cores 67
Figure 6.1: Age-depth curves based on AMS ^{14}C dates from MA4 83
Figure 6.2: Photographs of vegetation affected by debris flows 86

LIST OF TABLES

Table 3.1: Climate normals for Otter Falls, Yukon Territory (1971-2000) 16
Table 3.2: Climate normals for Pleasant Camp, British Columbia (1971-2000) 22
Table 5.1: Radiocarbon ages and related data for core MA4 50
Table 5.2: Radiocarbon ages and related data for core TG3 62

1. INTRODUCTION

This thesis uses lacustrine sediment records to examine debris flow activity at two sites in southwestern Yukon Territory and northwestern British Columbia. Debris flows are rapid mass movements initiated by hydroclimatic events and may occur wherever a rainstorm, rapid snowmelt, or thawing of icy permafrost mobilizes accumulated debris (Rapp, 1960; Johnson & Rodine, 1984; Selby, 1993). Due to their prevalence in steep mountainous terrain in a wide variety of climatic regimes, debris flows have been widely studied and the literature is extensive.

Debris flows are particularly active in southwestern Yukon Territory and northwestern British Columbia and occasionally pose a significant hazard to human life and infrastructure (*e.g.* Clague, 1981; Evans & Clague, 1989; Lowey, 2002). Several studies have reported debris flow return intervals of 100 years or more in this region (Clague, 1981; Harris & McDermid, 1998; Lowey, 2002). Therefore, any investigation of their magnitude and frequency must be conducted over large temporal scales, and this requires an intact, long-term record of debris flow activity. Although debris flows leave distinct erosional and depositional features, subsequent events alter and may completely destroy any terrestrial signature (Nieuwenhuijzen & van Steijn, 1990; van Steijn, 1996; Lewkowicz & Hartshorn, 1998). Conversely, sediments mobilized by sub-aerial debris flow events and deposited in sub-aqueous environments are often well preserved, and analysis of lacustrine sediments has been used in several investigations of the relationship between mass movement activity and climate (*e.g.* Gottesfeld *et al*, 1991; Hartshorn & Lewkowicz, 2000; Fuller, 2002). However, few of these studies have examined the effectiveness or accuracy of this methodology.

Therefore, the primary objective of this thesis is to test the efficacy of using lacustrine sediments as a means to obtain information regarding debris flow magnitude and frequency. Two research questions are posed relative this goal. First, is debris flow activity on slopes adjoining lakes in northwestern Canada detectable in lacustrine sediments? Second, can lacustrine sediments be used as indices of rates or changes in rates of debris flow activity in this region? A preliminary attempt is also made to investigate the relationship between precipitation regimes and debris flow magnitude and frequency.

2. Literature Review

2.1 Debris Flows

Debris flows are rapid mass movements that may be defined as the viscous or plastic flow of water-saturated material downslope under the influence of gravity. Many begin as highly erosive debris slides that glide over one or more slip planes on the substratum before evolving into debris flows as they become oversaturated (Rapp, 1985; Selby, 1993; French, 1996). Debris flows are capable of rapidly transporting tens of thousands of cubic metres of predominantly coarse-grained debris, over several kilometers as a coherent flow of a saturated, heterogeneous mixture of granular solids, water, and air (Bovis, 1993; Rebetez *et al*, 1997).

Rapp (1960) examined the role of mass movements in the periglacial environment of the Karkevägge, a glacial trough valley in northern Sweden. He concluded that debris flows and slides were the second most important method of sediment transfer after the transportation of dissolved salts. Bovis (1993) quantified the geomorphic capability of debris flows in coastal British Columbia stating, "coherent flows of saturated, heterogeneous debris, 2-5 m in depth, traveling at speeds of 5-10 m/s, were capable of transporting up to 50,000 m^3 of debris over distances of several kilometers" (p. 177). These observations make it clear that catastrophic debris flows are capable of considerable landscape modification and are a significant hazard in mountainous terrain (Clague, 1981; Eisbacher & Clague, 1984; Rapp, 1985; Evans & Clague, 1989; Haeberli, 1992; Bovis, 1993; Evans, 2001).

The classification scheme developed by Varnes (1978) separates debris flows, debris avalanches, and mudflows into separate types of mass movement based on rate of movement and the size of particles involved. However, Johnson & Rodine (1984) incorporate features

from all three within the term 'debris flow' because the mechanisms involved are similar. The latter scheme has been followed in this thesis and the term 'debris torrent', used by some researchers (*e.g.* Clague, 1981) to delineate very large debris flows has been included as well. In any case, debris flows are extremely hazardous and may occur wherever steep, debris mantled slopes are periodically saturated by water; consequently, the debris flow literature is very extensive (Rapp, 1985; Selby, 1993). However, the research presented in this thesis focuses on debris flow activity in mountainous environments underlain by permafrost and the scope of this literature review has been narrowed accordingly.

Debris flows are typically initiated by the saturation of slope material resulting in elevated pore water pressures and an increase in the shear stress to shear strength ratio until the slope stability threshold is exceeded (Selby, 1993; Hartshorn, 1995). The water required for saturation may be provided through intense precipitation events, the rapid melting of snow and ice, and/or thawing of icy permafrost if present. Overall, intense precipitation is generally considered to be the most important source of water for saturation of debris and initiation of flow (*e.g.* Rapp, 1960; Caine, 1980; Clague, 1981; Rapp & Nyberg, 1981; Larsson, 1982; Akerman, 1984; Rapp, 1985; Evans & Clague, 1989; Nyberg & Lindh, 1990; Kotarba, 1997; Rebetez *et al*, 1997; *etc.*). Semi-arid conditions in some mountain areas, however, may preclude the initiation of debris flows via intense rainstorms and water may be supplied by snowmelt (Jahn, 1976; Theakstone, 1982; Catto, 1993; Rebetez *et al*, 1997) and/or the degradation of permafrost containing segregated ice (Harris & Gustafson, 1988).

Although, rapid saturation of debris is important for debris flow initiation, not all studies and hydroclimatic threshold models take into account pre-existing moisture conditions. Several researchers have reported that relatively low intensity precipitation

events may trigger debris flows on slopes previously conditioned by rainfall and snowmelt (Rapp & Stromquist, 1976; Miles & Kellerhalls, 1981; Wieczorek, 1987, Rebetez *et al*, 1997). According to Jakob and Weatherly (2003), antecedent moisture conditions are as important for the development of a hydroclimatic threshold for landslide initiation in the North Shore Mountains of British Columbia as short-term rainfall intensities. Since precipitation, snowmelt, and the thawing of icy permafrost (where present) all influence moisture conditions, the initiation of debris flows may be the result of a combination of some or all of these processes. The origin of the water appears to matter little, as long as it is abundant and final saturation is intense and rapid.

The role of moisture in the initiation of debris flows generally overshadows the importance of debris supply, but without material available for transportation, a debris flow cannot occur. In the Coast Mountains of British Columbia, debris flows are only triggered by intense rain following a quiescent period that allows loose debris to accumulate in the initiation zone (Church & Miles, 1987). Furthermore, the volume of material entrained during a debris flow is more important for determining its magnitude than the volume of water involved in its initiation (Swanston & Swanson, 1976; Fannin & Rollerson, 1993). Therefore, debris flow magnitude and frequency may be controlled by the limiting factors of either debris supply and initiation zone recharge or localized exceedance of a slope stability threshold due to hydroclimatic events (Rebetez *et al*, 1997; Bovis & Jakob, 1999).

The presence or absence of permafrost further complicates the relationship between hydroclimatic conditions, debris supply, and debris flow magnitude and frequency. In periglacial environments, icy permafrost can inhibit drainage and provide a solid, impermeable slip plane that allows the rapid saturation of the active layer and results in

shallow, low-volume debris flows (Cogley & McCann, 1976; Akerman, 1984). Ice within the talus diminishes resistance to shear stress within the active layer because it increases porosity, preventing consolidation (Hartshorn, 1995) and thawing of icy permafrost, which may introduce enough moisture to trigger a debris flow (Harris & Gustafson, 1988). On non-permafrost slopes, longer or more intense precipitation and snowmelt events may be required to initiate debris flows because most of the water will percolate through the material and drain away. Without a frozen substrate, debris flows may extend to greater depths and consequently may be of much greater volume.

Several studies include observations of debris flows in action (Broscoe & Thompson, 1969; Larsson, 1982; Johnson & Rodine, 1984 as cited in Coussot & Meunier, 1996). While these qualitative and highly descriptive accounts provide insight into the processes taking place, most researchers will not observe debris flows in action due to their relatively unpredictable nature and the extreme hazard involved. Therefore, the depositional and erosional features of debris flows must be used to diagnose their occurrence.

Debris flows may be classified as one of two main types: (1) hillslope debris flows or (2) channelized debris flows. Hillslope debris flows result in well-defined failure scars, parallel levees on either side of an incised flow channel, and terminal lobate deposits. Channelized debris flows are initiated within steep, V-shaped catchments on the upper portions of slopes and may have narrow, well-defined tracks with distinct levees and lobes or wide, poorly defined tracks with discontinuous and chaotic deposits. A comparison of the two debris flow types on talus slopes in the Sawtooth Range, Ellesmere Island, Nunavut indicated that channelized debris flows, while less frequent, accomplished seven times the geomorphic work of hillslope debris flows (Lewkowicz & Hartshorn, 1998).

The outer sides of debris flow levees are characterized by coarse unconsolidated material with most stones oriented in the general direction of flow. The inner sides of levees are characterized by matrix-supported, coarsening-upwards, heterogeneous material with strong particle orientation in the direction of flow and decreasing matrix material downslope. Debris flow lobes generally consist of coarsening-upwards, heterogeneous material with scattered particle orientation and decreased grain size downslope. Fine material deposited during the initial event is removed from the surface of the debris flow by subsequent rain and runoff (Broscoe & Thompson, 1969; Bones, 1973; Nieuwenhuijzen & van Steijn, 1990; Catto, 1993; van Steijn, 1996; Lowey, 2002).

2.2 Debris Flows in Southwestern Yukon Territory and Northwestern British Columbia

A significant body of literature exists regarding debris flow activity in the Yukon Territory and British Columbia, especially in the Kluane Region. A variety of mass movements have been reported in the Kluane Region, including large catastrophic slope failures (*e.g.* rock avalanches), but debris flows present the greatest short-term hazard (Clague, 1981). In July of 1988, debris flows, debris avalanches, and related sediment-water flows severed the Alaska Highway at eight locations near Kluane Lake, as well as at six locations near Muncho Lake, British Columbia in the Sentinel Range of the Rocky Mountains (Evans & Clague, 1989). Although no loss of life occurred, the widespread damage to human infrastructure and the high financial cost of repairing the Alaska Highway (1.8 million dollars), illustrates the power of debris flows and the vulnerability of transportation routes that traverse active geomorphic surfaces. Debris flows are also

important agents of sediment transfer in the southern Yukon and can transport large volumes of debris (Lowey, 2002) as well as play a significant role in the development of valleys (Harris & Gustafson, 1988).

Debris flows in this region, particularly those at the southern end of Kluane Lake, are generally initiated by hydroclimatic events, especially intense rainstorms (Clague, 1981). When spring and autumn rain induce rapid melting of snow and ice, the potential for debris flow activity may be further enhanced. Intense rainstorms triggered flooding and catastrophic debris flow failures in the catchment area of the Kusawa Lake torrent system on 16 September 1982 (Lowey, 2002) as well as the debris flows of 1988 (Evans & Clague, 1989).

Earthquakes are a possible trigger for debris flows in the Kluane Range even though many significant seismic events in this region have not resulted in debris flows (Clague, 1981). Harris and Gustafson (1993) proposed that thawing of icy permafrost is responsible for saturation of debris and initiation of debris flows on Sheep Mountain at the southern end of Kluane Lake. However, large amounts of ground ice would be required and thawing would have to be exceptionally rapid in order to saturate the debris and induce a slope failure. On the other hand, thawing of ground ice may be important for releasing debris and making it available for transportation via debris flows.

Debris flows are quite frequent at the southern end of Kluane Lake. Harris and McDermid (1998) used dendrochronological and sedimentological analyses to determine that over the last 1200 years, an average of one major debris flow occurred every 150 years at Sheep Mountain with long periods of stability between major events. Lowey (2002)

determined that flooding related to catastrophic debris flows in the catchment area occurs on the Kusawa Lake torrent system approximately once every 200 years.

Debris flows are clearly an important geomorphic agent in southwestern Yukon Territory and northwestern British Columbia that pose a significant hazard to human life, infrastructure, and the environment. Since most of the debris flows in the Kluane Region are initiated by hydroclimatic events, improved understanding of the relationship between precipitation regimes and debris flow magnitude and frequency is especially important for this area.

2.3 Debris Flow Signatures in Lacustrine Sediment

Lacustrine sediment analyses can be useful additions to traditional studies of sediment transport processes because they may provide long-term data regarding geomorphic activity initiated in sub-aerial environments and terminating in sub-aqueous environments (Dearing & Foster, 1993). Physical, chemical, biological, and magnetic analyses of lacustrine sediments have been used to infer the rate, form, cause, and source of sediments in many different environments (Dearing, 1991). Sediment yield in lacustrine sediments is a valuable indicator of erosional and transport processes, hence it may also be used to make inferences regarding landscape change and hydroclimatic conditions in a catchment (Lamoureux, 2000; Lamoureux, 2002). When conducting lacustrine sediment studies in order to elucidate information regarding slope processes, samples must be taken from lakes with relatively small catchments. Lakes with catchment-to-lake ratios of ten or less may not be large enough to develop an extensive drainage network and may be more likely to have sediments derived from slope or surface processes than channel processes.

Conversely, sediments derived from channel deposits will dominate in lakes with relatively large catchments and this may overwhelm any signature from slope and surface processes (Dearing & Foster, 1993).

Lacustrine sediments have been used to determine the magnitude and frequency of mass movements and other geomorphic events in a variety of mountainous environments including northern Sweden, southern and central British Columbia, southern Poland, and the Canadian High Arctic (*e.g.* Jonasson, 1988; Gottesfeld *et al*, 1991; Kotarba, 1992; Doran, 1993; Kotarba, 1997; Hartshorn & Lewkowicz, 2000; Lamoureux, 2000; Fuller, 2002; Lamoureux, 2002). In the studies cited above, cores were collected using a variety of techniques including percussion coring from the frozen lake surface (*e.g.* Hartshorn & Lewkowicz, 2000) and piston coring from rafts (*e.g.* Fuller, 2002). In addition to thorough visual examinations, the lacustrine sediment cores were subjected to magnetic susceptibility, X-ray radiography, loss on ignition, grain size analysis, and radiocarbon dating techniques in order to interpret sedimentological activity.

Discrete layers of coarse particles with low organic content were generally interpreted as debris flow signatures, while fine sediments with high organic content were interpreted as autochthonous deposits laid down during quiescent periods between debris flows (Gottesfeld *et al*, 1991; Kotarba, 1992; Kotarba, 1997; Hartshorn & Lewkowicz, 2000; Fuller, 2002). The coarse debris flow layers in cores collected by Gottesfeld *et al* (1991) and Fuller (2002) in British Columbia were underlain and overlain by fine sediment interpreted as material washed into the lake by hydroclimatic events before and after the main debris flow pulse. In the latter study, fine sediment overlying the debris flow signature was topped by a thin layer of fine, woody debris and organic litter (Fuller, 2002).

Some studies simply used the lacustrine sediment signatures of mass movements to reach conclusions regarding local geomorphic activity (*e.g.* Gottesfeld *et al*, 1991; Doran, 1993; Fuller, 2002). In others, inferences were made regarding past changes in climate based on the long term magnitude and frequency of debris flows and other geomorphic events as determined from lacustrine sediment records (*e.g.* Kotarba, 1992; Kotarba, 1997; Hartshorn & Lewkowicz, 2000; Lamoureux, 2000; Lamoureux, 2002). However, the accuracy or effectiveness of using lacustrine sediments to analyze sub-aerial mass movements was not discussed in any of the publications. The collection of lacustrine sediment cores is difficult under ideal conditions (Glew *et al*, 2001) let alone from remote mountain lakes and identification of debris flow signatures in lacustrine sediments is open to many interpretations. The comprehensiveness of lacustrine sediment coring is also questionable because lake sediment cores cover a very small proportion of the entire lakebed area and debris flows can be highly localized events. The relatively small diameter of the core tubes also prevents sampling of large clasts deposited by debris flow activity with subsequent overestimation of the presence of finer materials. Furthermore, small debris flows might not possess enough energy to leave deposits in the lakes below the initiation zones and even if they do, sediment signatures might be very faint. Without an assessment of the effectiveness of this methodology, conclusions about debris flow magnitude and frequency based on lacustrine sediment records will remain questionable.

3. STUDY AREA

3.1 Site Selection

Southwestern Yukon Territory and northwestern British Columbia was selected as the study area because this mountainous region boasts many slopes affected by debris flows and contains many small lakes. These attributes made it ideal for the investigation of debris flow activity using lacustrine sediment signatures (Figure 3.1).

Individual field sites were selected through detailed examination and interpretation of maps and aerial photographs. Three criteria were used to evaluate potential field sites. First, evidence of debris flow activity into small lakes without glacial meltwater input and low catchment-to-lake ratios (<10) was required for the preservation of a long-term record of sub-aerial mass movement activity and to avoid blurring of those signatures by other depositional processes (Jonasson, 1988; Dearing & Foster, 1993). Second, locations underlain by carbonate rocks were avoided to facilitate radiocarbon dating of sediments. Third, field sites needed to be close to major transportation routes (*e.g.* Alaska and Haines Highways) or population centres to ease logistical constraints. Based on these criteria, Mount Aramis, Yukon Territory and Three Guardsmen Mountain, British Columbia, were selected as field sites. A third site between the two (St. Elias Lake, Yukon Territory) was investigated, but no cores were collected as there was no definitive terrestrial evidence of current debris flow activity and lake depths exceeded the maximum length of the coring apparatus.

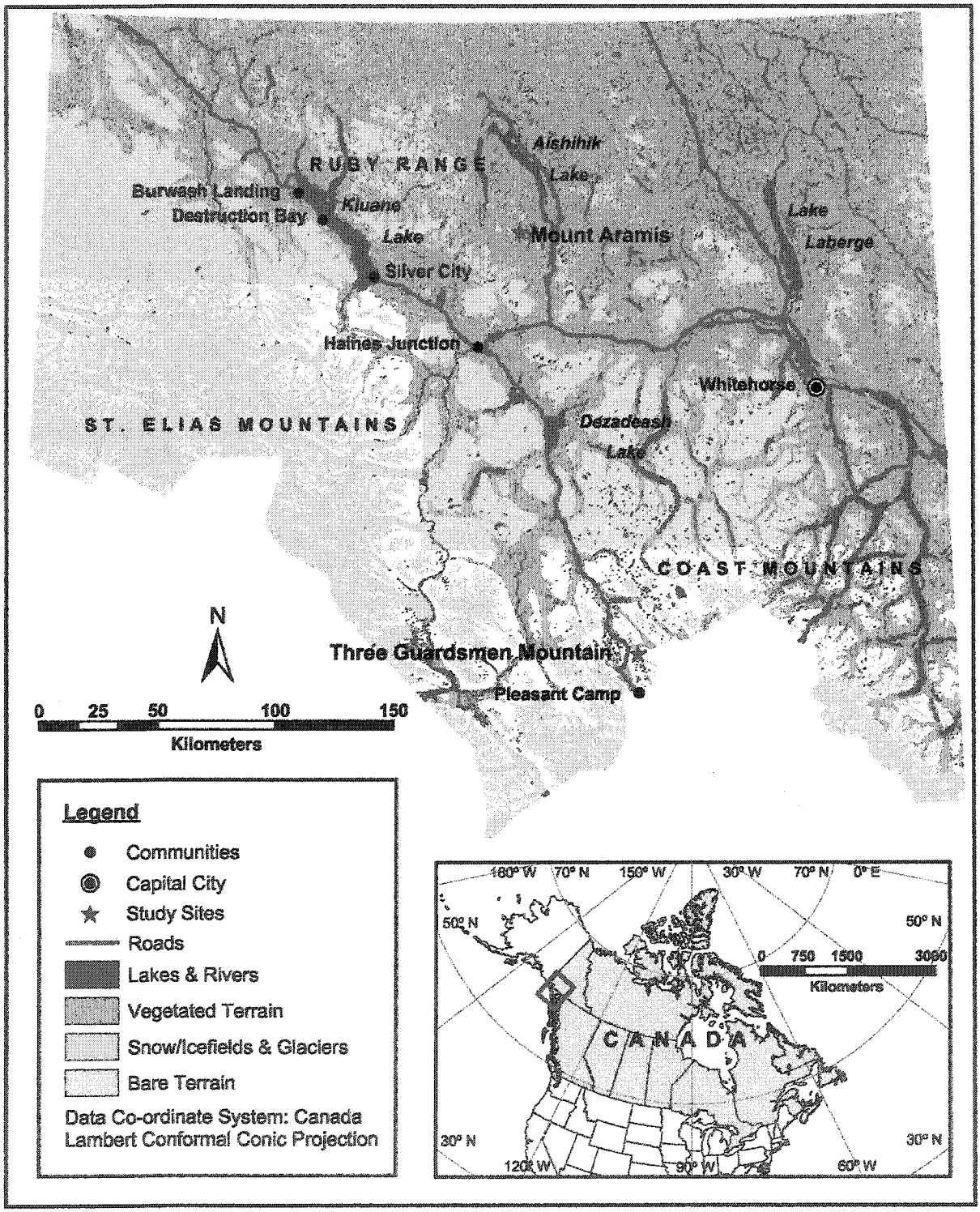

Figure 3.1: Study area map (Based on an extract of the topographic datasets 104M, 105D, 105E, 114P, and 115H at 1:250,000 © Her Majesty the Queen in Right of Canada. Reproduced with the permission of Natural Resources Canada).

3.2 Mount Aramis, Yukon Territory

3.2.1 Mount Aramis Site Description

Located at 61°11'N, 137°15'W with a summit of 1800 m, Mount Aramis is the westernmost peak in a series of three including Mount Porthos and Mount Athos (Figure 3.2). The three peaks are known collectively as the Three Guardsmen and are often confused with Three Guardsmen Mountain, British Columbia described below. The site is located northeast of the Ruby Range of the St. Elias Mountains and just west of Ittlemit Lake. Mount Aramis is underlain by Triassic granodiorite from the Ruby Range Batholith (Energy, Mines & Resources Canada, 1977). Mount Aramis Lake (unofficial name) is situated at 1200 m on the western side of Mount Aramis and is the second northernmost lake in a series aligned along a north/south glacial valley. The upper slopes of Mount Aramis are unvegetated bedrock and talus, but vegetation in the valley is abundant, consisting of grasses, willow, birch, and black spruce (Figure 3.3).

3.2.2 Mount Aramis Climate

The closest weather station to Mount Aramis is at Otter Falls, Yukon Territory, 28 km to the southeast and at an elevation of 830 m a.s.l. Although relatively close to the study site in terms of horizontal distance, the differences in elevation (approximately 600 m and 970 m from Otter Falls to Mount Aramis Lake and the peak of Mount Aramis respectively) indicate that climate normals for Otter Falls are not applicable to Mount Aramis without adjustment (Table 3.1). The mean annual temperature is predicted to be –5.3°C at the elevation of the lake, and –7.7°C on the upper slopes of Mount Aramis using the mean lapse rate of the standard atmosphere (6.5°C/km) cited by Whiteman (2000) and the mean

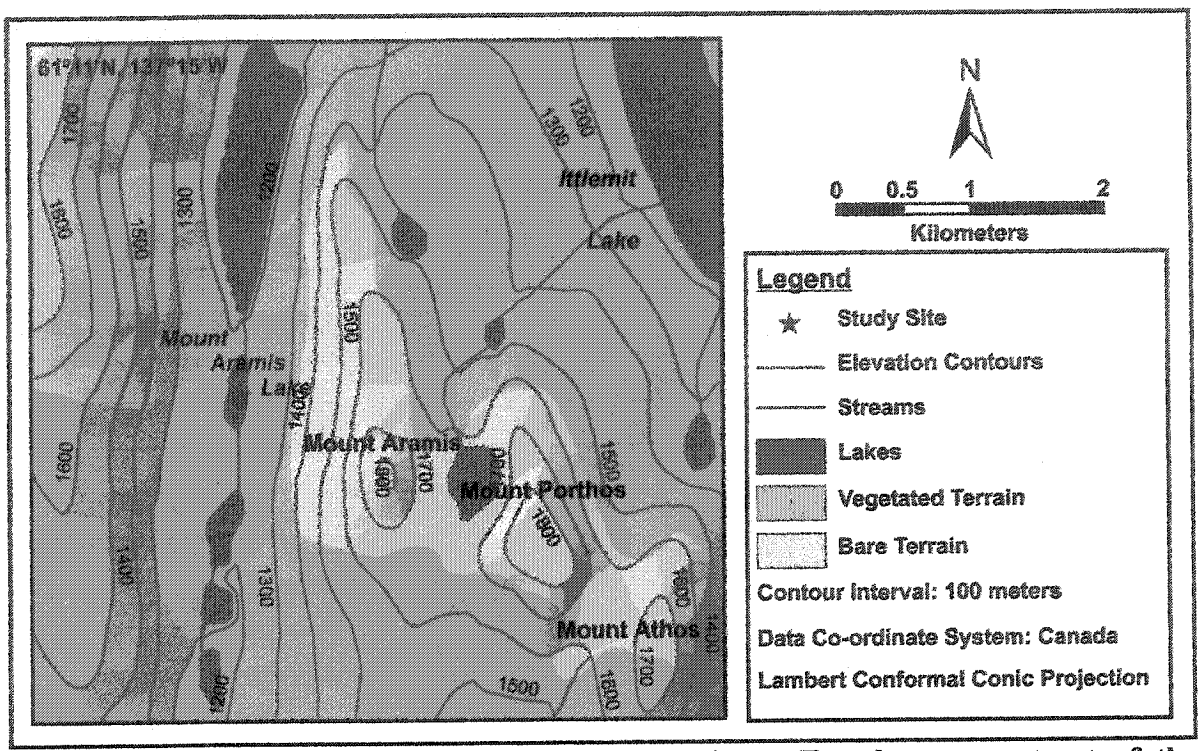

Figure 3.2: Map of Mount Aramis, Yukon Territory (Based on an extract of the topographic dataset 115H at 1:250,000 © Her Majesty the Queen in Right of Canada. Reproduced with the permission of Natural Resources Canada).

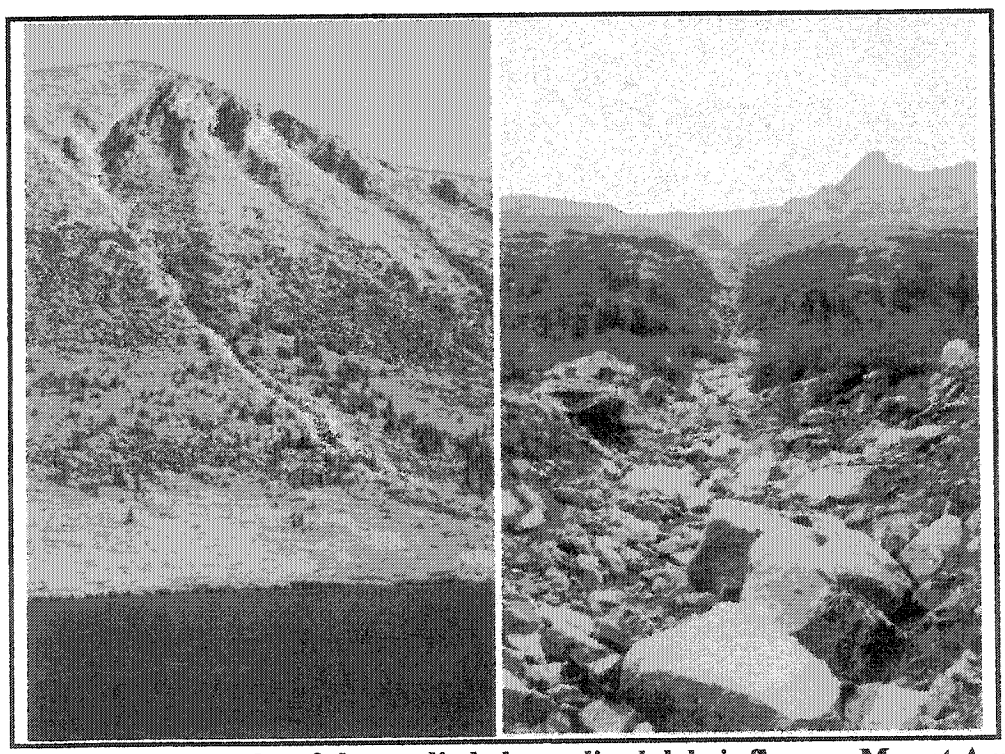

Figure 3.3: Photographs of the studied channelized debris flow on Mount Aramis.

temperature of –1.4°C at Otter Falls. However, because temperature inversions occur frequently in southwestern Yukon Territory, it is possible that the lapse rate is not this high and the actual temperatures are somewhat warmer. Mount Aramis probably receives similar amounts of annual precipitation as Otter Falls (297 mm/yr) although the higher elevation may increase this amount. Snowfall at Otter Falls constitutes 36% of the annual precipitation, and the greater elevation likely increases this proportion at Mount Aramis. Based on the predicted temperatures of –5.3°C and –7.7°C, it is probable that permafrost exists in the initiation zone of the Mount Aramis debris flow channel.

Table 3.1: Climate normals for Otter Falls, Yukon Territory (1971-2000).

Station Name:	Otter Falls NCPC, Yukon Territory
Latitude:	61° 02' N
Longitude:	137° 03' W
Elevation:	829.7 m

Temperature:	Jan	Feb	Mar	Apr	May	Jun	Jul	Aug	Sep	Oct	Nov	Dec	Year
Daily Mean (°C)	-16.4	-12.1	-7.3	-0.3	6.1	11.1	13.1	10.9	5.8	-1.5	-11.5	-14.4	-1.4
Standard Deviation	6.4	4.4	2.9	2.2	1.7	1.2	0.9	1.5	1.8	2.3	3.8	5.0	2.4

Precipitation:	Jan	Feb	Mar	Apr	May	Jun	Jul	Aug	Sep	Oct	Nov	Dec	Year
Rainfall (mm)	0.0	0.1	0.0	0.7	16.9	37.9	53.1	44.3	28.0	8.7	0.0	0.1	189.9
Snowfall (cm)	17.0	14.5	11.0	8.5	4.3	0.3	0.0	0.0	4.6	16.2	17.5	13.8	107.4
Precipitation (mm)	17.0	14.6	11.0	9.2	21.2	38.1	53.1	44.3	32.6	24.9	17.5	13.9	297.3

Source: Environment Canada (2004)

3.2.3 Mount Aramis Debris Flow Map and Profile

There are several track features associated with steep V-shaped catchments on the western slope of Mount Aramis, but only one reaches Mount Aramis Lake (Figure 3.4). The Mount Aramis debris flow channel is simple with a large, central track and related levees issuing from the largest of the catchments in the initiation zone (Figure 3.5). The track is 5 to 10 m wide and 2 to 4 m deep near the initiation zone but decreases in width and depth as it approaches the lakeshore until the track is nothing more than a thin stream along the northern edge of a wide, low-angled debris fan. The outer edges of the levees are generally

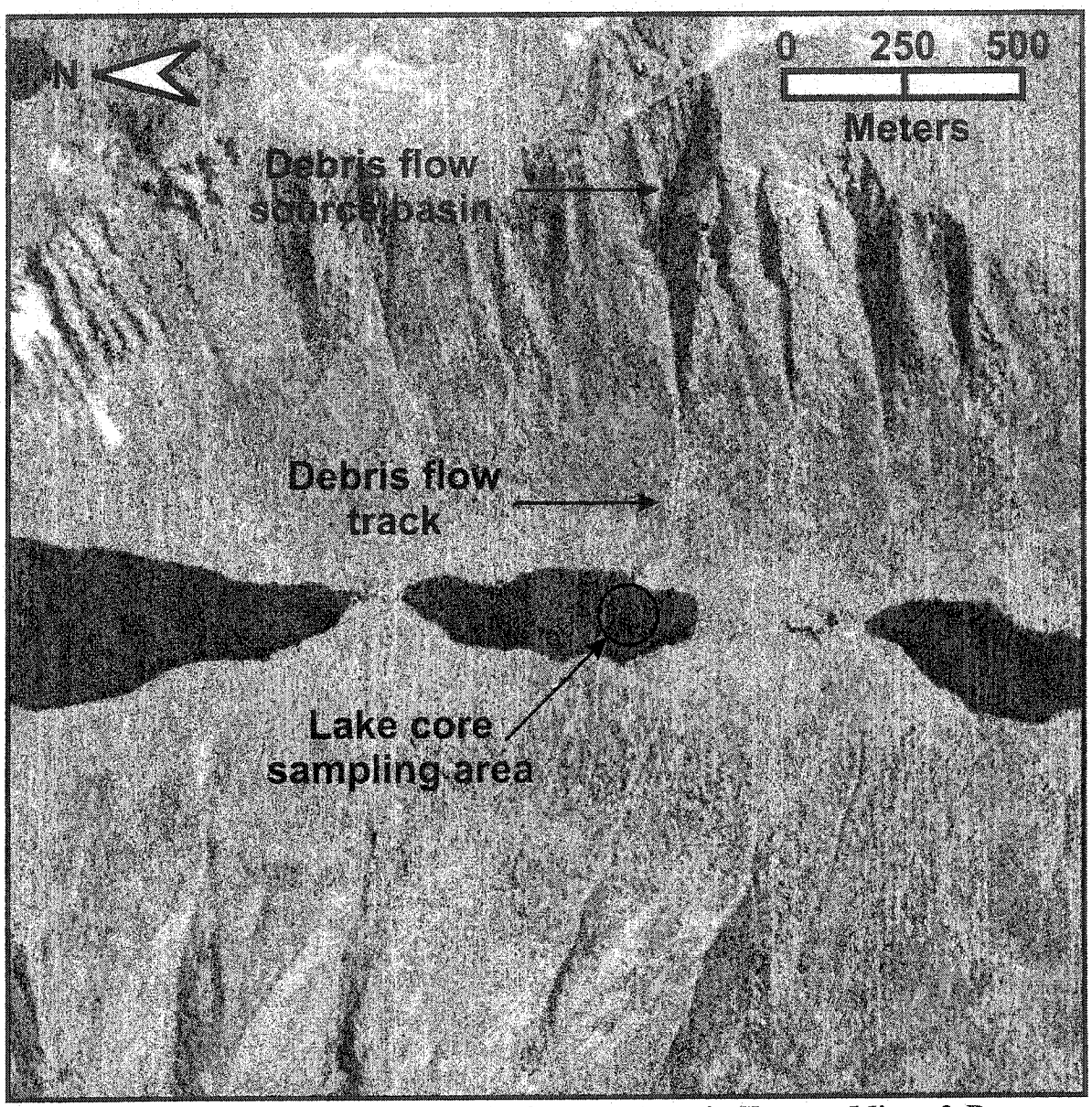

Figure 3.4: Aerial photograph (A27368) of Mount Aramis (Energy, Mines & Resources Canada, 1988).

vegetated, sometimes with mature black spruce trees, but usually with willows and grasses. Vegetation in the track is sporadic on the upper two-thirds of the debris flow but for the last 175 m, the track and levees are densely vegetated by willow and birch. Surface clasts are generally 20 to 300 cm in diameter and coarsen outwards on the levees. A 45 cm deep pit excavated on the inner side of the southern levee 250 m from the lakeshore contained 5 to 30

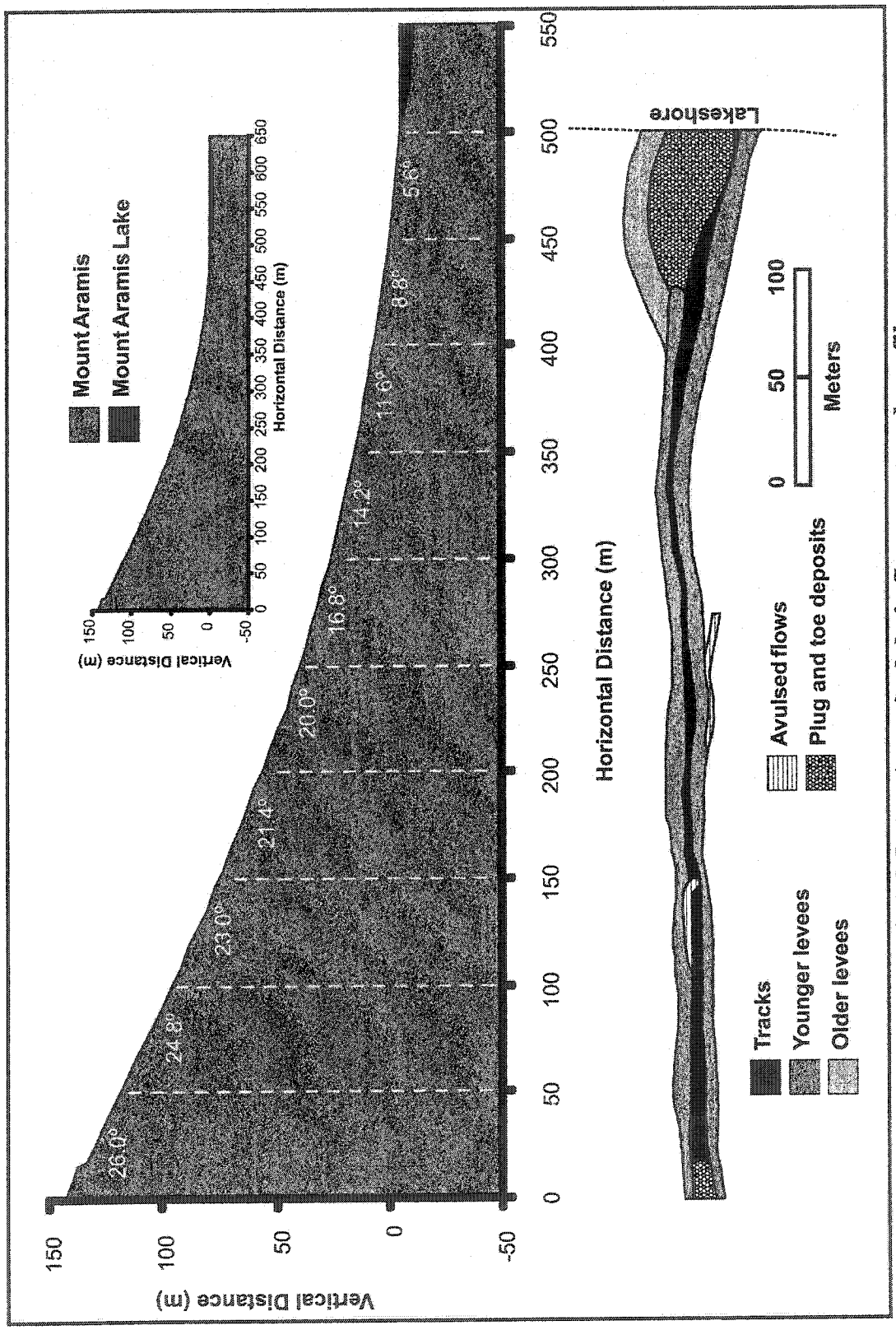

Figure 3.5: Mount Aramis debris flow map and profile.

cm diameter angular clasts, with long axes aligned downslope, supported by a sandy silt matrix, as well as a 1 to 2 m diameter boulder. These observations are similar to those reported in other studies as diagnostic characteristics of debris flows (*e.g.* Broscoe & Thompson, 1969; Bones, 1973; Nieuwenhuijzen & van Steijn, 1990; Catto, 1993; van Steijn, 1996; Lowey, 2002).

3.2.4 Mount Aramis Lake Bathymetry

Mount Aramis Lake is approximately 700 m long, 200 m wide, 6 m deep, and drains into the lake to the north of it via a narrow stream, while inflow comes from a narrow stream at the south end of the lake (flows of approximately 1L/min during the site visit in mid-summer) (Figure 3.6). The bathymetry is relatively simple with a central basin and shallow sides. Angular clasts (15 to 80 cm) are scattered across the unvegetated, silty bottom of the lake with higher concentrations near the toe of the debris flow channel.

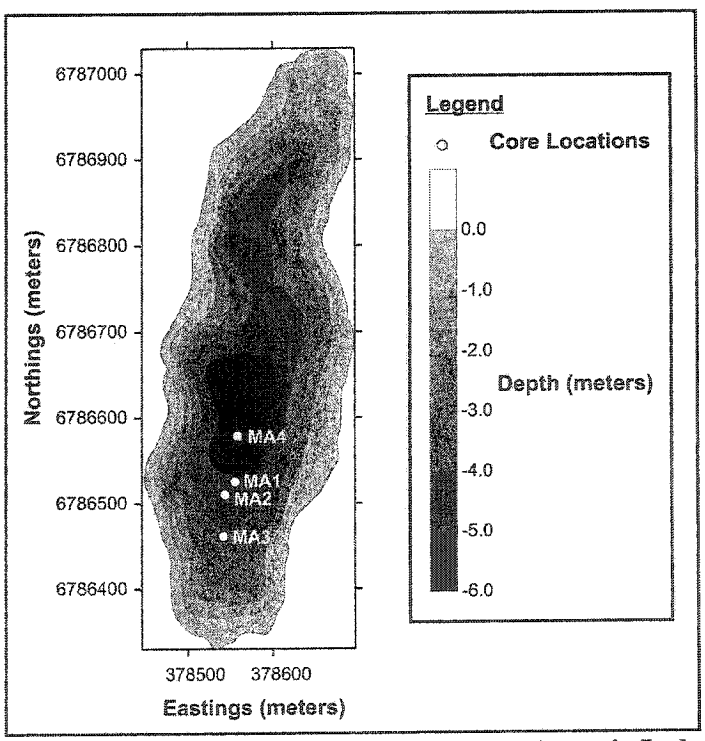

Figure 3.6: Bathymetric map of Mount Aramis Lake.

3.3 Three Guardsmen Mountain, British Columbia

3.3.1 Three Guardsmen Mountain Site Description

Located at 59°37'N, 136°27'W with a peak of 1840 m a.s.l., Three Guardsmen Mountain is part of the Alsek Range of the St. Elias Mountains (Figure 3.7). The immediate area is underlain by quartz diorite of Cretaceous and Tertiary age (Energy, Mines & Resources Canada, 1974). Three Guardsmen Lake is situated at the base of the mountain at 940 m a.s.l. and adjacent to the Haines Highway. The upper slopes on the western side of Three Guardsmen Mountain are unvegetated bedrock outcrops or talus (Figure 3.8). Vegetation is relatively abundant around Three Guardsmen Lake, especially on the lower slopes near the toe of the debris flow channel studied.

3.3.2 Three Guardsmen Mountain Climate

The closest weather station to Three Guardsmen Mountain is located 20 km south at Pleasant Camp, British Columbia at an elevation of 274 m a.s.l. Although relatively close to the study site in terms of horizontal distance, the differences in elevation (approximately 666 m from Pleasant Camp to Three Guardsmen Lake and 1566 m to Glave Peak) indicate that climate normals for Pleasant Camp are not applicable to Three Guardsmen Mountain without adjustment (Table 3.2). Using a mean lapse rate 6.5°C/km, the mean annual temperature of 2.7°C at Pleasant Camp drops to approximately –1.6°C at the lake and to –7.5°C on the upper slopes of Three Guardsmen Mountain. Given that Three Guardsmen Mountain is further inland but at a higher elevation, it may receive more precipitation than the 1416 mm that Pleasant Camp receives annually although the exact amount is impossible to quantify without direct measurement. More than 52% of the precipitation at Pleasant

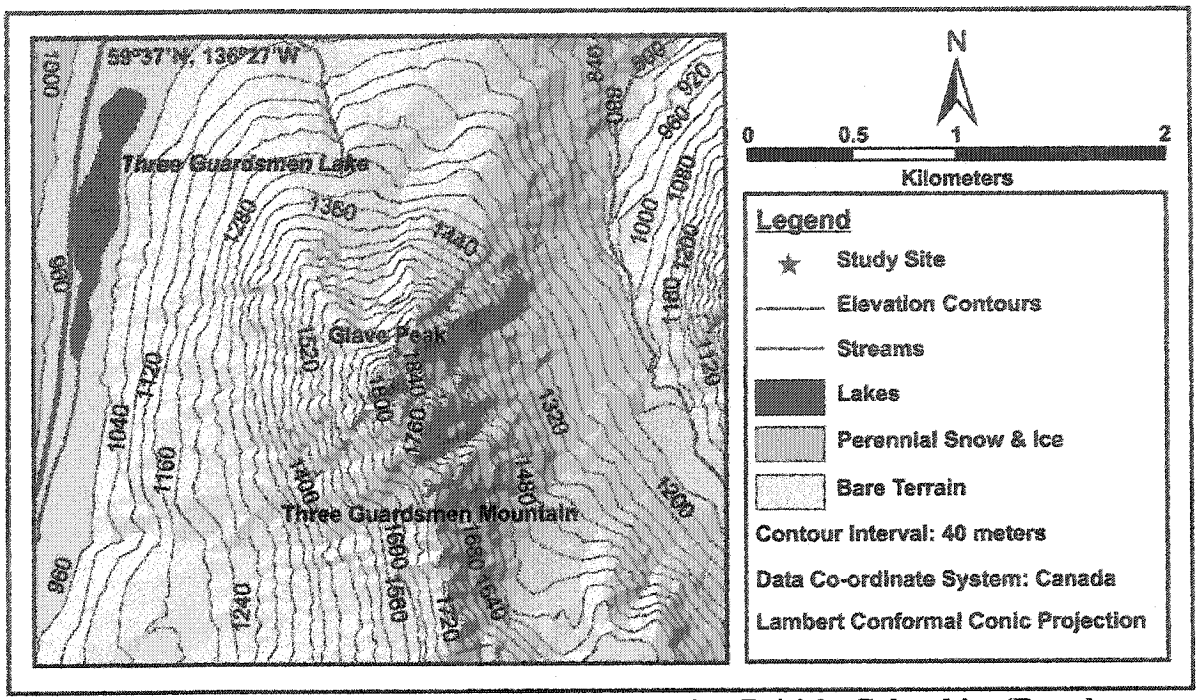

Figure 3.7: Map of Three Guardsmen Mountain, British Columbia (Based on an extract of the topographic dataset 114P at 1:250,000 © Her Majesty the Queen in Right of Canada. Reproduced with the permission of Natural Resources Canada).

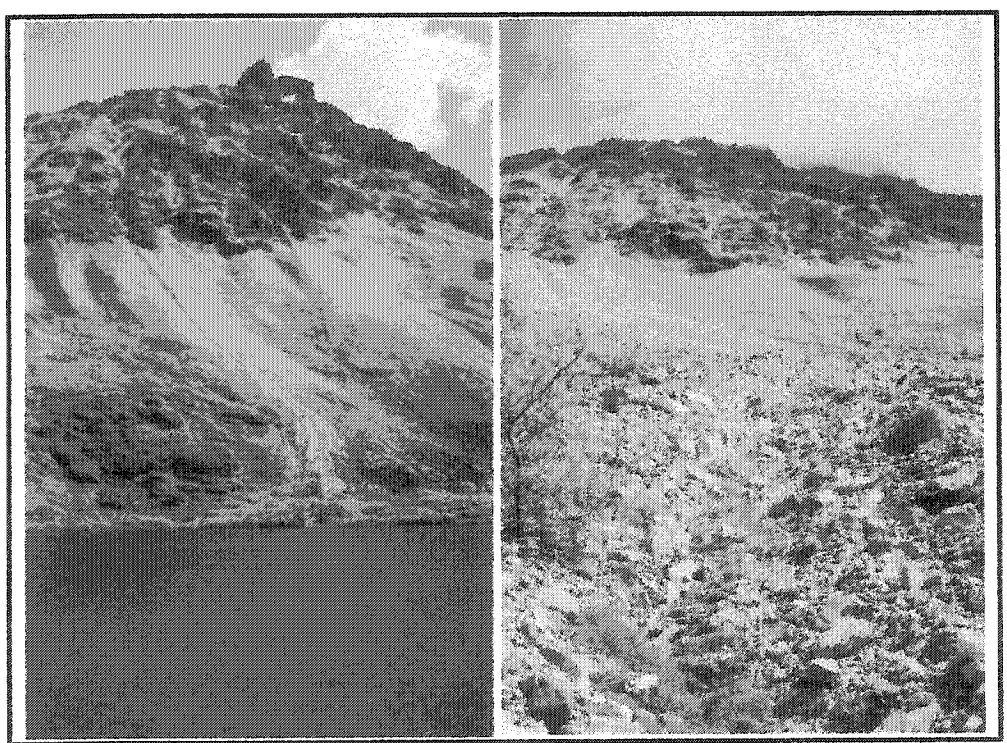

Figure 3.8: Photographs of the studied channelized debris flow on Three Guardsmen Mountain.

Camp falls as snow and due to lower temperatures, the study site probably receives an even greater percentage of its precipitation as snow. Based on a predicted mean temperature between –5.0 and –7.5°C at the elevation of the initiation zone, an active rock glacier on the western slope at 1300 m (toe profile of 37°), and the presence of perennial snow and ice on the north face of the mountain, there is a high probability of permafrost in the initiation zone of the debris flow channel at Three Guardsmen Mountain.

Table 3.2: Climate normals for Pleasant Camp, British Columbia (1971-2000).

Station Name:	Pleasant Camp, British Columbia
Latitude:	59° 27' N
Longitude:	136° 22' W
Elevation:	274.3 m

Temperature:	Jan	Feb	Mar	Apr	May	Jun	Jul	Aug	Sep	Oct	Nov	Dec	Year
Daily Mean (°C)	-8.6	-5.8	-2.1	2.6	7.5	11.7	14.2	13.1	8.7	2.7	-4.2	-7.2	2.7
Standard Deviation	3.9	3.7	1.7	1.4	1.3	1.2	1.0	1.1	1.2	1.2	2.9	3.0	2.0

Precipitation:	Jan	Feb	Mar	Apr	May	Jun	Jul	Aug	Sep	Oct	Nov	Dec	Year
Rainfall (mm)	20.3	24.4	15.4	49.0	44.6	35.0	41.5	64.9	139.8	175.3	40.3	26.1	676.4
Snowfall (cm)	156.1	118.7	82.6	24.8	2.7	0.0	0.0	0.0	1.1	36.5	149.2	168.2	739.8
Precipitation (mm)	176.4	143.1	97.9	73.8	47.2	35.0	41.5	64.9	140.9	211.8	189.6	194.3	1416.3

Source: Environment Canada (2004)

3.3.3 Three Guardsmen Mountain Debris Flow Map and Profile

Track features of variable age in the talus of Three Guardsmen Mountain indicate that mass movement activity is prevalent on its western slope and has been taking place for a long time (Figure 3.9). The most notable of these features is a distinct channelized debris flow complex surrounded by heavily lichenized and vegetated levees and tracks, modified by rockfalls, slushflows, and other slope processes (Figure 3.10). The debris flow is classified as channelized because of the narrow, well-defined central track with associated levees as well as a steep V-shaped catchment in the initiation zone (Lewkowicz &

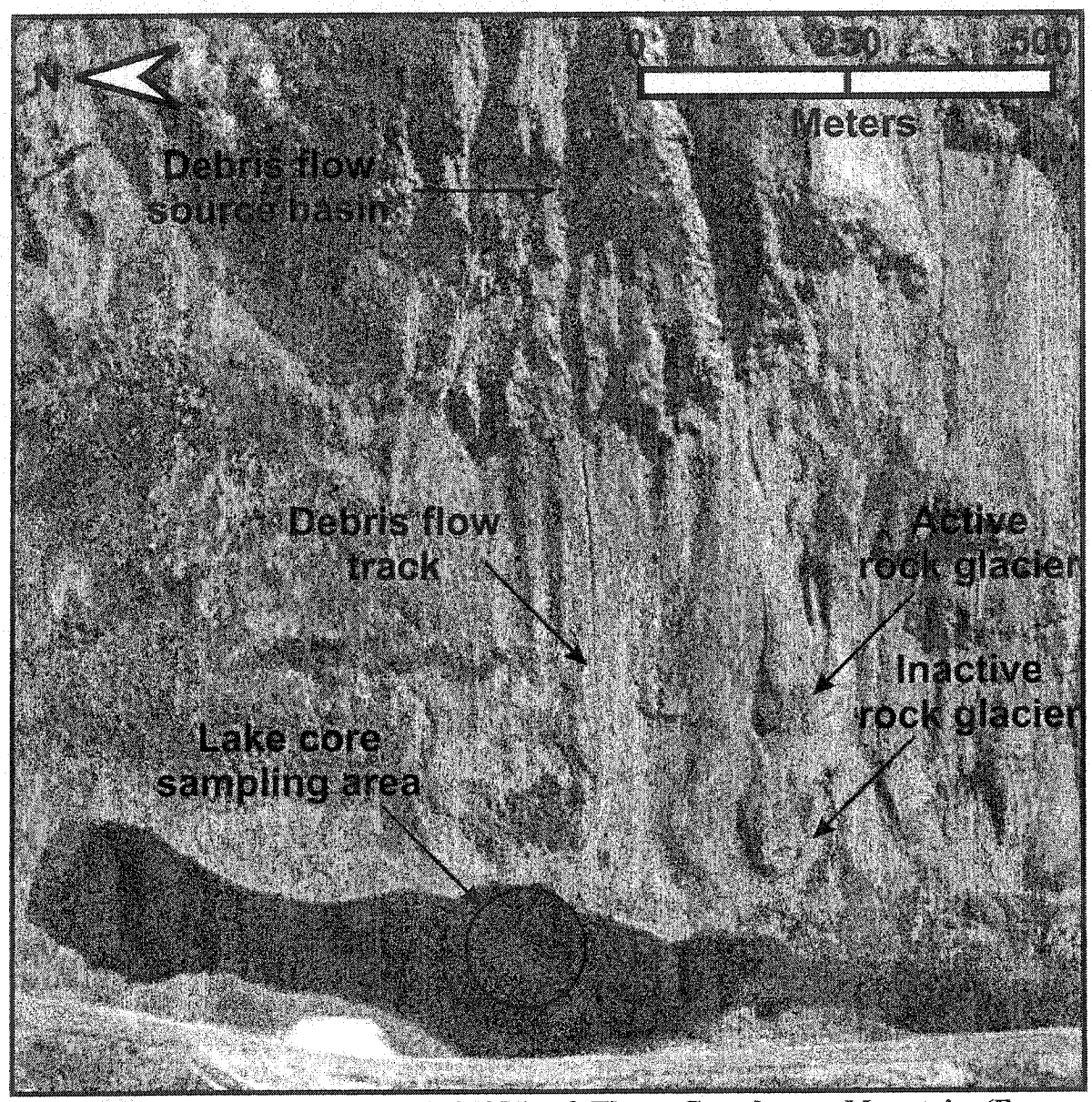

Figure 3.9: Aerial photograph (A27871) of Three Guardsmen Mountain (Energy, Mines & Resources Canada, 1992).

Hartshorn, 1998). The central track is 2 to 6 m wide and 1 to 3 m deep and generally decreases in width and depth with increasing distance from the initiation zone. The central channel and its levees are unvegetated but there are several tracks and levees related to debris flows that have avulsed from the central channel as well as some tracks and levees from older events that have been colonized by lichens and grasses. Surface clasts are

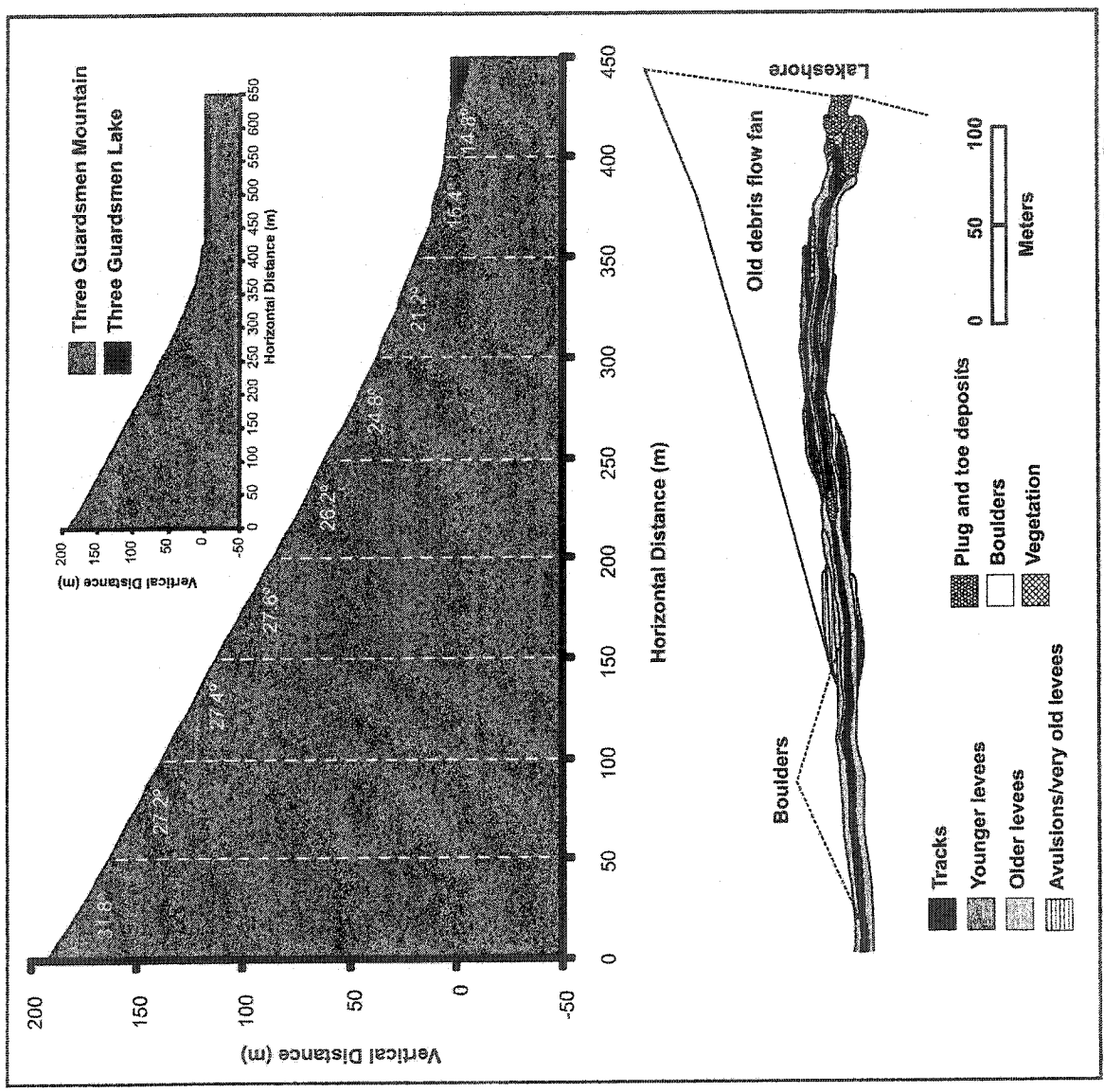

Figure 3.10: Three Guardsmen Mountain debris flow map and profile.

generally 5 to 100 cm in diameter although some boulders are as large as 5 m. Clasts on the debris flow levees coarsen outwards. Pits excavated down to 80 cm depth on the inner and outer edges of paired levees 170 m from the lakeshore, revealed that angular clasts are supported by a sandy silt matrix, and that they coarsen upwards and outwards with the long axes aligned downslope. The toe of the complex consists of several lobes of coarsening-upwards, heterogeneous material bordered by vegetation (willows) along the lakeshore. These observations are similar to those reported in other studies as diagnostic characteristics of debris flows (*e.g.* Broscoe & Thompson, 1969; Bones, 1973; Nieuwenhuijzen & van Steijn, 1990; Catto, 1993; van Steijn, 1996; Lowey, 2002).

3.3.4 Three Guardsmen Lake Bathymetry

Three Guardsmen Lake is approximately 1200 m long, up to 250 m wide, with a maximum depth of 16 m (Figure 3.11). The southern third of the lake is relatively shallow with a silty bottom supporting aquatic vegetation. The northern two-thirds of the lake is significantly deeper with steep sides and contains two sub-basins connected by a narrow trench. Angular clasts, 15 to 80 cm in diameter, are prevalent around the eastern side of the lake and the concentration is particularly high near the toe of the debris flow channel.

3.4 Comparison of the Mount Aramis and Three Guardsmen Mountain Sites

Mount Aramis and Three Guardsmen Mountain are underlain by granodiorite and quartz diorite respectively. The channelized debris flows on both mountains have a western aspect although the relief between the lake and initiation zone is greater at Three Guardsmen Mountain (900 m) than at Mount Aramis (600 m) (compare Figures 3.4 & 3.9). However,

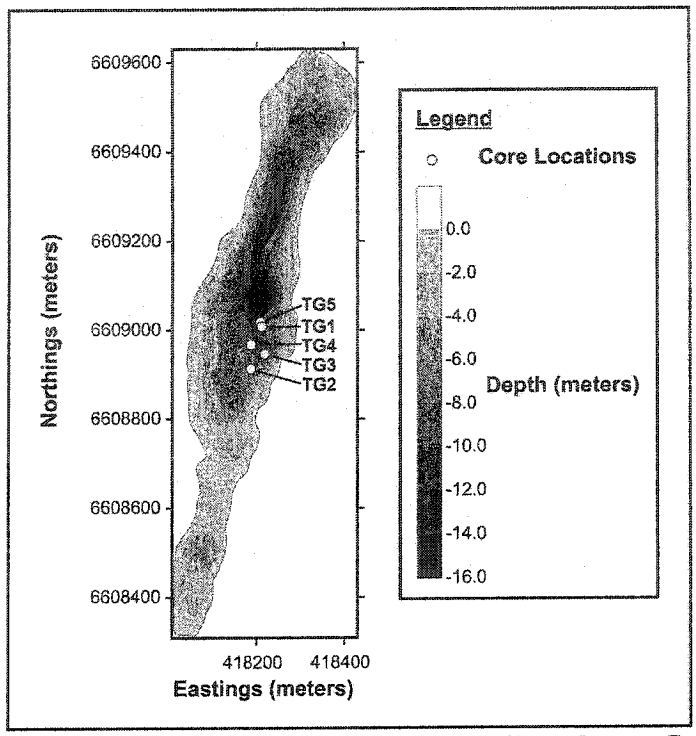

Figure 3.11: Bathymetric map of Three Guardsmen Lake.

the horizontal distances between the lakes and source catchments are similar and as a result the western slope of Three Guardsmen Mountain is steeper (mean gradient of 24°) than the western slope of Mount Aramis (mean gradient of 17°). Both debris flows originate from steep, V-shaped catchments but the morphology of the Three Guardsmen Mountain debris flow deposit is much more complex than the simple, single track debris flow at Mount Aramis. The dimensions of the Three Guardsmen Mountain debris flow are smaller than those of the Mount Aramis debris flow, which is wider, deeper, and contains larger clasts. Climatologically, both sites experience similar daily mean temperatures and probably have permafrost in the initiation zones of the debris flows. However, Three Guardsmen Mountain receives about five times the precipitation of Mount Aramis. Both sites are close to local treeline and the thick vegetation on the slopes of Mount Aramis is likely due to greater stability and less active talus on the lower-angled slopes.

4. METHODS

4.1 Terrestrial Methods

4.1.1 Mapping and Profiling of Debris Flows

Debris flow maps and profiles were created via morphometric surveys (van Steijn *et al*, 1988; Hartshorn, 1995). The quantitative dimensions of channel tracks, levees, lobes, and fans were measured at 10 m intervals, perpendicular to the long axes of the debris flows. An Abney level was used to determine the slope gradient alongside the debris flow for each interval. This data was recorded on grid paper and used to create a map. Qualitative information regarding clast characteristics (*e.g.* size, colouring, roundness), vegetation, and apparent relative ages of the various deposits was also noted on the maps. The maps were then computer-scanned at 600 dpi, imported into CorelDRAW 10, and traced to produce the versions presented in Figures 3.5 and 3.10.

4.1.2 Excavation of Levees

The sediment pits discussed in sections 3.2.3 and 3.3.3 of the previous chapter were excavated using a pick and shovel. Several attempts were made to excavate pits at Mount Aramis but the almost ubiquitous presence of very large clasts (1 to 3 m wide) just below the surface made this task extremely difficult. Only one 45 cm deep pit was successfully excavated 250 m from the shore of Mount Aramis Lake. Four 80 cm deep pits were excavated on the slopes of Three Guardsmen Mountain 170 m from the edge of Three Guardsmen Lake. The pits were dug on the inner and outer edges of the levees immediately adjoining the central debris flow track.

4.2 Lacustrine Methods

4.2.1 Bathymetric Mapping

The bathymetric maps of Mount Aramis Lake and Three Guardsmen Lake were created using a portable sonar (a Humminbird Piranha 2 Fish Finder) in conjunction with an e-Trek Summit hand-held Global Positioning System (GPS) (Figures 3.6 & 3.11). To ensure accuracy, several depth measurement readings from the sonar were compared to depths measured using a weighted, graduated line and differences were negligible. Following a diagonal grid pattern across each lake, geographic positions were recorded as waypoints using the GPS and the depth for each waypoint was determined using the sonar. This data was then used to create bathymetric maps in Golden Software Inc.'s Surface Mapping System Surfer (Win32) v. 6.04.

4.2.2 Collection of Lacustrine Sediment Cores

Sediment cores were collected from Mount Aramis Lake and Three Guardsmen Lake using a rod-driven piston corer from a small boat (Zodiac), following the techniques described by Glew *et al* (2001) and Fuller (2002). Rod-driven piston corers are limited to relatively shallow lakes due to the length and strength of the drive rods (no greater than 18 m deep for this study). However, the light weight and simplicity of the apparatus combined with the ability to penetrate compact sediment with minimal force and recover soft sediments without displacement within the core tube made these disadvantages a minor problem (Glew *et al*, 2001).

In order to secure the boat at the collection points, a rope line was run across the lake, over the desired location, and secured to the shore on either side by tying it to trees or

boulders. The boat was then attached to the line with U-bolts. Water depth was determined at the sampling point using a graduated line to determine the depths at which to begin and end coring. A double-ringed piston was then inserted into a 200 cm long, 6.4 cm diameter plastic core tube and pushed to the bottom of the tube. The tube was then taped to an aluminum drive rod. Once prepared, the apparatus was lowered vertically into the lake and additional drive rods were attached as necessary. The coring procedure began 25 cm above the lakebed by securing the position of the piston by wrapping the piston cable around the operator's foot and treading on it. The core tube was pushed into the lake sediment using the drive rods until the appropriate depth was reached or resistance was met. The core tube and collected sediment were then extracted by pulling upwards on the drive rods and maintaining the position of the piston in the core tube by locking the piston cable against the drive rods. When the bottom of the core tube was still below the surface of the water a rubber stopper was inserted to prevent loss of the core.

Onshore, the piston was removed by drilling a hole in the core tube just below the piston to relieve suction. With the core tube still in a vertical position, a drive rod was used to push against the bottom rubber stopper, forcing the core to the top of the tube where it was skimmed off and collected in 1 cm increments until the sediment had a firm consistency (usually 15 to 20 cm). The core tube was then lowered to a horizontal position and a drive rod was used to force the sediment core out onto 2 layers of plastic wrap and 2 layers of aluminum foil. The core was then wrapped in these materials, labeled, and placed between two halves of high-density plastic piping secured with tape. The encased cores were taped together in bundles for shipping by air to the University of Ottawa where they were refrigerated until analysis.

4.3 Laboratory Analyses

4.3.1 Magnetic Susceptibility

Magnetic susceptibility characterizes the relative ease of magnetization of sediments during the brief application of a magnetic field and varies with the relative content of magnetic minerals especially those from the iron-titanium solid solution series (*e.g.* magnetite) (Creer & Morris, 1996; Nowaczyk, 2001; Zolitschka *et al*, 2001). Given that the majority of iron-bearing minerals found in lake sediments are derived from erosion within the lake catchment and are transported by a variety of geomorphic processes, including debris flows, magnetic susceptibility may be regarded as a proxy indicator for allochthonous sediment input (Sandgren & Snowball, 2001; Zolitschka *et al*, 2001).

Magnetic susceptibility can be determined on whole cores, split cores, or small samples and is fast, simple, non-destructive, yields characteristic patterns, measures a wide range of values, and provides reliable proxy information regarding sedimentation events (Thompson *et al*, 1980; Thompson & Oldfield, 1986; Nowaczyk, 2001; Sandgren & Snowball, 2001; Zolitschka *et al*, 2001). As a result, magnetic susceptibility logging is one of the standard methods applied on sediment cores from marine, lacustrine, and terrestrial environments and has proven very useful for correlation and interpretation of the sediments within (Nowaczyk, 2001, Dearing, 1983; Dearing, 1986).

Whole-core magnetic susceptibility logging for each core was conducted using a Bartington MS2C Magnetic Susceptibility Meter with a loop sensor following the methodology outlined by Dearing (1994). Before sampling, the cores were unwrapped, allowed to warm to room temperature, and the calibration of the meter was checked against a standard core for which the magnetic susceptibility value was known. Once prepared,

each core was passed through the loop sensor and magnetic susceptibility was measured in Standard Industrial (SI) units at 1-cm intervals. However, the coil that generates and measures the magnetic field actually samples a 4 cm section of the core for each sample point (*i.e.* 2 cm on either side) resulting in a running-mean of magnetic susceptibility along the length of the core (Brown *et al*, 2002). Each core was sampled twice on two separate days to account for any inconsistencies in magnetic fields and power from the outlet. The mean value for each sample point was calculated and used to produce line graphs of magnetic susceptibility for each core. A logarithmic scale was applied to the graphs to emphasize some of the smaller peaks in magnetic susceptibility and de-emphasize some of the larger peaks.

4.3.2 X-Ray Radiography

X-ray radiographic techniques are fast, non-destructive, and very useful in the detection, interpretation, and correlation of primary and secondary sedimentary structures in lacustrine sediment cores (Axelsson, 1983). X-ray absorption depends on the radiation wavelength and the density, thickness, and atomic number of the sediments. As a result, high-density sediments are generally lighter in shade than organic rich sediments. Axelsson (1983) suggests that X-ray radiographs should normally be collected before extrusion from the core tube to avoid distortion of the sediments and to provide information about the soft, upper layers of the core. However, due to the lack of a portable X-ray imaging system, the upper sediments from Three Guardsmen Lake and Mount Aramis Lake were skimmed off and the cores were extruded and shipped to Ottawa.

X-ray radiographs of all nine cores in their intact state were taken at DiagnostiCare Inc.'s X-Ray Laboratory at the University of Ottawa Health Centre using a Raytheon RME-325R system set to 55 kV and 2.8 mA with an exposure time of 1/40 seconds (s). The X-ray images were then scanned and imported into CorelDRAW 10 for alignment and comparison with the magnetic susceptibility graphs.

4.3.3 Sketching

The cores were split into halves using a knife and then separated. One half of each core was re-wrapped and stored as an archive while the remaining half was sketched in detail. Qualitative variations in sediment texture, colour, consistency, density and the presence of discrete layers and bands of organic material were noted, measured and recorded on grid paper. This information was then used to create images of the cores in CorelDRAW 10, which were aligned with the graphs of magnetic susceptibility and x-ray images.

4.3.4 Loss on Ignition

Loss on Ignition (LOI) approximates the organic and carbonate content of sediment samples. Between 500 and 550°C, organic matter is oxidized to carbon dioxide and ash and between 900 and 1000°C, carbon dioxide will evolve from calcium carbonate and dolomite and leave behind oxide (Dean, 1974; Heiri *et al*, 2001). Not only is LOI fast, inexpensive, and straightforward, the results can be used to estimate the organic and carbonate content of sediments with the accuracy and precision of more sophisticated geochemical analyses provided that standardized techniques are applied (Dearing, 1986; Heiri *et al*, 2001).

Organic and carbonate contents were determined via LOI for all of the Mount Aramis Lake cores and cores TG3 and TG5 from Three Guardsmen Lake using the standardized methodology outlined by Heiri *et al* (2001). The length of each core was measured and compared with the length recorded immediately after extrusion in the field. The new measurement was divided by the old measurement to calculate a sampling interval ratio. However, the differences between the new and old measurements were minimal and the sampling intervals for the four cores ranged from 0.94 to 0.98 cm. The sample points were marked along the length of the cores using a clean, metal spatula. A series of crucibles were cleaned and weighed to determine the crucible weight (CW). Once cleaned, the crucibles were handled with clean metal tongs to avoid contamination and alteration of crucible weights. For each sampling point, 1 cm^3 of sediment (determined using a mold) was collected, placed in a crucible, and weighed to determine the wet weight (WW). The spatula and mold used for sampling were cleaned with de-ionized water and dried between samples to avoid contamination. The samples were collected from the central axis of the core to avoid inclusion of sediment from overlying layers due to the downwarping of sediments caused by core tube insertion. When a series of wet samples had been prepared they were dried for 14 to 24 hrs in a drying oven at 105°C. Upon removal, the samples were allowed to cool in a dessicator before they were weighed to determine the dry weight (DW).

The crucibles were then loaded into a muffle furnace for 4 hrs at 550°C after which the crucibles were allowed to cool in a dessicator and then weighed to determine the ignition weight (IW). The crucibles were placed at least 2.5 cm from the walls and were not in contact with each other when loaded in the furnace. The crucibles were re-loaded into a muffle furnace for 2 hrs at 950°C and then weighed to determine the carbonate weight

(AW). The percentage of organics (LOI at 550°C) and carbonates (LOI at 950°C) was then calculated using the following equations:

$$\text{LOI at 550°C (\%DW)} = ((DW - IW)/(DW - CW)) * 100$$

$$\text{LOI at 950°C (\%DW)} = ((IW - AW)/(DW - CW)) * 100$$

The organic and carbonate content data was then graphed in Microsoft Excel and the graphs were imported into CorelDRAW 10 and aligned with the core sketches, x-ray images, and magnetic susceptibility graphs.

4.3.5 Grain-size Analyses

Textural analysis of lacustrine sediment is critical in determining its source, the transport mechanisms involved in its deposition, the antecedent physical and chemical conditions within the basin, as well as the paleoclimatic and paleohydrological conditions of the watershed (Last, 2001). In particular, debris flow signatures in lake sediment have often been identified by textural characteristics (*e.g.* Gottesfeld *et al*, 1991; Kotarba, 1992; Kotarba, 1997; Fuller, 2002) and some researchers have interpreted even minor increases in the fine component of lake sediments to be indicative of disturbances in the catchment (*e.g.* Binford, 1983). The term 'texture' generally includes size, shape, and fabric arrangement among its attributes (Last, 2001). Although qualitative textural analysis was part of the core description outlined above, quantitative grain-size analysis was required to confirm the observations.

Two methods were used to determine grain size. Coarse materials were subjected to wet sieving and fine materials were subjected to Laser Particle Size Analysis (LPSA). However, initial preparation of the samples was similar. One cm sediment sections (7 to 14 g) were cut from the cores and placed in beakers. Samples for wet sieving were oven dried at 105°C for 14-24 hrs and weighed before placement in beakers. As per Kunze (1965) and Folk (1980), organic materials were removed via two treatments with 50 mL of 30% hydrogen peroxide (H_2O_2) over a 24 hr period followed by warming the solution on a hot plate. The samples were then allowed to dry before being soaked for 1-3 days in 50 mL of 50 g/L of sodium hexametaphosphate ($Na_6O_{18}P_6$), which is a dispersant that prevents clumping of sediments.

Wet sieving is a common, reliable, but time consuming, method of determining grain size of sediments that has been in use for many years (Last, 2001). The guidelines established for wet sieving by ASTM (2001) were followed in this study. Prepared samples were agitated using a Burrell Model 75 Wrist Action Shaker and then poured through sieves with openings of 63, 125, 250, 500, 1000, 2000, and 4000 μm (*i.e.* from 3 to -3 phi). Any sediment smaller than 63 μm (*i.e.* >4 phi) was collected and saved for LPSA. The sediments left on each sieve were collected, oven dried, weighed, and their respective percentages of the sample weight calculated.

LPSA is a more recent innovation in grain size analysis and is particularly useful for rapidly determining the size of silts and clays via measurement of the diffraction (*i.e.* scattering) of light when it strikes a particle (Last, 2001; Murray, 2002). LPSA was undertaken at the Geological Survey of Canada's Sedimentological Laboratory in Ottawa using the LECOTRAC™ LT-100 and ASVR system in conjunction with the LECOTRAC™

v. 7.01 and MICROTRAC™ v. 9.1.15 programs. Samples were wet-sieved at 500 μm into a plastic beaker, diluted by topping up the level of distilled water to 800 mL, and mixed for 4-6 min. using a modified Heidolph RZR-2000 mixer. During this time the LECOTRAC™ ASVR was set to four rinse cycles followed by a 1 min. flow cycle for de-aeration. The sample was then identified and the loading cycle initiated. A plastic syringe was used to collect 10 to 20 cc of the sample and deposit it in the LECOTRAC™ ASVR reservoir. Exposing the sample to ultrasonic waves during a 1 min ultrasound cycle broke up any aggregates before the run cycle analyzed the sample and provided percent cumulative grain sizes below 780 μm.

A variety of statistical parameters including mean, median, mode, sorting, and skewness, were calculated arithmetically, geometrically, and logarithmically using moment and Folk and Ward graphical methods in Gradistat 4.0. The Gradistat 4.0 program operates in Microsoft Excel and was developed by Simon Blott for rapid calculation of grain size statistics (Blott & Pye, 2001).

4.3.6 Accelerator Mass Spectrometry Dating

In order to establish rates of sedimentation and absolute ages of lacustrine sediment layers in Three Guardsmen Lake and Mount Aramis Lake, discrete organic material found in the cores was dated by accelerator mass spectrometry radiocarbon (AMS ^{14}C) dating. AMS ^{14}C dating is based on particle counting of the isotope and is less susceptible to errors than the conventional radiocarbon dating based on decay counting of the ^{14}C isotope (Linnick *et al*, 1989; Bjorck & Wohlfarth, 2001). Furthermore, AMS ^{14}C dating can be performed on very small samples, which makes it a suitable technique for dating the relatively small

volume of organic material available. Samples of plant material from 44 cm depth in TG3 and 44 and 69 cm depth in MA4 were collected with tweezers, rinsed with de-ionized water to remove sediment, dried in a dessicator, wrapped in aluminum foil, placed in a plastic bag, and shipped to the Beta Analytic Radiocarbon Dating Laboratory.

5. RESULTS

A total of nine cores were collected from Mount Aramis Lake, Yukon Territory and Three Guardsmen Lake, British Columbia and prefixed with the codes MA and TG respectively, followed by a number delineating the order of collection. The cores and their associated data are described in order of collection, followed by sections discussing the correlation and interpretation of layers in each lake. The figures for the individual cores include core diagrams, x-ray images, magnetic susceptibility graphs, and LOI and LPSA graphs where available. To facilitate understanding of the core descriptions, letters have been assigned to features of interest and are noted in the text and in the figures.

5.1 Core MA1

Four cores were collected from Mount Aramis Lake on 20 and 21 July 2003 (Figure 5.1). MA1 was comprised of homogeneous, very dark brown sandy silt with several distinct layers (Figure 5.2). Organic levels decreased slightly at 7, 13, and 21 cm depth (A, B, C). A 5 cm thick layer of organic material in a sandy silt matrix at 23 cm depth, a fining upward (medium sand to sandy silt) sequence of sediment from 30 to 35 cm depth corresponded to a distinct peak in magnetic susceptibility, a significant trough in organics, and increased density on the x-ray image (D). In fact, the range of magnetic susceptibility values for the individual Mount Aramis Lake cores was much higher than at Three Guardsmen Lake (below). A small increase in magnetic susceptibility and a small decrease in organics at 44 cm depth represented a 0.2 cm thick layer of light, yellowish brown sandy silt (E). This layer was found in all the Mount Aramis cores and therefore constitutes a marker horizon. Two 0.5 to 1 cm thick layers of organic material in a sandy silt matrix at 49.5 and 59.5 cm

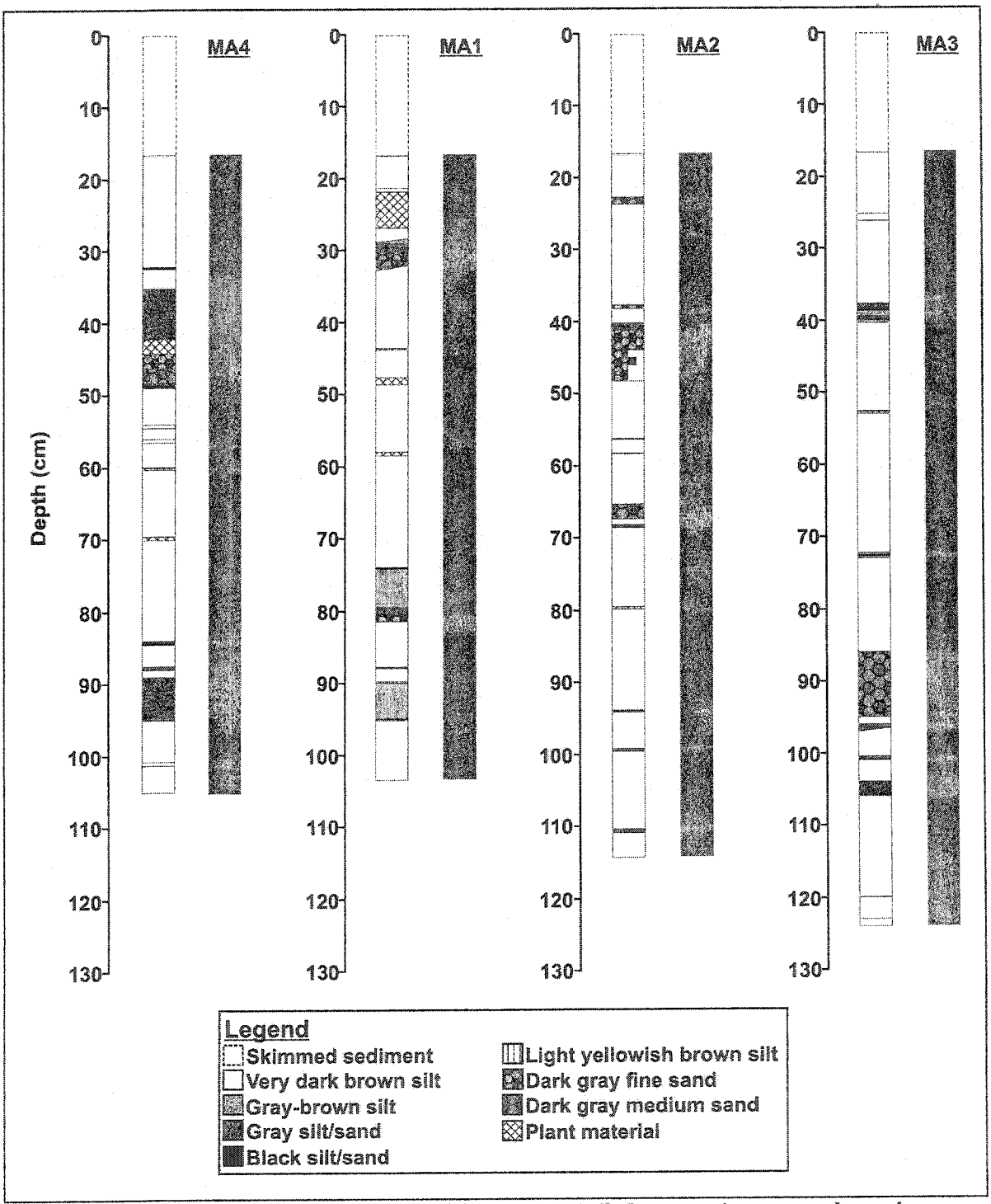

Figure 5.1: Diagrams and x-rays for Mount Aramis Lake cores (cores are shown in order from north to south, which corresponds with greatest to least water depth).

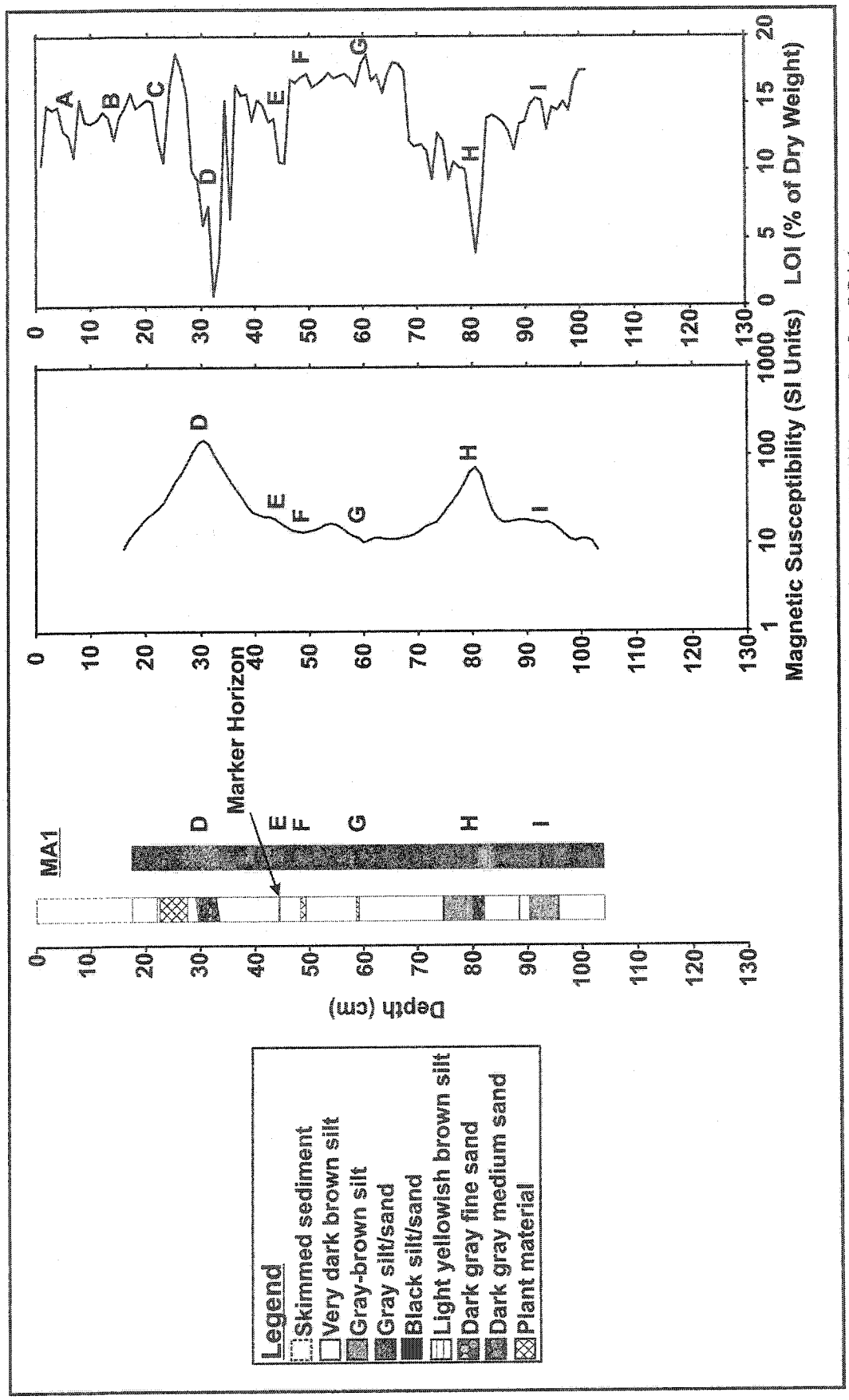

Figure 5.2: Diagram, x-ray, magnetic susceptibility, and LOI graphs for MA1.

depth corresponded to slight decreases in magnetic susceptibility and slight increase in organics but did not register as changes in density (F, G). A second fining upward (medium sand to sandy silt) sediment sequence from 75 to 82 cm depth appeared as a dense layer in the x-ray image of MA1 and as a sharp peak in magnetic susceptibility and a sharp trough in organics (H). A series of layers 0.2 to 5 cm thick, alternating between dark grayish brown and very dark grayish brown silty sand began at 88 cm depth but did not result in significant changes in magnetic susceptibility or organics and changes in density were very faint on the x-ray image (I).

5.2 Core MA2

Most of the sediment in MA2 consisted of homogeneous very dark brown sandy silt (Figure 5.3). There was a significant decrease in organic levels at 5 cm depth (A) and a slight decrease in organic levels at 15 cm depth (B). A 1 cm thick layer of medium sand at 23 cm depth and a 0.5 cm thick layer of fine sand at 38 cm depth corresponded to dense layers in the x-ray image of MA2, decreased organics, and in the former case, to a clear peak in magnetic susceptibility (C, D). The magnetic susceptibility signal from the second sand layer was subsumed by a peak in magnetic susceptibility that corresponded to an 8 cm thick, dense, fining upward (medium sand to sandy silt) sequence of sediment and decreased organics at 40 cm depth (E). Two 0.1 cm thick layers of organic material in very dark brown sandy silt at 57 and 58 cm depth were not visible in the x-ray image of MA2 but both corresponded to low but increasing magnetic susceptibility and slight increases in organics (F, G). A 2 cm thick layer of very dark grayish brown medium sand at 65 cm depth appeared in the x-ray image and corresponded to a peak in magnetic susceptibility that may

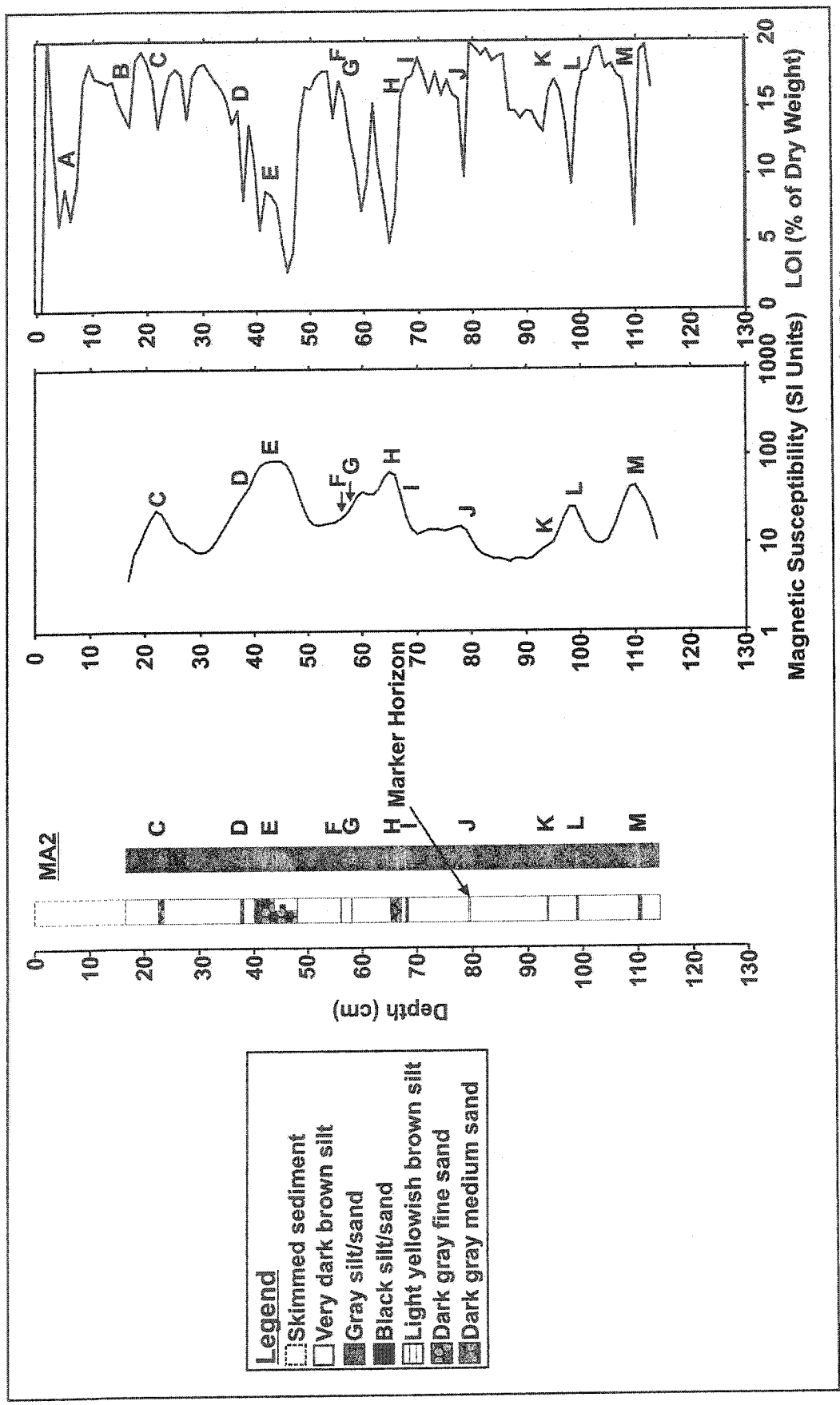

Figure 5.3: Diagram, x-ray, magnetic susceptibility, and LOI graphs for MA2.

have overwhelmed the signal from a 0.4 cm thick layer of dark gray silty sand at 68 cm depth (H, I). The former was also related to a significant decrease in organics while the latter was related to a slight increase in organics. The light yellowish brown layer of sandy silt found in all of the Mount Aramis cores was 0.2 cm thick at 79 cm depth and was represented by a slight increase in magnetic susceptibility, a decrease in organics, and a dense layer in the x-ray image (J). Three layers of dark gray to very dark gray silty sand ranging from 0.3 to 0.6 cm thick were also present at 93, 98, and 110 cm depths and all three corresponded to dense layers visible in the x-ray image, decreased organics, and increases in magnetic susceptibility with the last two related to distinct magnetic susceptibility peaks (K, L, M).

5.3 Core MA3

Most of the sediment in MA3 was very dark brown silt (Figure 5.4). Mean and median values for organics were 12.9% and 14.48% but 16% was the baseline from which the organic values fluctuated downward in abrupt troughs. The first three troughs in organics occurred within the skimmed sediment at 6, 10, and 14 cm depth (A, B, C). A fourth trough in organic levels corresponded to a slightly denser but faint 1 cm thick layer of very dark brown sandy silt at 25 cm (D). A small peak in magnetic susceptibility at this depth was subsumed within the increase resulting from four 0.5 cm thick layers of alternating dark gray and black silty sand at 38 cm depth (E). These layers were also denser than the surrounding silt and corresponded to a decrease in organics. A decrease in organic levels and an increase in magnetic susceptibility marked the 0.3 cm thick, light yellowish brown layer of sandy silt at 53 cm depth which was overlain by a 0.1 cm thick layer of black

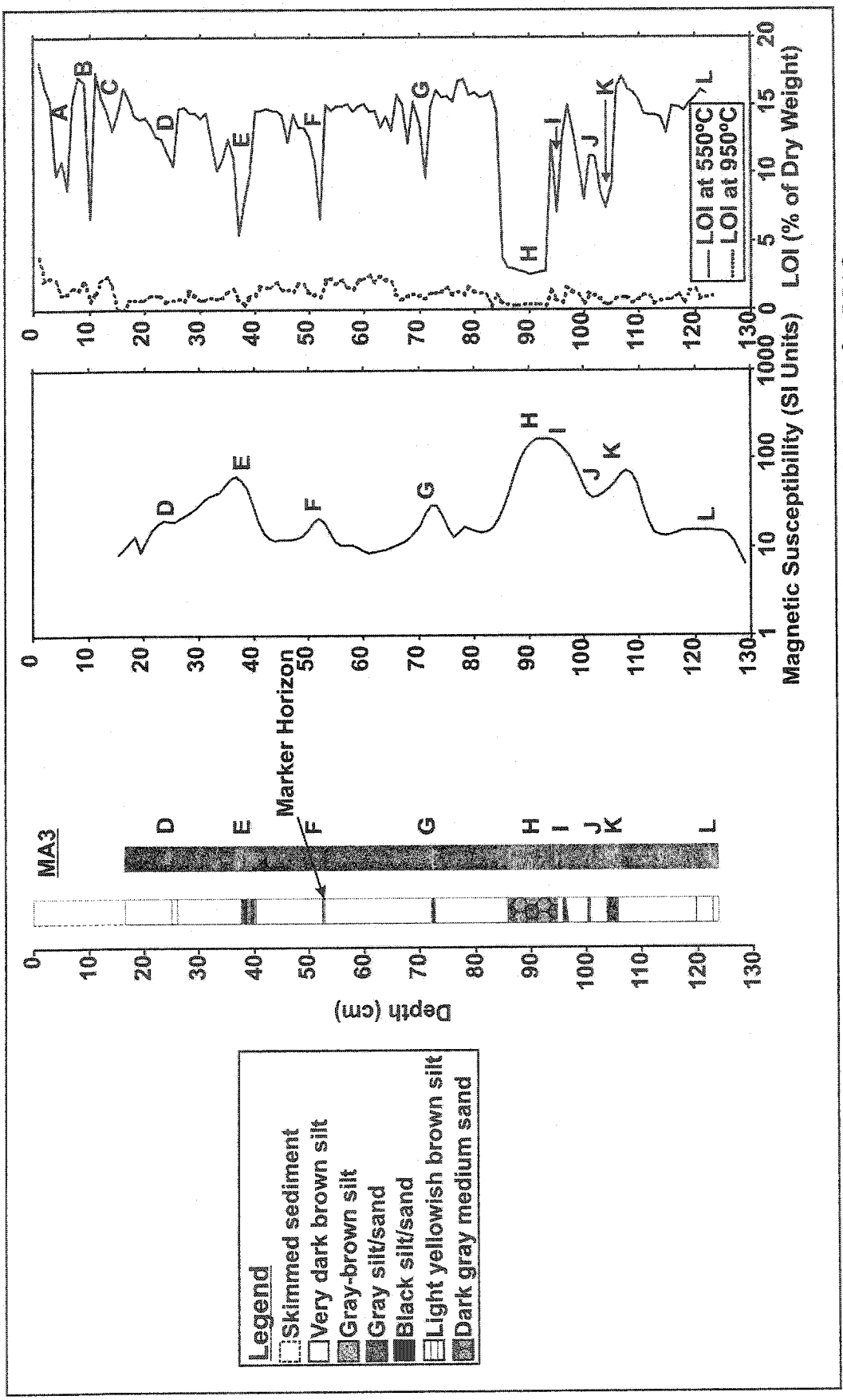

Figure 5.4: Diagram, x-ray, magnetic susceptibility, and LOI graphs for MA3.

sandy silt (F). At 72 cm depth an increase in magnetic susceptibility and a decrease in organics represented three 0.25 cm thick, adjoining bands of dense dark grayish brown and black silty sand (G). A 9 cm thick fining upward (medium sand to fine sand) sequence of sediment from 86 to 95 cm depth corresponded to increases in density and magnetic susceptibility, as well as a significant reduction in organics (H). A 0.75 cm thick layer of dark gray silty sand at 96 cm depth also corresponded with increased density and magnetic susceptibility, and a decrease in organic levels although the signals were partially overwhelmed by those from the thick layer of sand (I). Increased density, a trough in magnetic susceptibility, and a local increase in organics at 101 cm depth represented two layers of 0.25 cm thick gray to very dark gray silty sand (J). At 104 cm depth, a 1.75 cm thick layer of very dark gray silty sand was overlain by a 0.25 cm thick layer of gray silty sand and both were represented by increased magnetic susceptibility and decreased organic levels (K). A faint, 3 cm thick layer of very dark brown sandy silt at 120 cm was visible in the core but did not appear in the x-ray image or the magnetic susceptibility graph but there was a slight increase in organic levels. Although carbonate levels were never greater than 3.90%, they had a well-correlated, positive relationship with organic levels ($R^2 = 0.9487$, p-value < 0.001, $n = 123$).

5.4 Core MA4

MA4 was mainly comprised of homogenous very dark brown sandy silt with median grain-sizes typically between 35 and 40 μm interspersed with discrete layers of coarser and finer sediment (Figure 5.5). Organic levels decreased significantly at 4 and 13 cm depth (A, C) and increased locally at 8 cm depth (B) although there were no significant differences in

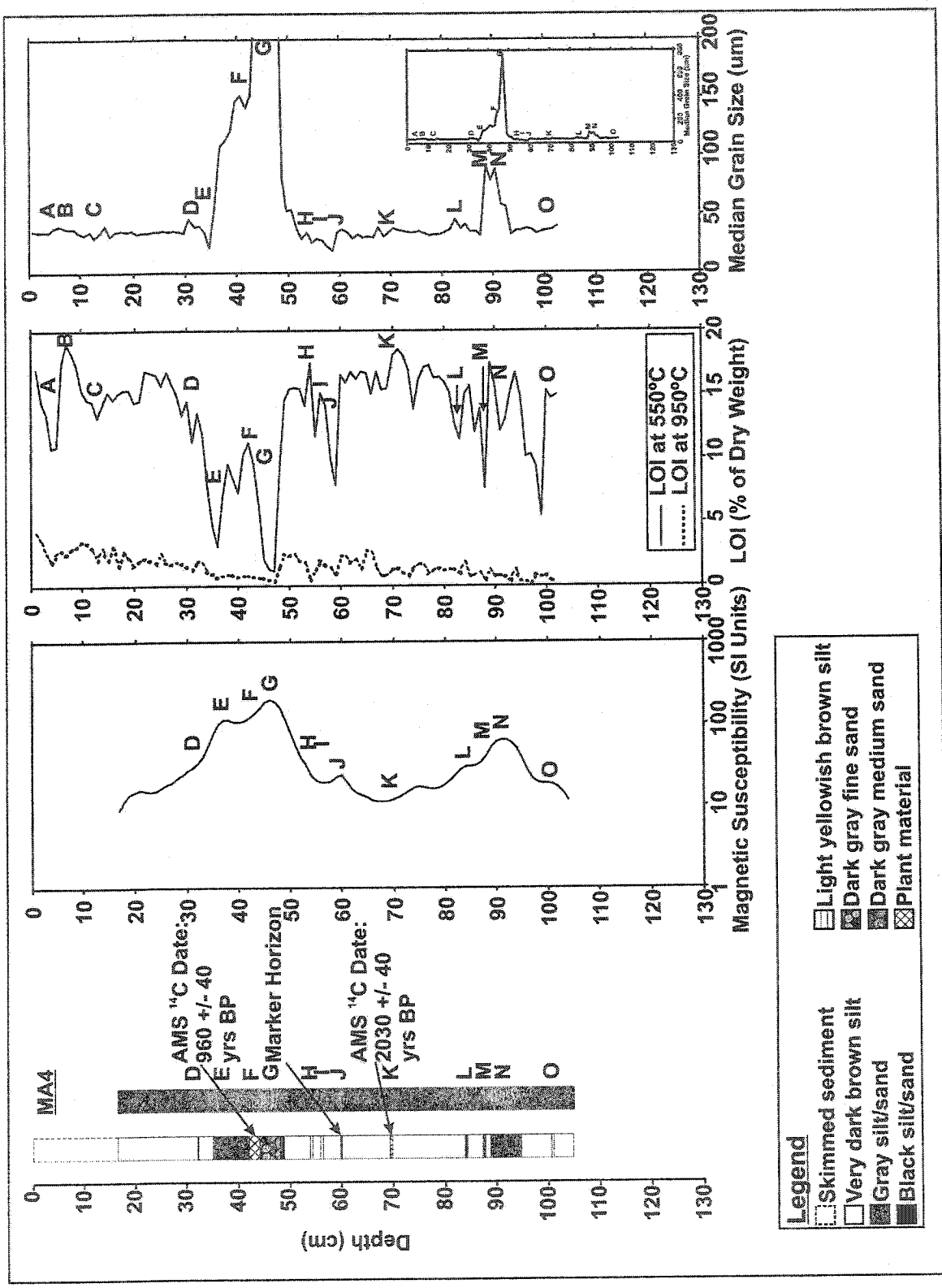

Figure 5.5: Diagram, x-ray, magnetic susceptibility, LOI, and LPSA graphs for MA4.

median grain-size. A 0.25 cm thick layer of black sandy silt at 32 cm depth appeared as a dense layer in the x-ray image of MA4 and corresponded to a decrease in organics and slight increases in median grain-size and magnetic susceptibility (D). The double-peaked increase in magnetic susceptibility that resulted from a fining upward (medium sand to sandy silt) sediment sequence from 35 to 48 cm depth (E, G) probably overwhelmed the magnetic susceptibility signal from the sandy silt layer at 32 cm depth. The dense, fining upward sediment sequence also corresponded to two troughs in organics (E, G) and was immediately underlain by two 0.25 cm thick layers of gray and black sandy silt. A local increase in organics at 44 cm depth correlates with a 2 cm thick layer of organic material immediately above the fine sand layer (F). Two 0.5 cm thick faint layers of very dark brown sandy silt at 54 and 56 cm corresponded with a decrease in magnetic susceptibility, localized increases organic levels, and negligible change in median grain-size (H, I). The light yellowish brown layer of sandy silt was 0.2 cm thick at 60 cm depth, overlain by a 0.1 cm thick layer of black sandy silt, and corresponded to increases in density, magnetic susceptibility, and median grain-size, as well as a decrease in organics (J). An increase in organics corresponded to decreased magnetic susceptibility and median grain-size and was related to a 0.5 cm thick layer of organic material in a matrix of very dark brown sandy silt at 69.5 cm depth (K). Decreased organics at 84 cm depth corresponded with slight increases in magnetic susceptibility and median grain-size as well as a dense 0.25 cm thick layer of black sandy silt (L). Gray to very dark gray layers of dense sand at 88 and 95 cm depth were correlated with increased magnetic susceptibility, decreased organics, and a notable increase in median grain-size (M, N). A 0.5 cm thick faint layer of very dark brown silt at 101 cm depth had no significant magnetic susceptibility, organic, or median grain-size

signature and did not appear as a dense layer in the x-ray image of MA4 (O). As in MA3, carbonate levels fluctuated down-core with a maximum carbonate concentration of 3.70%. The relationship between carbonates and organics was non-significant ($R^2 = 0.3453$, p-value = 0.165, n = 102).

A ternary plot of median grain-sizes clearly shows more variability in MA4 than in TG3 (Figure 5.6). Although most of the samples are classified as sandy silt, they are spread out within this range. The samples at the higher end of the sandy silt classification and in the silty sand range represent the discrete layers mentioned above. Sediment grain-size parameters can also be compared to discriminate between the processes responsible for deposition (Greenwood, 1969). In particular, sorting and skewness can be used to make inferences regarding the kinetic energy (velocity) fluctuations of a geomorphic process and the frequency of those fluctuations respectively. A bivariate plot of sorting *versus* skewness (Figure 5.7) demonstrates that the processes involved in the deposition of these layers may be distinct because many of them can be distinguished from samples from the matrix.

AMS ^{14}C dates from plant material retrieved from 44 and 69 cm depths indicate that the vegetation died at 960 +/- 40 yrs. BP and at 2030 +/- 40 yrs BP respectively (Table 5.1). The organic layer at 44 cm depth is part of the 13 cm thick sediment sequence from 35 to 48 cm underlain by thin layers of sandy silt; therefore, the bottom of this sequence (48.5 cm depth) was deposited no later than 960 +/- 40 yrs BP. Assuming that the dates represent the actual time of deposition, the sedimentation rate between the two dates is 0.18 to 0.21 mm/yr. This implies that the light yellowish brown layer at 60 cm was deposited between 1520 and 1560 yrs BP in all of the cores. However, the assumptions that AMS ^{14}C dates represent the actual time of deposition and that the age-depth relationship is linear may not

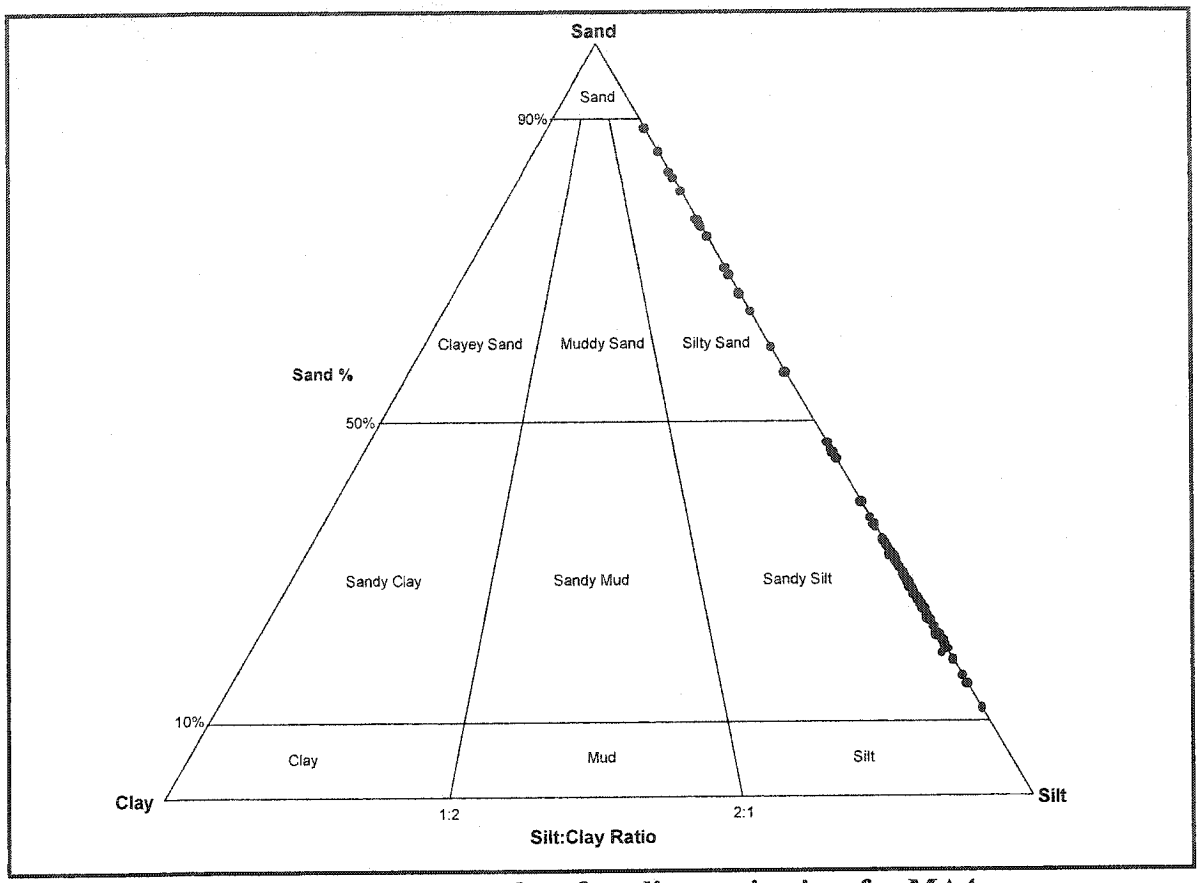

Figure 5.6: Ternary plot of median grain-sizes for MA4.

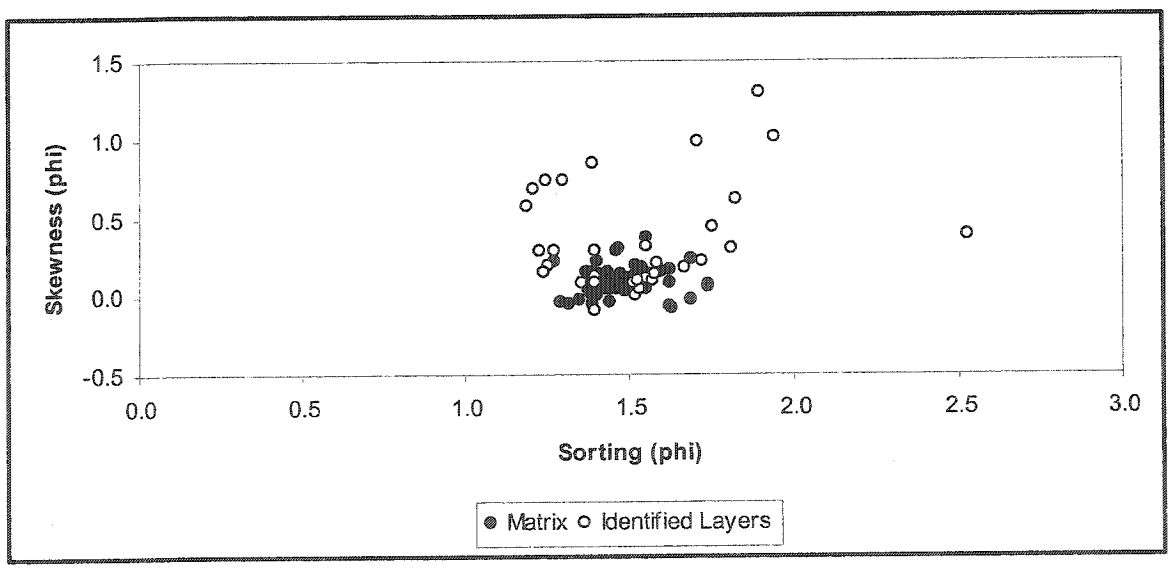

Figure 5.7: Bivariate plot of sediment sorting *versus* skewness for MA4 (sorting and skewness determined using method of moments).

be accurate and the errors associated with this and the dating of the light yellowish brown layer are discussed below in Section 5.12.1: Interpretation of Mount Aramis Lake Cores and Chapter 6: Discussion. Discounting the layers between 35 and 48.5 cm as a near-instantaneous event, the rate of sedimentation for the portion of sediment above 35 cm depth was 0.35 to 0.38 mm/yr. Assuming that the sedimentation rate of 0.18 to 0.21 mm/yr also applies to all of the sediment below 69 cm and discounting the layers between 89 and 95 as a near-instantaneous event, the base of MA4 was deposited at 3595 +/- 40 yrs BP.

Table 5.1: Radiocarbon ages and related data for samples of organic material taken from core MA4 at 44 and 69 cm depth (analysis performed by Beta Analytic Inc.).

Sample Data	Measured Radiocarbon Age	13C/12C Ratio	Conventional Radiocarbon Age
Beta Sample Number: 187645 **Sample:** MA4 44 cm **Analysis:** AMS **Material:** Plant material **Pretreatment:** Acid/alkali/acid **2 Sigma Calibration:** Cal AD 1000 to 1180 (Cal BP 950 to 780)	930 +/- 40 yrs BP	-23.1 o/oo	960 +/- 40 yrs BP
Beta Sample Number: 187646 **Sample:** MA4 69 cm **Analysis:** AMS **Material:** Plant material **Pretreatment:** Acid/alkali/acid **2 Sigma Calibration:** Cal BC 160 to Cal AD 60 (Cal BP 2100 to 1890)	2160 +/- 40 yrs BP	-32.8 o/oo	2030 +/- 40 yrs BP

5.5 Correlation of Mount Aramis Lake Cores

Correlating the cores from Mount Aramis Lake was relatively straightforward because distinct layers were visible in the cores and x-ray images, because there were large variations in magnetic susceptibility, and because a marker horizon was present in all of the cores. A complicating factor, however, was that some cores contained layers that were absent in the others. In Figure 5.8 the diagrams, x-ray images, and magnetic susceptibility graphs for each core have been placed in order from greatest to shallowest depth of collection, which also corresponds with the north to south alignment of the cores.

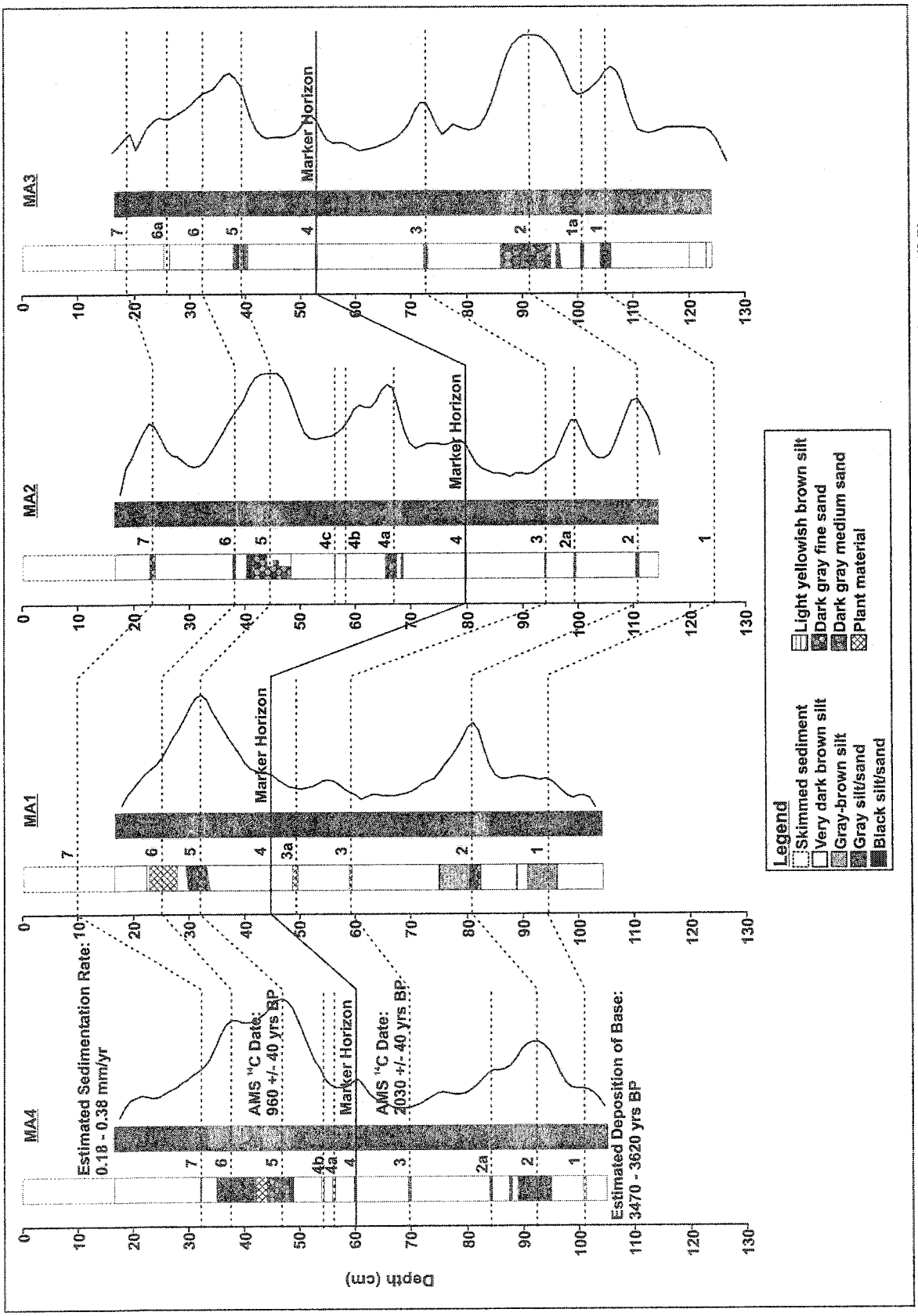

Figure 5.8: Correlation of Mount Aramis Lake cores based on core diagrams, x-rays, and magnetic susceptibility.

Seven correlatable layers were identified in the four cores and were labeled in order of deposition. Ten additional layers that did not appear in all four cores were also identified and labeled by number, and letter (*e.g.* MA3 1a between correlated layers one and two in MA3). Therefore, there are total of seventeen layers in the Mount Aramis Lake cores but only seven of these can be correlated.

Layer 1 corresponded to layers of gray to very dark grayish brown silty sand in MA4, MA1, and MA3 as well as increased magnetic susceptibility and decreased organics for MA3 and MA4. Layer 1 was absent from MA2 because this core is thought to represent the shortest time period of the four cores. Two adjoining layers of sandy silt in MA3 that corresponded to decreased magnetic susceptibility and increased organics were not correlated with layers in the other cores and were labeled MA3 1a. The magnetic susceptibility of all four cores increased for layer 2, which is associated with fining upward sediment sequences in MA1 and MA3 and layers of gray to very dark grayish brown silty sand and sandy silt in MA4 and MA2. Organic levels decreased in all four cores for layer 2. Silty sand layers in MA4 and MA2 were correlated with a decrease in organics and increased magnetic susceptibility and median grain-size and were labeled MA4 2a and MA2 2a respectively. Although these layers have similar characteristics they are probably unrelated given that an additional layer is not found between layers 1 and 2 in MA1, which was collected between MA4 and MA2.

The correlation between the cores for layer 3 was weak because it is related to decreases in magnetic susceptibility for MA4, MA1, and MA2 and an increase in magnetic susceptibility for MA3. Additionally, organic material decreased in MA3 and increased in the other three cores at the projected location of layer 3. However, the correlation of layer 3

was logical based on the sedimentation rates of the individual cores and the presence of organic material layers in MA4 and MA1 and bands of dark gray to black sandy silt in MA2 and MA3. A thin layer of organic material in a sandy silt matrix that corresponded to decreased magnetic susceptibility was found only in MA1 and was labeled MA1 3a.

Layer 4 was identified based simply on the presence of the thin layer of light yellowish brown sandy silt found in all four cores. This layer was particularly important as a marker horizon and was used as a guide for correlation of the other layers. In MA2 a layer of very dark grayish brown medium sand (MA2 4a) corresponded with increased magnetic susceptibility and decreased organics but was not found in the other cores. Two additional layers were found in MA4 (MA4 4a & MA4 4b) and MA2 (MA2 4b & MA2 4c) and although all of them corresponded with low magnetic susceptibility and consisted of organic material in very dark brown sandy silt they are probably unrelated because they are not found in core MA1.

Layer 5 was correlated with a fining upward sequence of sediment in all four cores, coincident with marked increases in magnetic susceptibility and decreases in organic levels. A dramatic increase in median grain-size in MA4 was also evident. Layer 6 corresponded to upper layers of the fining upward sediment sequence associated with layer 5 in MA4, a thick layer of organic material in MA1, a layer of sand in MA2, and a faint layer of very dark brown sandy silt in MA3. A faint layer of dark brown sandy silt found only in MA3 corresponded to slightly increased magnetic susceptibility as well as a decrease in organics and was labeled MA3 6a.

The visible evidence for layer 7 appeared in MA2 as a band of medium sand and in MA4 as a band of black silty sand. Layer 7 correlated with increased magnetic susceptibility in MA4, MA2, and MA3 and a reduction in organics in all four cores.

5.6 Core TG1

Five cores were collected from Three Guardsmen Lake between 7 and 9 July 2003 using the techniques described in Chapter 4: Methods (Figure 5.9). TG1 consisted almost entirely of homogeneous olive brown sandy silt (Figure 5.10). However, at 18 cm depth there was a faint, 1 cm thick layer of small dark grains within the matrix (A). This layer also corresponded with a peak in magnetic susceptibility values. Magnetic susceptibility dropped significantly between 40 and 47 cm depth, but this decrease did not correspond with any layers noted in the core sketch or x-ray image (B). Two 0.2 cm thick layers of dark grayish brown sandy silt were present at 58 and 59 cm depth that corresponded with two dense layers in the x-ray image and a local increase in magnetic susceptibility (C).

5.7 Core TG2

The top two-thirds of TG2 consisted largely of homogeneous olive brown sandy silt with a faint 2 cm thick layer of red grains within the sandy silt matrix at 20 cm depth (B) (Figure 5.11). This layer did not appear in the x-ray image and there was no major variation in magnetic susceptibility values. Apart from a peak in magnetic susceptibility between 13 and 16 cm (A), magnetic susceptibility values slowly decreased down to 58 cm depth (D) with a noticeable drop at 42 cm (C). It is also possible that the C and D are actually related

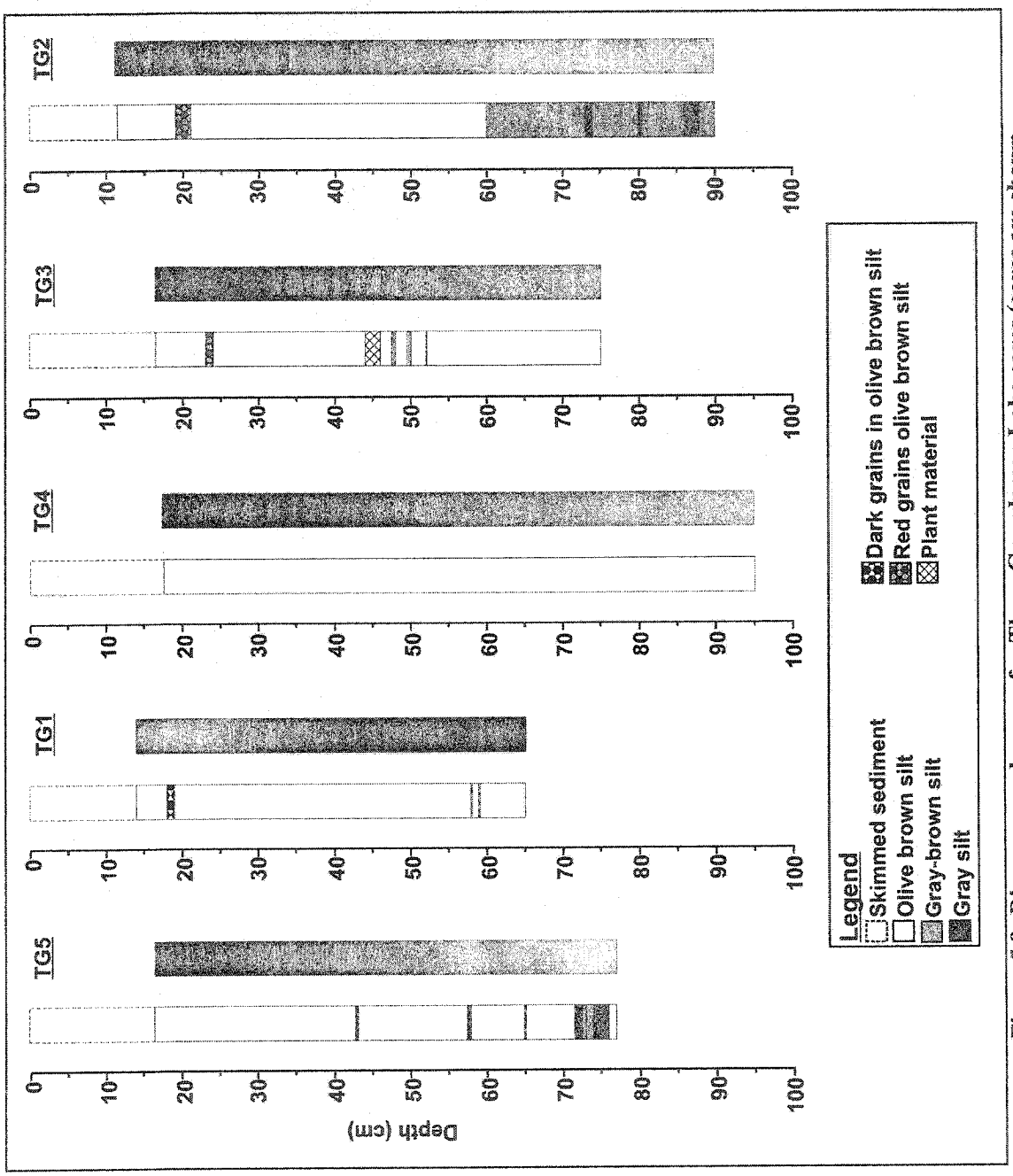

Figure 5.9: Diagrams and x-rays for Three Guardsmen Lake cores (cores are shown in order from north to south, which corresponds with greatest to least water depth).

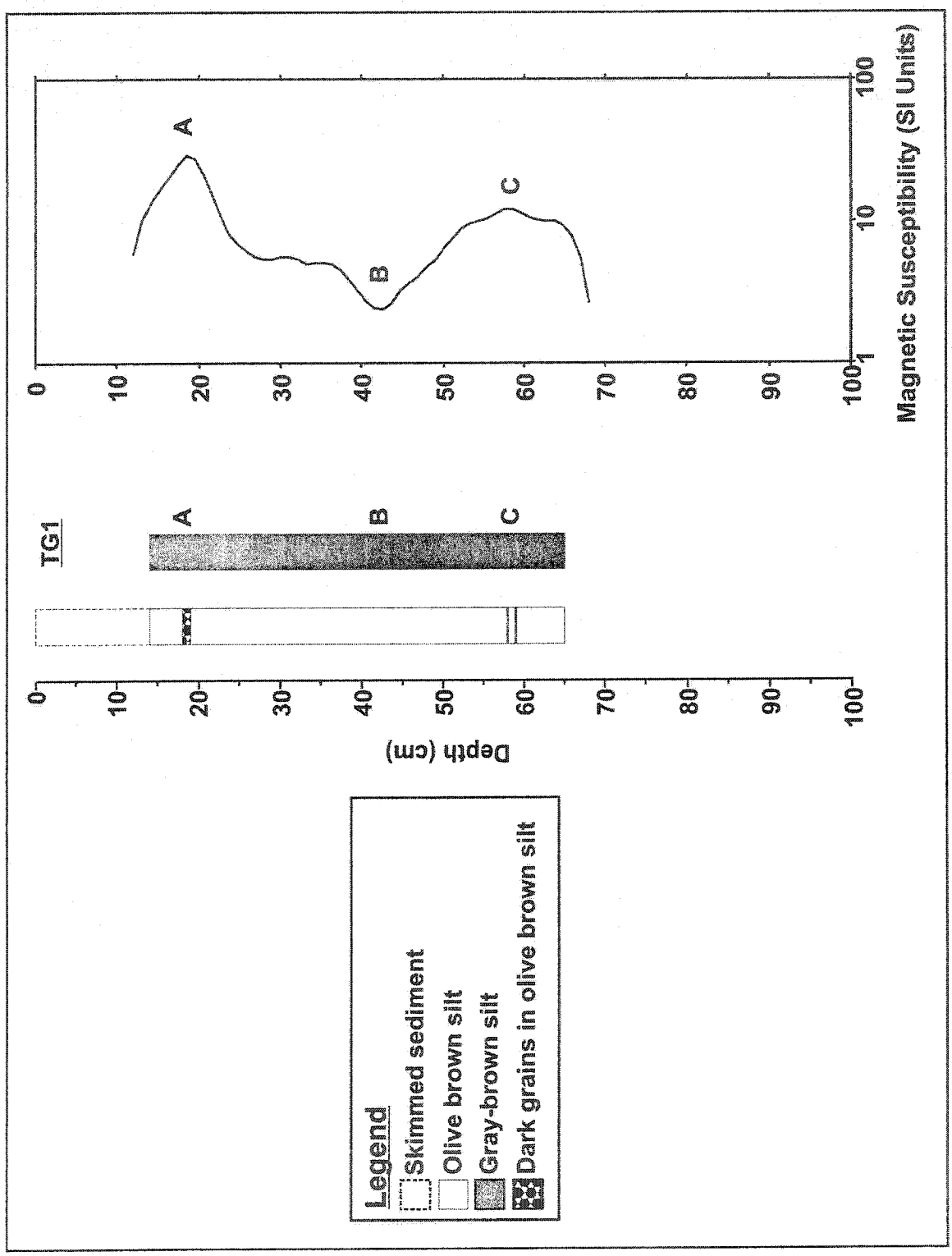

Figure 5.10: Diagram, x-ray, and magnetic susceptibility graph for TG1.

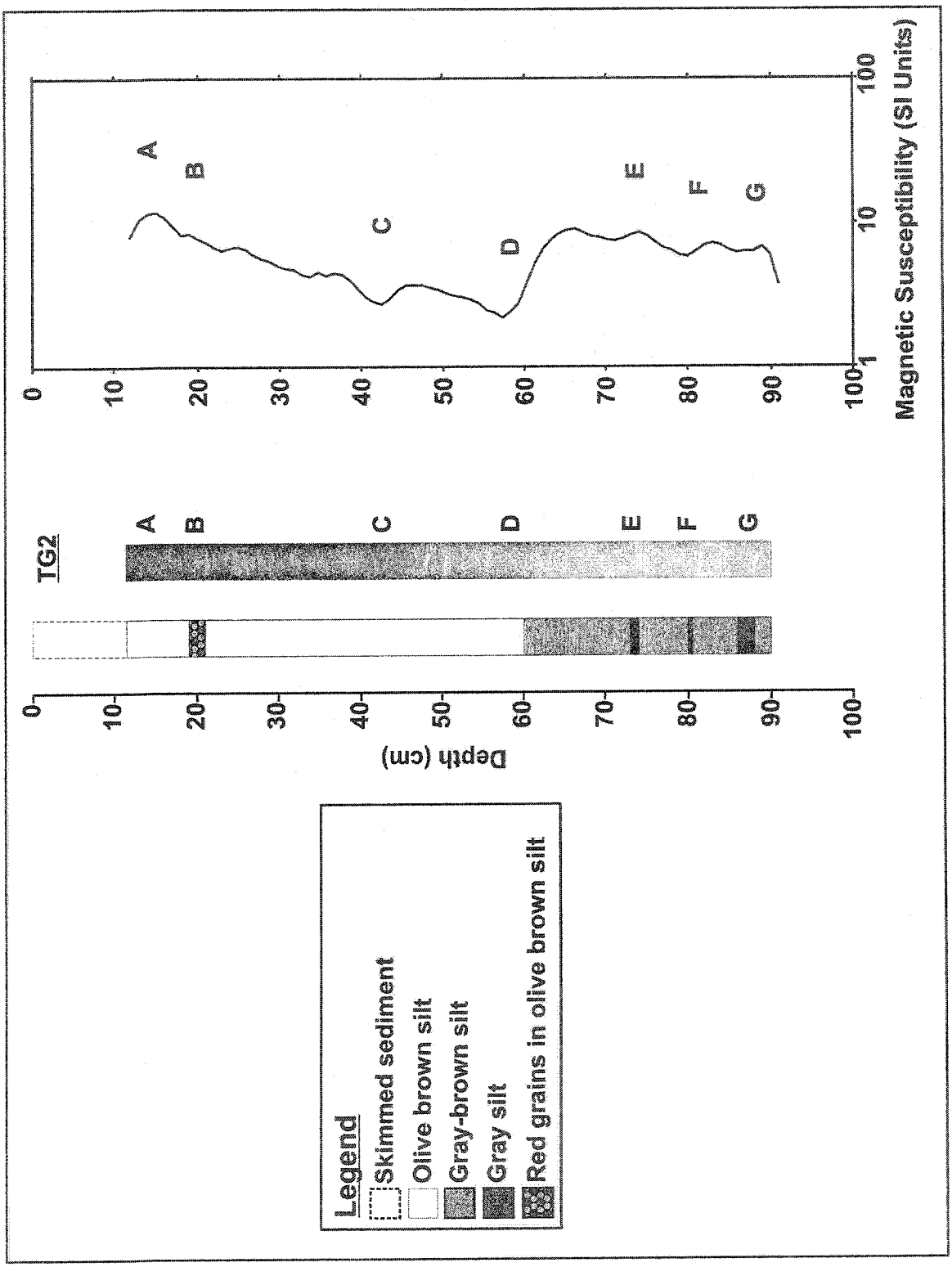

Figure 5.11: Diagram, x-ray, and magnetic susceptibility graph for TG2.

to an increase in magnetic susceptibility at 50 cm depth. None of these increases or decreases had a visible signature in the sketch or x-ray images. Below 60 cm depth, the sediment changed to dark grayish brown sandy silt, which continued to the bottom of the core. This change corresponded with a marked increase in magnetic susceptibility values but there was no change in density based on the x-ray image except for the gradual increase in density with depth. Three grayish layers of sandy silt between 0.5 and 2 cm thick were present in the bottom one-third of the core at 75, 82, and 88 cm (E, F, G). These layers appeared faintly in the x-ray image and registered as slight increases in magnetic susceptibility.

5.8 Core TG3

The majority of the sediment in TG3 was homogeneous olive brown sandy silt with median grain-sizes typically between 25 and 30 μm (Figure 5.12). From 1 to 17 cm depth, organics (based on LOI at 550°C as a percentage of dry weight) decreased down-core with several depressions that corresponded to decreases in median grain-size (A, B, C). Organic levels reached a minimum of 6.4% at 22 cm depth which corresponded to a peak in magnetic susceptibility, a peak in median grain-size, a faint 1 cm thick layer of red grains in a matrix of olive brown sandy silt, and a slightly denser layer in the x-ray image (D). Increased median grain-size at 24, 34, 44, 48, and 59 cm depth corresponded with increased organic values and magnetic susceptibility (E, F, G, H, J). However, the first three (E, F, G) were correlated with an increase in organic levels while the last two (H, J) were correlated with a decrease in organics. E, F, and J were not visible as distinct layers in the core but G and H were associated with a 2 cm thick layer of organic material and 0.5 cm thick layer of

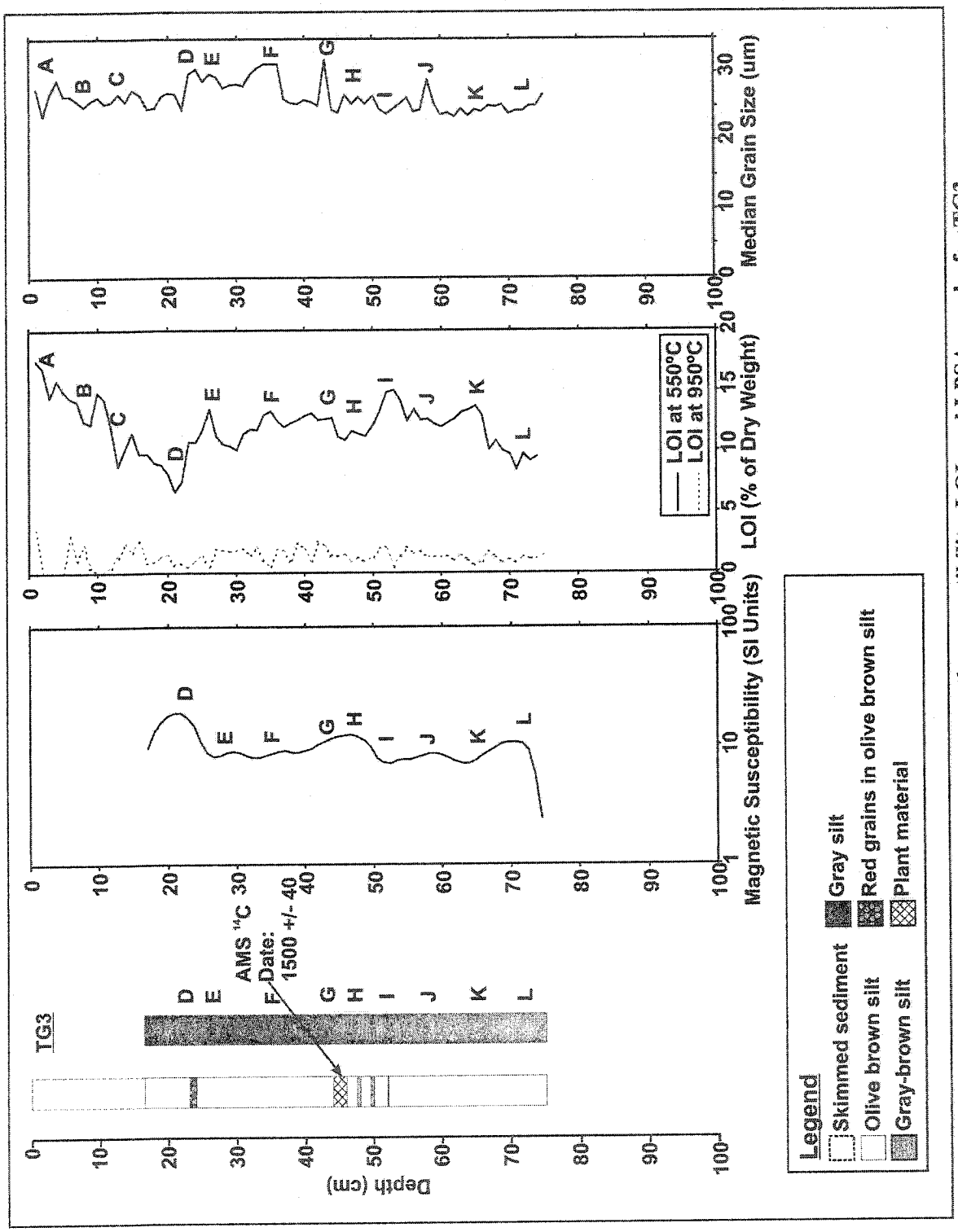

Figure 5.12: Diagram, x-ray, magnetic susceptibility, LOI, and LPSA graphs for TG3.

faint dark grayish brown sandy silt respectively. The signature from H probably subsumed the magnetic susceptibility, organic, and median grain-size signature from an additional 0.5 cm thick layer of faint dark grayish brown silt at 50 cm. A decrease in median grain-size at 53 cm depth was correlated with increased organics, decreased magnetic susceptibility, and a faint 0.5 cm thick layer of dark red silt (I). A decrease in magnetic susceptibility at 65 cm depth, correlated with increased organic levels, did not leave a visible signature in the core or x-ray image (K) and a visible core and x-ray signature for an increase in magnetic susceptibility and decreased organic levels at 74 cm depth was similarly absent (L). Carbonate levels (based on LOI at 950°C values) were never greater than 3.70% and have no relationship with organic levels ($R^2 = 0.0010$, p-value = 0.784, n = 75).

A ternary plot of median grain-sizes demonstrates the homogeneity of the sediment with all of the samples clustered in the sandy silt range and containing negligible amounts of clay (Figure 5.13). A bivariate plot of sorting *versus* skewness (Figure 5.14) further illustrates the uniformity of the sediment in TG3 because samples of the layers identified in the correlation of all of the Three Guardsmen Lake cores are not readily distinguishable from samples of the matrix.

Organic matter at 44 cm depth was AMS ^{14}C-dated at 1500 +/- 40 yrs BP (Table 5.2). If the material was deposited immediately after death, representing a maximum age for this level in the core, the sedimentation rate was 0.29 to 0.30 mm/yr for the last 1500 yrs. Assuming that the rate remained constant throughout the late Holocene, sediments at the base of the core were deposited 2490 to 2625 yrs BP.

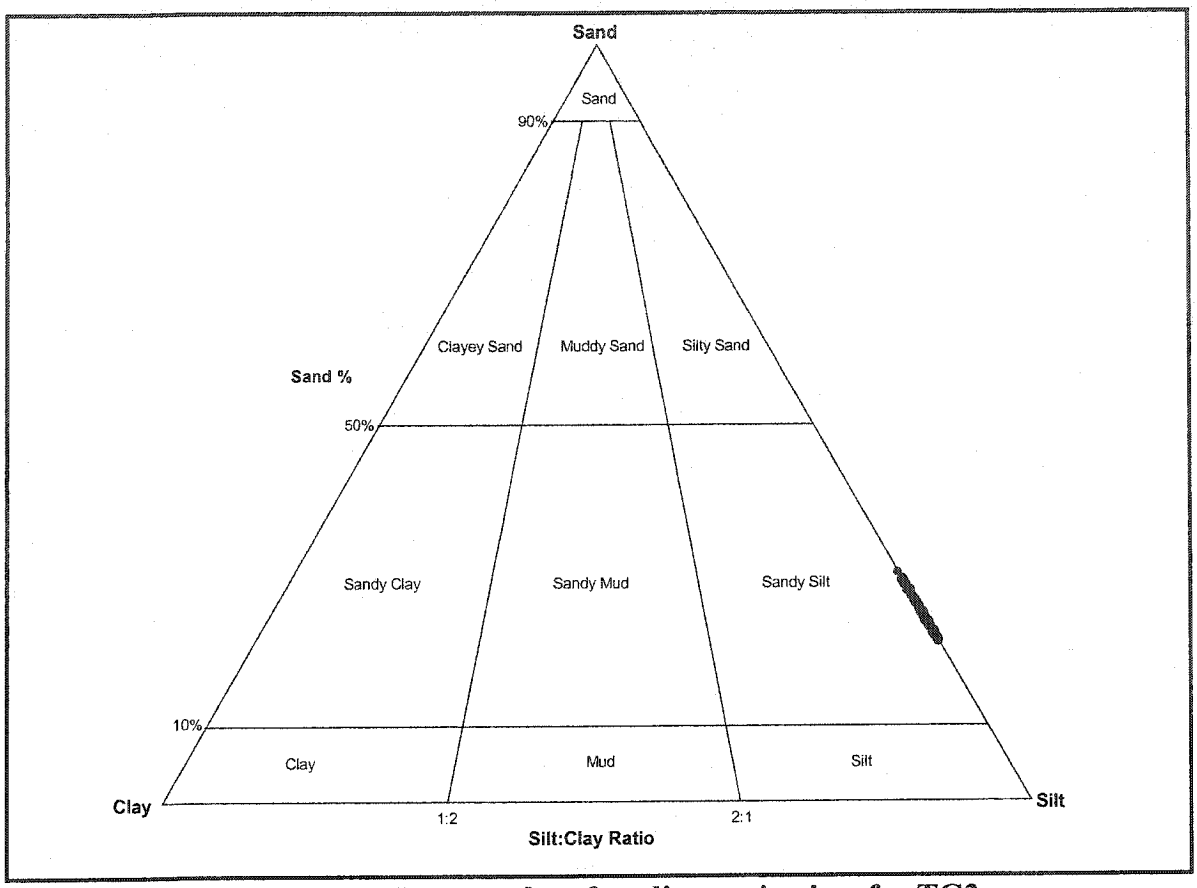

Figure 5.13: Ternary plot of median grain-sizes for TG3.

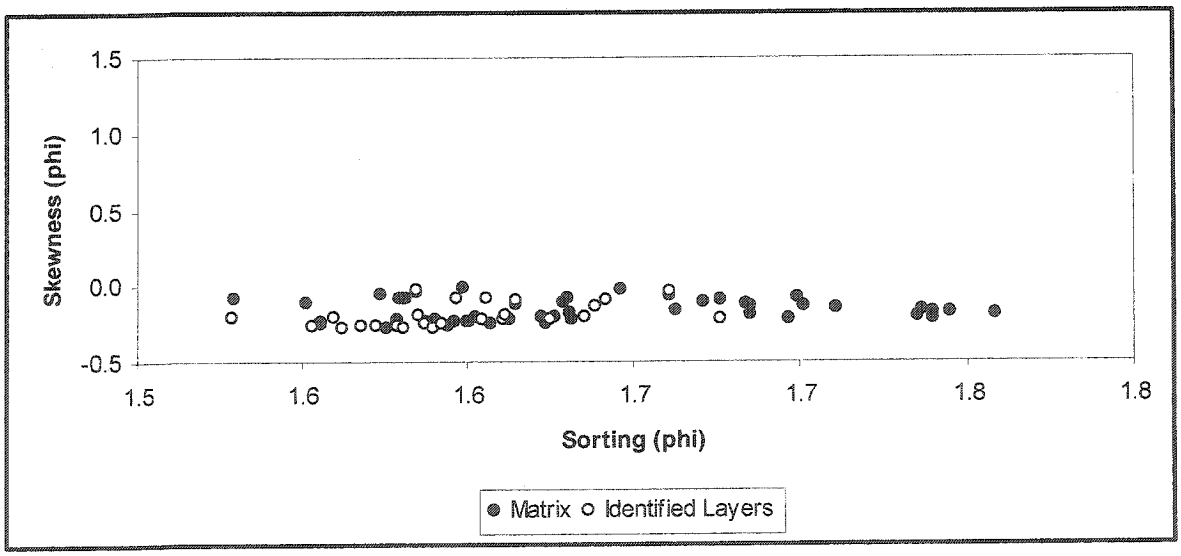

Figure 5.14: Bivariate plot of sediment sorting *versus* skewness for TG3 (sorting and skewness determined using method of moments).

Table 5.2: Radiocarbon ages and related data for a sample of organic material taken from core TG3 at 44 cm depth (analysis performed by Beta Analytic Inc.).

Sample Data	Measured Radiocarbon Age	13C/12C Ratio	Conventional Radiocarbon Age
Beta Sample Number: 187644	1540 +/- 40 yrs BP	-27.7 o/oo	1500 +/- 40 yrs BP
Sample: TG3 44 cm			
Analysis: AMS			
Material: Plant material			
Pretreatment: Acid/alkali/acid			
2 Sigma Calibration: Cal AD 450 to 640 (Cal BP 1500 to 1310)			

5.9 Core TG4

The entire length of TG4 consisted of homogeneous olive brown sandy silt (Figure 5.15). The x-ray image of TG4 was similarly massive with no visible increases in density except for a gradual increase in density with an increase in depth. Magnetic susceptibility values were steady with slight increases at 26, 36, 64, 79, and 95 cm depth (A, B, C, D, F) and a decrease at 83 cm depth (E).

5.10 Core TG5

Most of the sediment in TG5 consisted of homogeneous olive brown sandy silt (Figure 5.16). Organics decreased from a maximum of 25% at 1 cm depth to 12% at 17 cm depth with one increase in organic levels at 7 cm depth (A). A decrease in organics at 18 cm depth was related to a slight peak in magnetic susceptibility but there were no visible signatures in the core diagram or x-ray image (B). A trough in magnetic susceptibility at 28 cm depth was associated with a decrease in organics, but no visible layers in the core diagram or x-ray image (C). Magnetic susceptibility increased from 28 cm depth and steadily rose to a peak at 43 cm depth that corresponded with decreased organic levels, a dense layer on the x-ray image, and a faint, 0.4 cm thick layer of dark grains in the olive brown sandy silt matrix (D). Decreased magnetic susceptibility at 49 and 64 cm depth

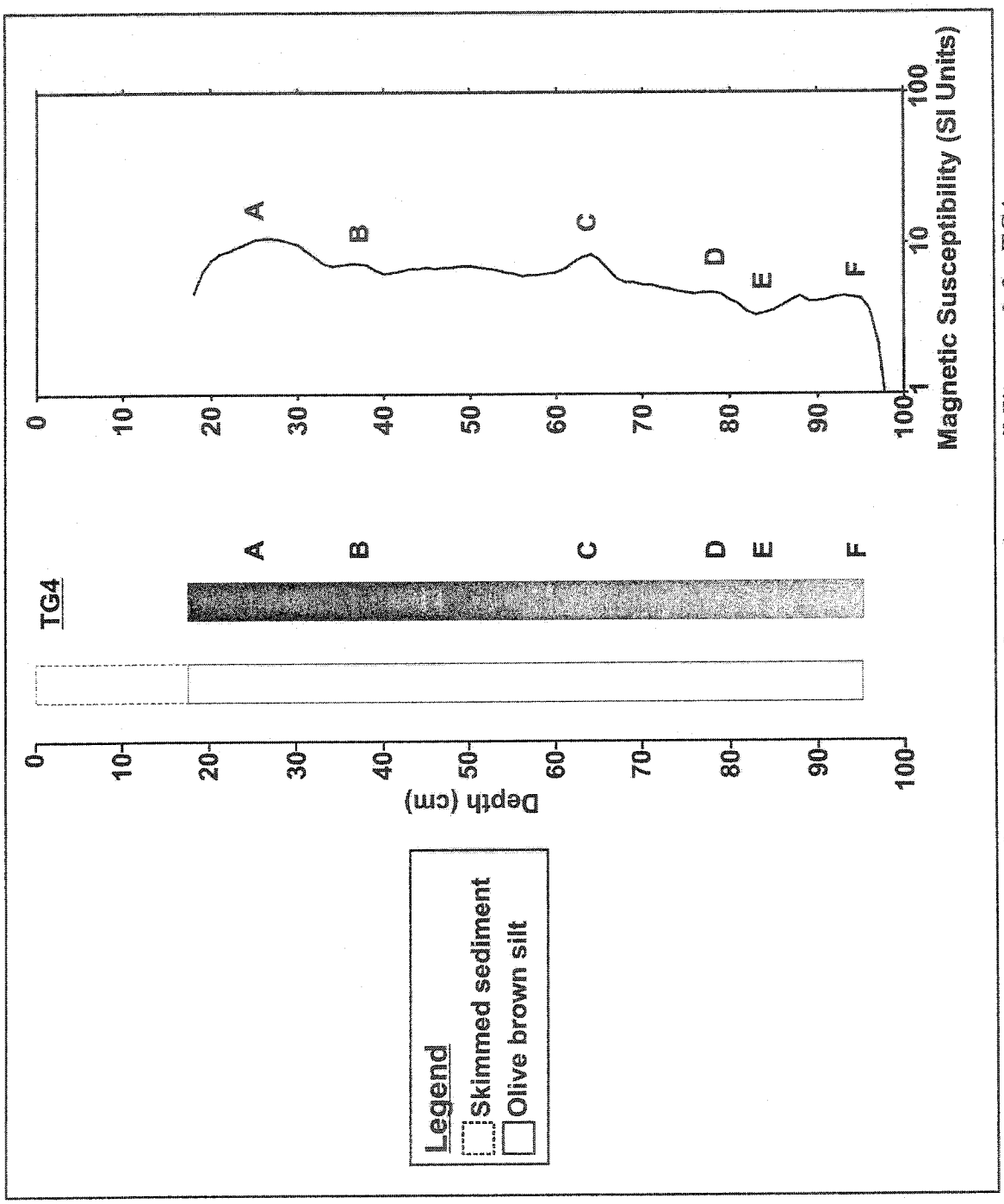

Figure 5.15: Diagram, x-ray, and magnetic susceptibility graph for TG4.

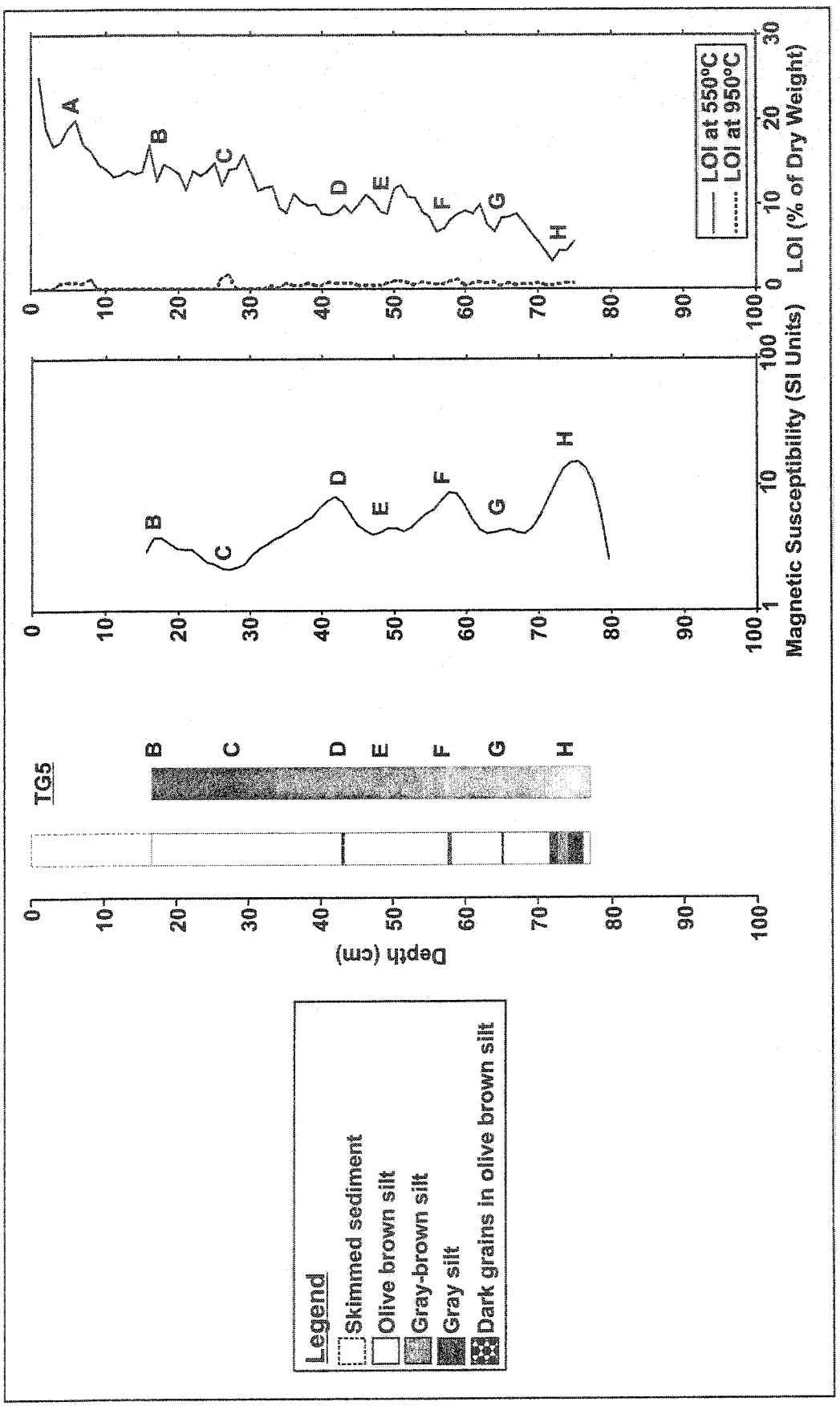

Figure 5.16: Diagram, x-ray, magnetic susceptibility, and LOIgraphs for TG5.

corresponded with decreased organics (E, G). E was not related to any visible layers in the core diagram or x-ray image while G was associated with a dense, 0.2 cm thick layer of dark grains in a matrix of olive brown sandy silt. Peaks in magnetic susceptibility at 57 and 74 cm depth were correlated with a decrease in organics and several dense, 0.5 to 2 cm thick layers of dark gray, very dark gray, and very dark grayish sandy silt (F, H). Carbonate levels fluctuated down-core and like TG3 had a low correlation with organics ($R^2 = 0.0928$, p-value = 0.008, n = 75) and were never greater than 1.70%.

5.11 Correlation of Three Guardsmen Lake Cores

Due to the relatively featureless appearance of the Three Guardsmen Lake cores, correlation of the sediments was very difficult and was largely based on graphs of magnetic susceptibility as well as visible layers in the cores and core x-rays for five reasons. First, visible layers in the cores and core x-rays are reliable, physical evidence that a distinct sedimentation event has occurred. Second, magnetic susceptibility provides information regarding relative differences in concentration, grain-size, and mineralogy of sediments that signal variations in the sediment sources and the balance between allochthonous and autochthonous depositional processes (Chen *et al*, 1999). Third, magnetic susceptibility generally has a well-correlated, negative relationship with organic levels, albeit at a lower resolution, so it does account for changes in organics. Fourth, many researchers have derived sedimentological information from lake cores using magnetic susceptibility (*e.g.* Thompson *et al*, 1980; Dearing, 1983; Dearing, 1986; Creer & Morris, 1996; Chen *et al*, 1999, Brown *et al*, 2002). Five, although useful, fluctuations in organic levels were often unrelated to physical layers in the core diagrams or x-ray images, which suggests that LOI

picks up even minor limnological processes and is therefore, too noisy to be reliable. Given that debris flows are known to be highly effective agents of sediment transfer, it was logical to correlate and interpret the cores based on visible layers and magnetic susceptibility.

In Figure 5.17 the diagrams, x-ray images, and magnetic susceptibility graphs for each core have been placed in order from greatest to shallowest depth of collection, which also corresponds, with the north to south alignment of the cores. Nine corresponding layers and three uncorrelated layers were identified in the five cores and labeled in order of deposition (*i.e.* one to nine from the bottom of the cores to the top). The first three layers were only found near the bottom of TG2 as gray sandy silt with slight increases in magnetic susceptibility. Layer 4 corresponded to increased magnetic susceptibility in TG5, TG4, TG3, and TG2 and decreased organics in TG5 and TG3 as well as layers of dark gray to dark grayish brown sandy silt in TG5. Layer 5 was correlated with decreased magnetic susceptibility in TG5, TG4, TG3, and TG2 and increased organics in TG5 and TG3 as well as a layer of dark grains in TG5 and the boundary between olive brown and dark grayish brown sandy silt in TG2. Layer 6 was associated with dark gray sandy silt in TG5 and increased magnetic susceptibility in TG5, TG4, TG3, and TG2 as well as decreased organics in TG5 and TG3 and increased median grain-size in TG3. Layer 7 was coincident with increased magnetic susceptibility in all five cores, increased grain-size in TG3, decreased organics in TG5 and TG3, and layers of dark grains, grayish brown sandy silt, dark red sandy silt, and organic material.

In TG3 it was difficult to elucidate which of four layers between 43 and 52 cm depth corresponded with layer 7, so all were labeled as being possibly related to layer 7. The same problem was found with two layers in TG1. Given the spacing of the additional layers and

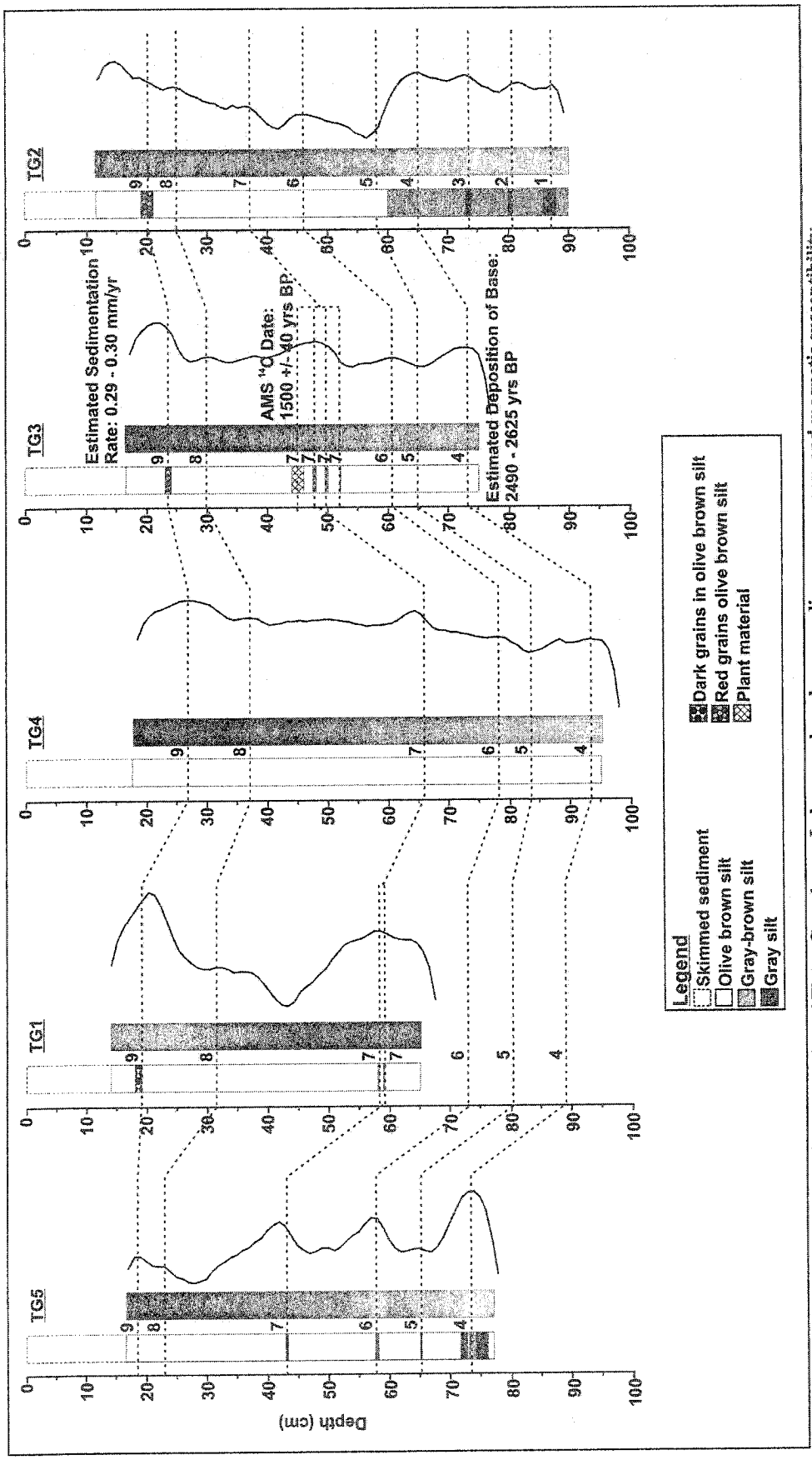

Figure 5.17: Correlation of Three Guardsmen Lake cores based on core diagrams, x-rays, and magnetic susceptibility.

the sedimentation rate in Three Guardsmen Lake, they cannot all be attributed to one event. Layer 8 was identified by a slight increase in magnetic susceptibility in all five cores as well as a decrease in organic levels in TG5 and TG3. Layer 9 was relatively easy to identify based on the layers of dark or red grains found in TG1, TG3, and TG2, increased magnetic susceptibility in all five cores, decreased organic levels in TG5 and TG3, and increased grain-size in TG3. Assuming that the additional layer in TG1 associated with layer 7 is related to one of the additional three layers in TG3, there are a total of twelve layers in the Three Guardsmen Lake cores but only nine of these can be correlated.

5.12 Interpretation of Results

The Mount Aramis Lake cores contained a total of seventeen layers (seven of which could be correlated), calculated to have been deposited over the last 3400 to 3800 yrs (assuming linear age-depth relationships in the cores). The Three Guardsmen Lake cores contained a total of twelve layers (nine of which could be correlated) calculated to have been deposited over the last 3000 to 3500 yrs (assuming linear age-depth relationships in the cores). Since these layers are distinct from the bulk of the sediment in each core they are probably the result of allochthonous sedimentation resulting from geomorphic events. Given the size of the catchments, the presence of channelized debris flows, and the locations of the core collection points at each site, it is reasonable to suggest that the layers are related to geomorphic activity occurring in the debris flow channels. However, association with a debris flow channel does not automatically imply that debris flows were involved in transportation and deposition of the layers. Fluvial activity in the debris flow channels and slushflows may also be responsible for transportation and sub-aqueous deposition of

sediment at both sites. Sub-aqueous mass movements are unlikely to be the cause of any of the deposits given the relatively shallow bathymetry of both lakes. If sub-aqueous mass movements have occurred in either lake, they are probably related to remobilization of recently deposited debris from sub-aerial mass movements.

An attempt is made in this section to infer which geomorphic processes were involved in depositing the layers found in the lacustrine sediment cores from Mount Aramis Lake and Three Guardsmen Lake. Layers characterized by increased grain size, fining upward sediment sequences, increased magnetic susceptibility, and decreased organics are attributed to debris flow activity for the following reasons. First, the deposition of coarse particles on lakebeds requires a process with sufficient energy to transport coarse sediment from a sub-aerial environment to a sub-aqueous environment and debris flows are capable of transporting large amounts of material over a considerable distance in a very short period of time (Kotarba, 1992; Kotarba, 1997; Hartshorn & Lewkowicz, 2000). Second, a fining upward lacustrine sediment sequence is suggestive of large debris flow events that deposit the coarsest sediment first followed by the deposition of finer materials as the sediment plume settles out and rainfall and snowmelt washes finer sediment into the lake (Gottesfeld *et al*, 1991; Fuller, 2002). Rainfall and snowmelt that precedes the initiation of a debris flow may also result in the deposition of thin layers of fine sediment immediately below the deposits. Third, an increase in magnetic susceptibility emphasizes the presence of iron-bearing minerals that are generally derived from erosion of magnetic minerals in the lake catchment and can be transported to the lake by various geomorphic processes including debris flows (Chen *et al*, 1999; Sandgren & Snowball, 2001; Zolitschka *et al*, 2001). Fourth, a decrease in organics is suggestive of debris flows that have transported large

amounts of sediment from unvegetated upper slopes. However, the material transported by debris flows is not limited to mineral sediments and may include plant material entrained during the event or deposited post-event (Fuller, 2002). As a result, an increase in organics may also be indicative of debris flow activity if there is an increase in magnetic susceptibility and/or grain size at the same level or slightly below.

Layers with medium (*i.e.* neither high nor low) magnetic susceptibility, organic content, and median grain-size point to autochthonous sedimentation. The origins of layers possessing a mixture of characteristics are less clear. For example, layers with increased magnetic susceptibility, organic content, and median grain-size and not associated with a fining upward sediment sequence could be attributed to debris flows or to fluvial activity in the debris flow channel. Both debris flows and fluvial events are capable of entraining organic material and sandy material. Unless the layer contains particularly coarse clasts that could have only been transported by a debris flow event, determining which process is responsible is almost impossible. Therefore, when the origins of a layer are unclear more than one possibility will be suggested.

A final point to note before detailed interpretations are presented, is that there are many notable reductions in the organic levels of the Mount Aramis Lake cores and TG3 and TG5 from Three Guardsmen Lake, which based on the criteria detailed above, could be indicative of debris flows. However, as stated above, the fluctuations in organic levels were often unrelated to physical layers or changes in magnetic susceptibility and median grain-size. LOI may in fact be one of the best indicators of allochthonous sedimentation events but without additional evidence of debris flow activity (*e.g.* visible layers, increased magnetic susceptibility and median grain-size) it is impossible to comment on the

geomorphic origins of the reductions in organics. Instead it must be conceded that it is possible that more than twelve geomorphic events and more than seventeen geomorphic events have deposited sediment layers in Three Guardsmen Lake and Mount Aramis Lake respectively.

Since the layers in the Mount Aramis Lake cores were more distinct than the layers in the Three Guardsmen Lake cores, interpretation was easier and presumably more accurate. Therefore, the interpretation for the Mount Aramis Lake cores is presented first in order to clarify the results from Three Guardsmen Lake.

5.12.1 Interpretation of Mount Aramis Lake Cores

At least seventeen sedimentation events occurred in Mount Aramis Lake over the last few thousand years (Figure 5.8). Of these, seven were distinct, correlated layers. Layer 7 was associated with dense sediment, increased magnetic susceptibility, decreased organics in MA4 and MA3, and medium sand in MA2. Based on the criteria stated above, layer 7 was probably deposited by a debris flow, albeit a relatively small one because visible layers are only found in MA4 and MA2. However, fluvial activity in the debris flow channel could also deposit similar sediments and therefore is a possible cause for layer 7. Additionally, gullies on the western side of Mount Aramis Lake may also contribute sediment via fluvial activity although they are heavily vegetated and show no signs of recent geomorphic activity capable of reaching the lake. Deposition of coarse sediments due to fluvial input from the stream entering the southern end of Mount Aramis Lake is unlikely due its small size (50 cm wide with a flow of approximately 1 L/min in summer) and its nearby source in a lake 350 m south that would attenuate any significant flood wave.

Layer MA3 6a is found only in MA3 and is probably related to a debris flow or fluvial activity in the debris flow channel. It is characterized by increased magnetic susceptibility and decreased organics. Given the faint physical signature of layer MA3 6a and its presence at only one core site, it is probably related to a relatively low magnitude geomorphic event.

Layer 6 is associated with increased magnetic susceptibility, decreased organics, and increased median grain-size in MA4. The complication with layer 6 is that in MA4 it appears to be related to the upper layers of the fining upward sediment sequence labeled as layer 5, while it is related to separate layers of plant material and coarse sediment in MA1, sand in MA2, and silt in MA3. Layers 5 and 6 may represent the bottom and top, respectively, of a sediment sequence deposited by a large debris flow. However, the separation of the two layers in MA1, MA2, and MA3 suggests that this scenario is unlikely and that they are the result of two separate geomorphic events. Another possible explanation is that layer 6 is absent from MA4 because it was collected 60 m away from the next closest core (MA1). However, a slight peak in magnetic susceptibility, as well as a vegetation layer between layers 5 and 6 support the suggestion that layer 6 is found in MA4 and that the two layers are indeed from separate events. Layer 6 is probably related to a debris flow event although fluvial activity could also be involved.

Layer 5 was almost definitely deposited by a large debris flow event, as it is associated with thick fining upward sediment sequences and increased magnetic susceptibility, decreased organics, and a significant increase in median grain-size in MA4. All of these characteristics are suggestive of a high-energy debris flow that deposited coarse sediment, which was overlain by finer sediment that settled out from a plume following the

event or was washed into the lake by subsequent rainfall or snowmelt. It is unlikely that fluvial activity in the debris flow channel would be capable of transporting such a large volume of coarse sediment more than 80 m out into Mount Aramis Lake.

Layers MA4 4a, MA4 4b, MA2 4b, and MA2 4b were all characterized by decreased magnetic susceptibility and increased organic levels, and hence are probably not related to debris flow activity. They are probably the result of organic material washed into the lake from the debris flow channel or the gullies on the western side of the valley by fluvial activity. Despite their similar characteristics, these four layers cannot be cross-correlated because they are not found in MA1, which was collected between MA4 and MA2. Layer MA2 4a is another uncorrelated layer found only in MA2 but it is associated with increased magnetic susceptibility, decreased organics, and a dense layer of sand. Since layer MA2 4a is absent from the other cores but it possesses several characteristics of debris flow activity it was probably deposited by a debris flow of narrow extent, similar to the one that is thought to have deposited layer 7. As with layer 7, however, fluvial activity from either side of the lake cannot be ruled out entirely.

As noted previously, layer 4 proved very useful as a marker horizon due to its distinctive light yellowish brown colouring and its presence in all four Mount Aramis Lake cores. Initially it was thought to be a signature from the eastern lobe of the White River Ash deposited 1147 yrs BP following the volcanic eruption of Mount Churchill, Alaska (Clague *et al*, 1995; Doig, 1998). According to Turney and Lowe (2001), ash from ryholitic materials is often light in colour and the White River Ash is known to be a ryhodacite composed of glass, andesine, hornblende, hypersthene, and magnetite (Lerbekmo & Campbell, 1969). When compared with slide samples of sediment known to be White River

Ash from Silver City and Kluane Wilderness Village, Yukon Territory, layer 4 was similar in colour but much finer in texture. Horizon thickness and grain-size generally decrease with increasing distance from the source (Pyle, 1989; Sparks *et al*, 1992). Mount Aramis Lake is 50 km further away from the origin of the White River Ash than Silver City and Kluane Wilderness Village and is 420 m higher. Therefore, it is logical that if the White River Ash reached Mount Aramis it would be finer in texture than samples collected at Silver City and Kluane Wilderness Village.

However, linear interpolation between AMS ^{14}C dates collected at 44 cm and 69 cm in MA4 suggests that layer 4 was deposited between 1520 and 1600 yrs BP, which would eliminate the possibility of it being the White River Ash. This would be the case even though Beierle and Bond (2002) found in Doal Lake, Yukon Territory that White River Ash migrated downward through low-density, organic lake sediments and created tephra layers at stratum dated at approximately 10,000 yrs BP. When tephra with a relatively high density is rapidly deposited above relatively low-density gyttja, the inverted density gradient may allow vertical penetration of the tephra until it reaches a layer with sufficient density to stop it. The sandy silt forming the majority of the sediment in the Mount Aramis Lake cores was actually quite dense and organic levels were not particularly high so it is improbable that tephra could have migrated any great distance. However, as discussed previously, the assumption of a linear age-depth relationship may be inaccurate and since layer 4 is in close to the appropriate location for White River Ash there is a reasonable chance that it is this tephra layer.

A microscopic examination of layer 4 revealed that it was not significantly different sedimentologically from samples in other parts of the cores and a preliminary examination

of this layer by Dr. T. Fowler (Department of Earth Sciences, University of Ottawa) was inconclusive. However, if layer 4 is not White River Ash then where did it come from? Doig (1998) has noted that the settling of lake sediments in resuspension due to seismic activity may result in significant changes in colour. Following seismic resuspension of lake sediments, the silicate fraction settles relatively quickly to form a chalky white or beige layer of silt overlain by organic material. Layer 4 matches this description and the location of Mount Aramis Lake between the active Denali and Tintina Faults suggests that it may experience seismic events.

Therefore, layer 4 may be evidence of a seismic event or it may be the White River Ash. X-ray Diffraction (XRD) and X-ray Fluorescence (XRF) techniques are currently (June 2004) being undertaken in an attempt to elucidate the mineral and chemical content of layer 4. However, the results are not yet available, so in this thesis, layer 4 is used strictly as a marker horizon. The effect of it being White River Ash, if that is the outcome of the current investigations, is discussed in Chapter 6.

Layer MA1 3a was only found in MA1 and was similar to layers 4c and 4b in that it was associated with decreased magnetic susceptibility as well as organic material in a sandy silt matrix. Therefore, layer MA1 3a was probably deposited by fluvial activity in the debris flow channel or from the gullies west of Mount Aramis Lake.

Interpretation of layer 3 was difficult because of conflicting characteristics between the cores. Magnetic susceptibility decreased in MA4, MA1, and MA2 and increased in MA3. Organic levels decreased in MA3 in increased in the other three cores. However, the correlation of layer 3 was logical based on the sedimentation rates of the individual cores and the presence of organic material layers in MA4 and MA1 and bands of sandy silt in

MA2 and MA3. One possible explanation is that the layer in MA3 is from a debris flow that did not leave a signature in the other three cores, while the layers found in MA4, MA1, and MA2 were deposited by fluvial activity that did not leave a signature in MA3. A second possibility is that a low magnitude debris flow deposited coarse material near the location of MA3 and the organic material found in MA4 and MA1 was washed into the lake by rainfall or snowmelt post-event. The third, and possibly best, explanation for layer 3 is that it is the result of fluvial activity in the gullies on the western side of Mount Aramis Lake. Although there is no evidence of recent activity in these gullies, aerial photographs suggest that Mount Aramis Lake may have been separated from the lake south of it by deposition of alluvial fans at the base of the gullies (see Figure 3.9). A large fluvial event from one of these gullies centered on the location of MA3 could have deposited coarse material at that position, while finer sediment and organic material took longer to settle and were transported northwards into the deeper parts of the lake.

Layers MA4 4 2a and MA2 2a were found in MA4 and MA2 as layers of silty sand with increased magnetic susceptibility, decreased organics in MA4, and increased median grain-size in MA4. Therefore, these layers are probably debris flow deposits although fluvial activity in the debris flow channel or the gullies west of the lake could also be involved. If these layers were related a similar layer should be present between layers 1 and 2 in MA1. However, no such layer exists and MA4 2a and MA2 2a probably represent two separate debris flow events.

Fining upward sediment sequences in MA1 and MA3, increased magnetic susceptibility, decreased organics, and a notable increase in median grain-size in MA4 are strong indications that layer 2 was deposited by a debris flow. Since the signal of this event

is strongest in MA3 it is likely that the debris flow was directed across the southern portion of the debris flow fan. Conversely, the signals for layers 5 and 6 are weakest in MA3 and strongest in MA4, which suggests that those debris flows were directed across the northern portion of the debris flow fan. When all four cores and their locations are taken into consideration it is likely that over time, the Mount Aramis debris flow channel has migrated northwards across the fan towards the deepest sections of Mount Aramis Lake.

Layer MA3 1a was only present in MA3 as two adjoining layers of sandy silt associated with decreased magnetic susceptibility and increased organic levels. Based on the criteria stated at the beginning of this section layer MA3 1a is probably not a debris flow. Layer MA3 1a was likely the result of fluvial activity in the debris flow channel or from the gullies on the western side of Mount Aramis Lake that carried in debris with high organic content.

Layer 1 was absent from MA2 because this core represents the shortest time period of the four cores, but it was associated with increased magnetic susceptibility in the other three cores (particularly MA3), reduced organics, and layers of silty sand. These characteristics indicate that layer 1 is probably a debris flow deposit although fluvial activity in the debris flow channel cannot be discounted. It is notable that the peak in magnetic susceptibility related to this layer is best-developed in MA3, towards the southern end of the core transect, which further supports the idea that the debris flow channel has shifted northwards over the last 3800 years.

In summary, two of the seventeen layers in the Mount Aramis Lake cores are *definitely* debris flow deposits (layers 5 & 2), seven are *probably* debris flow deposits (layers 7, MA3 6a, 6, MA2 4a, MA4 2a, MA2 2a, & 1), seven are *probably* related to fluvial

activity (layers MA4 4b, MA4 4a, MA2 4c, MA2 4b, MA1 3a, 3, & MA3 1a), and one is due to seismic or volcanic activity (layer 4).

5.12.2 Interpretation of Three Guardsmen Lake Cores

At least twelve sedimentation events occurred in Three Guardsmen Lake over the last 3000 to 3500 years. Of these, nine could be correlated between the cores. As noted previously, correlation of the Three Guardsmen Lake cores was difficult because the visible layers in the cores and x-ray images were faint, as were the signals in the organic/carbonate levels and median grain-size. Consequently, although the layers may exhibit characteristics of debris flows or fluvial activity, the interpretation lacks certainty. Furthermore, the ternary diagram of median grain-size and bivariate plot of sorting *versus* skewness for TG3 demonstrate that samples down-core are remarkably similar which suggests that the matrix and the identified layers are the result of similar depositional processes.

Layer 9 was associated with increased magnetic susceptibility in all five cores, decreased organics in TG5 and TG3, increased median grain-size in TG3, and layers of dark or red grains in TG1, TG3, and TG2 (Figure 5.17). Above layer 9 there is an increase in organics in TG5 and TG3. This sequence is indicative of rapid deposition of relatively coarse sediment from the unvegetated upper slopes of Three Guardsmen Mountain during the initial stages of a debris flow, followed by organic material and finer sediment settling out and/or being washed into the lake by subsequent rainfall or snowmelt. Therefore, layer 9 was probably deposited by a debris flow event.

Layer 8 was not related to any visible evidence in the cores but did correspond to slightly increased magnetic susceptibility in all five cores, decreased organics in TG5 and

TG3. There was no change in median grain-size in TG3. The increase in magnetic susceptibility and decrease in organics suggest that layer 8 is the result of allochthonous deposition by a debris flow or fluvial activity in the debris flow channel. Immediately above layer 8, organics increased in TG3 and TG5, which is similar to the debris flow scenario described for layer 9 so it is probable that layer 8 is the faint signature of a debris flow.

Increased magnetic susceptibility, decreased organics in TG5 and TG3, increased median grain-size in TG3, and layers of dark grains, grayish brown sandy silt, dark red sandy silt, and organic material suggest that layer 7 is probably a debris flow deposit. Two layers in TG1 and four layers in TG3 are associated with layer 7. The uppermost of these layers in TG3 is probably a debris flow deposit because it corresponds with an increase in magnetic susceptibility and median grain-size. However, it is also associated with a band of vegetative material, which does not rule out the possibility of a debris flow but does indicate that fluvial activity may have been involved. The two middle layers in TG3 are probably debris flows because they correspond with increased magnetic susceptibility and median grain-size. The bottommost of these layers in TG3 is probably not a debris flow because it corresponds with a decrease in magnetic susceptibility and an increase in organics, which is suggestive of autochthonous depositional processes.

Layers 4 and 6 were probably deposited by debris flows because of increased magnetic susceptibility, decreased organics in TG5 and TG3, and increased median grain-size in TG3. Of course fluvial activity in the debris flow channel could also be responsible but debris flows are more likely to transport coarse sediment out into the lake. In contrast, layer 5 is probably the result of a change in autochthonous depositional processes as it is associated with a decrease in magnetic susceptibility, increased organics in TG5 and TG3, as

well as a layer of dark grains in TG5 and the boundary between olive brown and dark grayish brown sandy silt in TG2.

Layers 1, 2, and 3 were only found in TG2, which is thought to represent the longest time period. This paucity of data makes any suggestions regarding their origin purely speculative. However, all three are characterized by increased magnetic susceptibility and layers of gray sandy silt. Therefore, they were probably deposited by debris flows or fluvial activity in the debris flow channel.

In summary, ten of the twelve layers in the Three Guardsmen Lake cores are *probably* debris flow deposits (layers 9, 8, top three layers associated with layer 7, 6, 4, 3, 2, & 1) although fluvial activity may have been involved. The remaining two layers (bottom layer associated with layer 7 & layer 5) are *probably* the result of changes in autochthonous depositional processes.

6. Discussion

Lacustrine sediment cores from Mount Aramis Lake contained seventeen distinct layers, nine of which were interpreted as debris flow signatures over the last 3400 to 3800 yrs (*i.e.* one debris flow every 378 to 422 yrs based on linear age-depth relationships in the cores). Cores from Three Guardsmen Mountain contained twelve distinct layers, ten of which were inferred to be debris flow signatures over the last 3000 to 3500 yrs (*i.e.* one every 300 to 350 yrs based on linear age-depth relationships in the cores). These debris flow return intervals are longer than those calculated by other researchers working in the southern Yukon Territory. Harris and McDermid (1998) found that debris flows on Sheep Mountain at the southern end of Kluane Lake (61°25'N, 138°72'W) had a return interval of 150 yrs. Lowey (2002) estimated that catastrophic flooding related to debris flow activity occurs on the Kusawa Lake (60°35'N, 136°37'W) torrent system approximately once every 200 years.

The lower debris flow frequency at Mount Aramis is not surprising given that it is further inland than Kluane and Kusawa Lakes so there is less moisture available to initiate debris flow activity. The vegetated slopes, lichenized debris flow features, and large debris flow channel at Mount Aramis are indicative of a high magnitude, low frequency debris flow regime. Debris flow frequency is also partially controlled by debris supply, which is influenced by site-specific conditions such as lithology, stratigraphy, ruggedness, and slope gradient (Bovis & Jakob, 1999). Sheep Mountain and the torrent catchment at Kusawa Lake both have greater local relief and steeper slopes than Mount Aramis, as well as local differences in stratigraphy and terrain stability, hence shorter debris flow return intervals are not surprising. The possibility also exists that Harris and McDermid (1998) and Lowey

(2002) miscalculated the debris flow return interval at their sites by basing their calculations on terrestrial debris flow features altered by subsequent events.

Conversely, the debris flow return interval calculated for Mount Aramis may be an overestimation for two reasons. First, small magnitude debris flows may not penetrate far enough into the lake to leave a deposit and very small ones may not reach the lake at all. Second, as noted in the previous chapter, there is strong physical evidence supporting the interpretation that nine of the seventeen identified layers in the Mount Aramis Lake sediment are debris flows but decreases in organics may also be indicative of more than nine debris flow events over the past 3400 to 3800 yrs at Mount Aramis. However, these could not be confirmed because there is no additional evidence (visible layers in the cores, x-ray images, increased magnetic susceptibility, increased grain size) to suggest that they are related to debris flows and not some other geomorphic activity. Therefore, the debris flow return intervals calculated for Mount Aramis probably represent a maximum return interval based on accurate identification of the minimum number of events recorded in lacustrine sediments.

Furthermore, the assumption of a linear age-depth relationship between AMS ^{14}C dates in MA4 and the supposed deposition of the plant material subjected to radiocarbon dating immediately after death meant that the origin of layer 4 in the Mount Aramis Lake cores could not be conclusively identified. In Figure 6.1, age-depth curves illustrate that if layer 4 *is* White River Ash (deposited 1147 yrs BP) the lacustrine sediment record extends back to 4800 to 5200 yrs BP with a corresponding increase in the debris flow return interval at Mount Aramis. Additionally, the slope of the age-depth curve changes over time if layer 4 is White River Ash, which may be indicative of changes in sedimentation rates in Mount

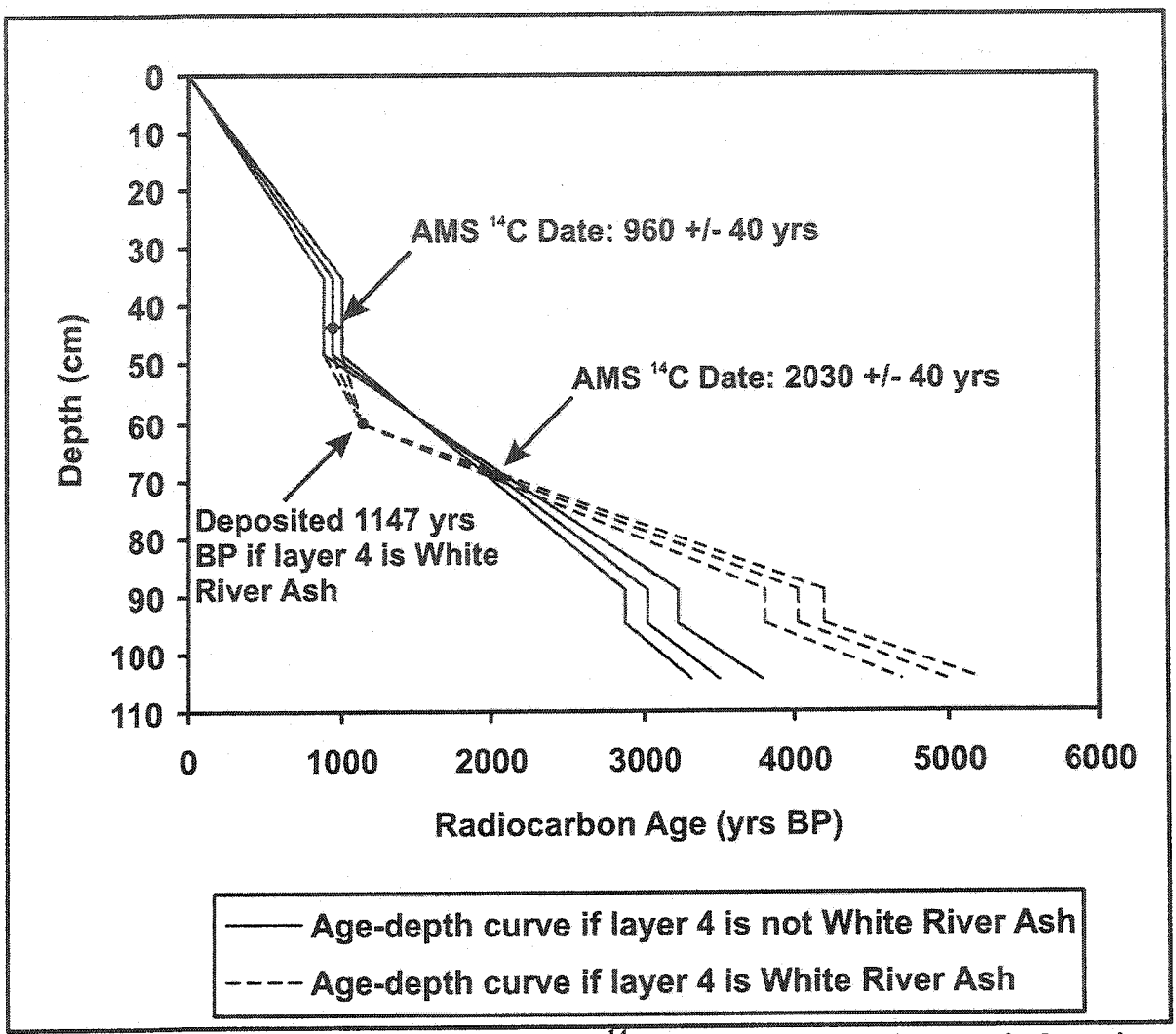

Figure 6.1: Age-depth curves based on AMS ^{14}C dates from MA4 (the vertical portions of the curves represent instantaneous sedimentation events).

Aramis Lake. The assumption of a linear age-depth relationship could not be avoided without more radiocarbon dating at much finer intervals than that allowed by the relative lack of organics, small amounts of material available, and financial constraints. However, it is clear that without more data regarding the age-depth relationship of the lacustrine sediments, the debris flow recurrence intervals calculated for both Mount Aramis and Three Guardsmen Mountain may be flawed.

The results from Three Guardsmen Mountain are surprising because it was expected that the relatively higher volume of precipitation in northwestern British Columbia would result in greater frequency but lower magnitude debris flow activity than at Mount Aramis. This proved to be true based on the layers observed in the cores but the difference in debris flow recurrence interval was only about 75 yrs. It was also expected that Three Guardsmen Mountain would have a shorter debris flow return interval than the sites studied at Kluane and Kusawa Lakes. However, most of the arguments used to defend the Mount Aramis debris flow return interval above also apply to the return interval calculated for Three Guardsmen Mountain.

What is most troubling is that the interpretation of the results from both lakes could be incorrect. For example, all of the identified layers may be related to debris flows. If this is the case, the recurrence interval changes to one debris flow every 200 to 225 yrs for all seventeen layers in Mount Aramis Lake and one debris flow every 250 to 290 yrs for all twelve layers in Three Guardsmen Lake (in both cases assuming linear age-depth relationships). Furthermore, while the ternary diagrams and bivariate plots of sorting *versus* skewness for MA4 indicate that a variety of geomorphic processes have deposited layers in Mount Aramis Lake, those for TG3 suggest that the depositional processes in Three Guardsmen Lake were very similar throughout. Therefore, it is also possible that sediment deposition in Three Guardsmen Lake is entirely due to autochthonous depositional processes and that there is no distinct debris flow record. Although misinterpretation of all the layers seems unlikely, the possibility must be considered especially given the relatively weak signatures of geomorphic activity in the cores from Three Guardsmen Lake. The differences in the sedimentary structures within the cores in the two lakes is itself an interesting

question. Why were there distinct debris flow signatures in the lacustrine sediment of Mount Aramis Lake and only weak indicators of geomorphic activity in the lacustrine sediment of Three Guardsmen Lake? The numerous factors that could be responsible for the difference are examined below.

First, are the slope deposits due to debris flow activity? The terrestrial geomorphological evidence presented in Chapter 3, clearly establishes that channelized debris flows have occurred several times on the western slope of Three Guardsmen Mountain based on the complex system of levees, tracks, and plug and toe deposits of varying age. The terrestrial geomorphological evidence indicates that debris flows have also occurred at Mount Aramis but the larger and less complex channel suggests that they may be of greater magnitude and lower frequency than those at Three Guardsmen Mountain.

Second, do the lacustrine sediment cores extend far enough back in time to include events on the adjacent slopes? Willows and balsam poplar that appear to have been impacted during deposition of the debris flow toes and levees at both Mount Aramis and Three Guardsmen Mountain indicate that the slopes at both sites have been active in the last 30 to 50 years based on estimated age of the affected vegetation (Figure 6.2). Therefore, the Mount Aramis and Three Guardsmen Lake cores were certainly long enough to include a record of recent debris flow events on the surrounding slopes. Any debris flow event that occurred within the last 30 yrs should be present in the skimmed sediment of either site, but while LOI and LPSA data for MA4 show potential evidence of debris flow activity at Mount Aramis in the last 30 yrs, LOI and LPSA data for TG3 show no distinctive evidence for debris flow activity in the last 30 yrs at Three Guardsmen Mountain (Figure 5.12). Clearly, not all debris flow events are recorded in the lacustrine sediments of Three Guardsmen Lake

Figure 6.2: Photographs of a balsam poplar affected by deposition of a debris flow levee at Mount Aramis, Yukon Territory (left) and a willow affected by deposition of a debris flow toe at Three Guardsmen Mountain, British Columbia (right).

Furthermore, although the cores from Mount Aramis Lake contain an obvious record of debris flow activity there is no way to tell whether all debris flow events are recorded in the lacustrine sediments.

Third, were debris flow signatures subsumed by high sedimentation rates? This seems unlikely because the sedimentation rate calculated for TG3 (0.29 to 0.30 mm/yr) was comparable to values calculated for Mount Aramis Lake (0.18 to 0.38 mm/yr) and the latter contained clear evidence of debris flow activity in the lacustrine sediment. Furthermore, the catchment to lake ratios of both sites were small enough to prevent the development of an extensive drainage network and the corresponding channel deposits that would have inundated sediments derived from slope or surface processes (Dearing & Foster, 1993). However, debris flow magnitude does appear to be greater at Mount Aramis than at Three Guardsmen Mountain. The sedimentation rate in Three Guardsmen Lake may overwhelm

the smaller events at Three Guardsmen Mountain while a similar rate of sedimentation in Mount Aramis Lake has less effect on the larger events at Mount Aramis.

Fourth, could differences in the core locations or lake bathymetry have influenced the results? Although coring took place directly offshore from the terrestrial debris flow channels near the centre of each lake, the coring apparatus was not long enough to collect cores in the deepest water at Three Guardsmen Lake where theoretically, all sedimentation events are recorded. However, only one of the cores taken from Mount Aramis Lake was collected in the deepest section and yet the other three contained a record of debris flow activity. The possibility exists, though, that some of the layers identified in the Mount Aramis Lake cores were fluvial deposits from gullies on the ridge west of the lake. The distance between Three Guardsmen Lake and the base of the ridge to its west probably precludes sub-aqueous deposition of slope deposits and the Haines Highway has provided a barrier in recent times. Therefore, the variations in the lacustrine sediment records could be related to differences in core location. Lake bathymetry may have had some influence because Mount Aramis Lake has a very simple bathymetry and a debris flow could more easily spread out and leave a widespread deposit. Three Guardsmen Lake has a more complex bathymetry with steeper banks that may direct debris flows to specific locations upon reaching the lake. Still, post-event deposition of finer sediment should leave a relatively widespread debris flow signature and it seems doubtful that the bathymetry of Three Guardsmen Lake could result in such a major difference.

Fifth, are there geological differences that may have affected the results? Lithologically, Mount Aramis and Three Guardsmen Mountain are similar, with the former underlain by Triassic granodiorite of the Ruby Range Batholith and the latter by Cretaceous

and Tertiary quartz diorite. Local stratigraphic differences, however, may be a significant factor because they are expressed by variations in weathering rates, clast size, and debris supply that influence debris flow magnitude and frequency (Bovis & Jakob, 1999) and the nature of lacustrine sediment signals. For example, if debris supply is limited, debris flow events may be small and infrequent with weak lacustrine sediment signals. If debris supply is abundant, debris flow events may be larger and occur more often with stronger lacustrine sediment signals.

Sixth could differences in the debris flow initiation zones and upper slopes have influenced the results? Although it was not possible to safely investigate the debris flow initiation zones at Mount Aramis or Three Guardsmen Mountain, there do not appear to be significant differences in their morphology. Both are deep, steep-sided, V-shaped clefts in the spine of the ridges that form the individual mountains and both are probably underlain by permafrost. The upper slopes at Three Guardsmen Mountain are unstable, unvegetated, and consist mostly of loose talus from 5 to 30 cm in diameter while the upper slopes at Mount Aramis are more stable, vegetated, and the clasts are generally much larger (50 to 300 cm) in diameter. While the upper slopes of Three Guardsmen Mountain are not part of the initiation zone, the smaller clasts and less stable talus may be more susceptible to mobilization. This could result in more frequent, but smaller, events that may cause deposition without appearing in the lacustrine sediment record.

Seventh, could differences in slope aspect or gradient have affected the results? Although both slopes have a western aspect, the upper slopes of Three Guardsmen Mountain have gradients ranging from 27° to 32° compared to 21° to 26° for Mount Aramis (see Figures 3.5 & 3.10). While these ranges of angles are sufficient for the initiation of debris

flows (Rapp & Nyberg, 1981; Larsson, 1982) the steeper slopes of Three Guardsmen Mountain may result in a lower threshold for shear stress and hydroclimatic initiation of debris flows. Consequently, debris flows may occur more frequently at Three Guardsmen Mountain, reducing the quiescent period required for the accumulation of debris in the initiation zone with a subsequent reduction in the magnitude of the events. Low magnitude events may not carry enough sediment to leave a significant signature or have enough energy to cross the built up toe deposits and enter Three Guardsmen Lake. Conversely, if the shallower slopes of Mount Aramis result in less frequent exceedance of hydroclimatic thresholds, more debris may accumulate, resulting in higher magnitude debris flows that are capable of traversing the flat toe deposits and leaving distinct layers in the lacustrine sediment.

Eighth, could precipitation be responsible for the difference in results? Higher precipitation at Three Guardsmen Mountain may result in more opportunities for the initiation of debris flows via rainfall and snowmelt than at Mount Aramis. With a higher frequency, magnitude could be expected to decrease, resulting in faint lacustrine evidence of debris flow activity or possibly none at all. At Mount Aramis, lower precipitation may result in fewer opportunities for the initiation of debris flows via rainfall and snowmelt but with a corresponding increase in magnitude and the deposition of distinct debris flow signatures in lacustrine sediment. Since Three Guardsmen Mountain receives almost five times the average annual precipitation of Mount Aramis the precipitation gradient could have a significant influence on the differences in the lacustrine sediment records of debris flow activity.

Despite the efforts made to select sites with similar conditions of rock type and topography, leaving climate as the main variable between them, it is evident that the experimental design was not entirely successful. Thus it is impossible to simply attribute the differences in sediment signatures in the two lakes to the magnitude and frequency of debris flows on the surrounding slopes. It would be surprising if the differences in precipitation – Three Guardsmen Mountain receives almost five times that of Mount Aramis – did not play a major role, but differences in slope gradient and variations in weathering rates could be just as significant. Given only two study sites and no information regarding debris supply conditions, it is not possible to reach definitive conclusions regarding the relationship between precipitation regimes and debris flow magnitude and frequency.

7. CONCLUSIONS

This thesis used lacustrine sediment records to examine debris flow magnitude and frequency at two sites along a precipitation gradient between northwestern British Columbia and southwestern Yukon Territory. The primary objective was to test the efficacy of using lacustrine sediments as a means to obtain information regarding debris flow magnitude and frequency.

Nine of seventeen layers observed in the lacustrine sediment of Mount Aramis Lake over the last 3400 to 3800 yrs (based on linear age-depth relationships), were interpreted as debris flows. Two of the nine were almost definitely debris flows and the other seven were probably debris flows but could have also been deposited by fluvial activity. Seven of the remaining layers were probably related to fluvial activity although debris flows may have been involved with those as well. The final layer observed in Mount Aramis Lake was probably the result of either resuspension of bottom sediments due to a seismic event or a thin layer of tephra deposited after a volcanic eruption. Ten of twelve layers observed in the lacustrine sediment of Three Guardsmen Lake over the last 3000 to 3500 yrs (based on linear age-depth relationships) were inferred to probably be debris flow deposits while the remainder were attributed to changes in autochthonous deposition. Therefore, debris flow activity on slopes adjoining lakes in northwest Canada is detectable in lacustrine sediments and the signatures may be used as broad indices of rates of debris flow activity. However, collection of multiple cores is necessary as some may not contain a complete record of geomorphic activity.

While lacustrine sediments provide information regarding debris flow frequency only the largest events are definitively recorded in lacustrine sediments. Smaller events

leave faint signatures without distinct debris flow characteristics making interpretation difficult. Consequently, lacustrine sediments may only contain a record of the minimum number of events over a given period and return intervals may be overestimated. From a hazard management perspective, this may be acceptable because less frequent but high magnitude debris flows have the most significant impacts on human infrastructure, activities, and life. From a research perspective, using lacustrine sediments to characterize debris flow activity may not be acceptable because geomorphic studies require a complete accounting of events. Therefore, lacustrine sediments should be used to determine debris flow magnitude and frequency in conjunction with other techniques (*e.g.* lichenometry, dendrochronology, and analysis of remotely sensed imagery).

The interpretation of the lacustrine sediment cores and the terrestrial and climatic evidence suggests that the high annual precipitation at Three Guardsmen Mountain may support a low magnitude but high frequency debris flow regime. Conversely, the low annual precipitation at Mount Aramis may support a regime with high magnitude but low frequency debris flows. Unfortunately, little is known about debris supply conditions at Three Guardsmen Mountain and Mount Aramis and what effects these may have on debris flow magnitude and frequency. Until more research is conducted on this subject any conclusions regarding the role of precipitation in debris flow activity based on research at Three Guardsmen Mountain and Mount Aramis remain speculative.

8. REFERENCES

Akerman, H.J., 1984: Notes on talus morphology and processes in Spitsbergen. *Geografiska Annaler*, 66A: 267-284.

American Society for Testing and Materials (ASTM), 2001: *American Standard Test Method D422-63, 1998: Standard Test Method for Particle-Size Analysis of Soils*. West Conshohocken, Pennsylvania.

Axelsson, V., 1983: The use of X-ray radiographic methods in studying sedimentary properties and rates of sediment accumulation. *Hydrobiologia*, 103: 65-69.

Beierle, B. and Bond, J., 2002: Density-induced settling of tephra through organic lake sediments. *Journal of Paleolimnology*, 28: 433-440.

Binford, M.W., 1983: Paleolimnology of the Peten Lake District, Guatemala, 1, Erosion and deposition of inorganic sediment as inferred from granulometry. *Hyrdobiologia*, 103: 199-203.

Bjorck, S. and Wohlfarth, B., 2001: ^{14}C Chronostratigraphic techniques in paleolimnology. *In* W.M. Last and J.P. Smol (eds.) *Tracking Environmental Change Using Lake Sediments Volume 1: Basin Analysis, Coring, and Chronological Techniques*. Dordrecht, The Netherlands: Kluwer Academic Publishers, 205-245.

Blott, S.J. and Pye, K., 2001: Gradistat: A grain size distribution and statistics package for the analysis of unconsolidated sediments. *Earth Surface Processes and Landforms*, 26: 1237-1248.

Bones, J. G., 1973: Process and sediment size arrangement on High Arctic talus, southwest Devon Island, N.W.T., Canada. *Arctic and Alpine Research*, 5: 29-40.

Bovis, M.J., 1993: Hillslope geomorphology and geotechnique. *Progress in Physical Geography*. 17(2): 173-189.

Bovis, M.J. and Jakob, M., 1999: The role of debris supply conditions in predicting debris flow activity. *Earth Surface Processes and Landforms*. 24(11): 1039-1054.

Broscoe, A.J. and Thompson, S., 1969: Observations on an alpine mudflow, Steele Creek, Yukon. *Canadian Journal of Earth Sciences*. 6(2): 219-229.

Brown, S., Biermen, P., Lini, A., Davis, P., and Southon, J., 2002: Reconstructing lake and drainage basin history using terrestrial sediment layers: analysis of cores from a post-glacial lake in New England, USA. *Journal of Paleolimnology*, 28: 219-236.

Caine, N., 1980: The rainfall intensity-duration control of shallow landslides and avalanches. *Geografiska Annaler*. 62A: 23-27.

Catto, N.R., 1993: Morphology and development of an alluvial fan in a permafrost region, Aklavik Range, Canada. *Geografiska Annaler*, 75A: 83-93.

Chen, F., Shi, Q., and Wang, J., 1999: Environmental changes documented by sedimentation of Lake Yiema in arid China since the Late Glaciation. *Journal of Paleolimnology*, 22: 159-169.

Church, M. and Miles, M.J., 1987: Meteorological antecedents to debris flow in southwestern British Columbia: some case studies. *In* J.E. Costa and G.F. Wieczorek (eds.) *Debris flows/avalanches: process, recognition and mitigation*. Reviews in Engineering Geology 7. Boulder, Colorado: Geological Society of America, 63-79.

Clague, J.J., 1981: Landslides at the south end of Kluane Lake, Yukon Territory. *Canadian Journal of Earth Sciences*. 18(5): 959-971.

Clague, J.J., Evans, S.G., Rampton, V.N., and Woodsworth, G.J., 1995: Improved age estimates for the White River and Bridge River tephras, western Canada. *Canadian Journal of Earth Sciences*, 32: 1171-1179.

Cogley, J.G. and McCann, S.B., 1976: An exceptional storm and its effects in the Canadian High Arctic. *Arctic and Alpine Research*, 8(1): 105-110.

Coussot, P. and Meunier, M., 1996: Recognition, classification and mechanical description of debris flows. *Earth-Science Reviews*, 40: 209-227.

Creer, K.M. and Morris, A., 1996: Proxy-climate and geomagnetic palaeointensity records extending back to ca. 75,000 BP derived from sediments cored from Lago Grande Di Monticchio, Southern Italy. *Quaternary Science Review*, 15: 167-188.

Dean, W.E., 1974: Determination of carbonate and organic matter in calcareous sediments and sedimentary rocks by loss on ignition: comparison with other methods. *Journal of Sedimentary Petrology*, 44: 242-248.

Dearing, J.A., 1983: Changing patterns of sediment accumulation in a small lake in Scania, southern Sweden. *Hydrobiologia*, 103: 59-64.

Dearing, J.A., 1986: Core correlation and total sediment influx. *In* B.E. Berglund (ed.), *Handbook of Holocene Palaeoecology and Palaeohydrology*. Toronto: John Wiley & Sons Ltd., 247-273.

Dearing, J.A., 1991: Lake sediment records of erosional processes. *Hydrobiologia*, 214: 99-106.

Dearing, J.A. and Foster, I.D.L., 1993: Lake Sediments and Geomorphological Processes: Some Thoughts. *In* J. McManus and R.W. Duck (eds.) *Geomorphology and Sedimentology of Lakes and Reservoirs*. Toronto: John Wiley & Sons Ltd., 5-14.

Doig, R., 1998: Paleoseismological evidence from lake sediments for recent movement on the Denali and other faults, Yukon Territory, Canada. *Tectonophysics*, 296: 363-370.

Doran, P., 1993: Sedimentology of Colour Lake, a non-glacial High Arctic lake, Axel Heiberg Island, N.W.T., Canada. *Arctic and Alpine Research*, 25: 353-367.

Eisbacher, G.H. and Clague, J.J., 1984: *Destructive mass movements in high mountains: Hazard and management.* Ottawa: Geological Survey of Canada Paper, v. 84-16: 230 pp.

Energy, Mines and Resources Canada, 1974: *Iskut River* [map]. Geological Atlas 1:1,000,000, sheet 104, 114 Map 1418 A. Ottawa: Geological Survey of Canada.

Energy, Mines and Resources Canada, 1977: *MacMillan River* [map]. Geological Atlas 1:1,000,000, sheet 105, 115 Map 1398 A. Ottawa: Geological Survey of Canada.

Energy, Mines and Resources Canada, 1988: *A27368* [aerial photograph]. 1:40,000. Ottawa: Energy, Mines and Resources Canada.

Energy, Mines and Resources Canada, 1992: *A27871* [aerial photograph]. 1:15,000. Ottawa: Energy, Mines and Resources Canada.

Environment Canada, 2004: *Canadian Climate Normals, 1971-2000.* URL: http://www.climate.weatheroffice.ec.gc.ca/climate_normals/index_e.html. Date: 1 March 2004.

Evans, S.G., 2001: Landslides. *In* G.R. Brooks (ed.) *A synthesis of geological hazards in Canada.* Ottawa: Geological Survey of Canada Bulletin 548: 43-79.

Evans, S.G. and Clague, J.J., 1989: Rain-induced landslides in the Canadian Cordillera, July 1988. *Geoscience Canada.* 16(3): 193-200.

Fannin, R.J. and Rollerson, T.P., 1993: Debris flows: some physical characteristics and behaviour. *Canadian Geotechnical Journal*, 30: 71-81.

Folk, R.L., 1980: *Petrology of Sedimentary Rocks.* Austin: Hemphill Publishing Company.

French, H.M., 1996: *The Periglacial Environment 2nd Edition.* Edinburgh Gate: Addison Wesley Longman Ltd.

Fuller, T., 2002: Sediment coring at Swansea Point fan delta, Mara Lake, British Columbia - Application of a coring method to determine historical debris flow events. *Terrain Stability and Forest Management in the Interior of British Columbia: Workshop Proceedings.* May 23-25, 2001 Nelson, British Columbia, Canada. Edited by: Jordan, P. and Orban, J. British Columbia Ministry of Forests Forest Sciences. Technical Report 003: 103-110.

Glew, J.R., Smol, J.P., and Last, W.M., 2001: Sediment core collection and extrusion. *In* W.M. Last and J.P. Smol (eds.) *Tracking Environmental Change Using Lake Sediments Volume 1: Basin Analysis, Coring, and Chronological Techniques*. Dordrecht, The Netherlands: Kluwer Academic Publishers, 73-105.

Gottesfeld, A.S., Mathews, R.W., and Johnson Gottesfeld, L.M., 1991: Holocene debris flows and environmental history. *Canadian Journal of Earth Sciences*, 28: 1583-1593.

Greenwood, B., 1969: Sediment parameters and environmental discrimination: an application of multivariate statistics. *Canadian Journal of Earth Sciences*, 28: 1347-1358.

Haeberli, W., 1992: Construction, environmental problems and natural hazards in periglacial mountain belts. *Permafrost and Periglacial Processes*. 3: 111-124.

Harris, S.A. and Gustafson, C.A., 1988: Retrogressive slumps, debris flows and river gully development in icy, unconsolidated sediments on hills and mountains. *Zeitschrift fur Geomorphologie*, 32: 441-455.

Harris, S.A. and McDermid G., 1998: Frequency of debris flows on the Sheep Mountain fan, Kluane Lake, Yukon Territory. *Zeitschrift fur Geomorphologie*. 42(2): 159-175.

Hartshorn, J., 1995: High energy geomorphic events in the Sawtooth Mountains, Ellesmere Island, High Arctic Canada – Unpublished M.Sc. Thesis. Department of Geography, University of Toronto, 136 pp.

Hartshorn, J. and Lewkowicz, A.G., 2000: Lacustrine record of high energy geomorphic events in the Sawtooth Range, Ellesmere Island, Canadian High Arctic. *Zeitschrift fur Geomorphologie*, 44(4): 417-434.

Heiri, O., Lotter, A.F., Lemcke, G., 2001: Loss on ignition as a method for estimating organic and carbonate content in sediments: reproducibility and comparability of results. *Journal of Paleolimnology*, 25: 101-110.

Jahn, A., 1976: Contemporaneous geomorphological processes in Longyeardalen, Vestspitsbergen (Svalbard). *Biuletyn Peryglacjalny*, 26: 253-268.

Jakob, M. and Weatherly, H., 2003: A hydroclimatic threshold for landslide initiation on the North Shore Mountains of Vancouver, British Columbia. *Geomorphology*. 54(3-4): 119-136.

Johnson, A.M. and Rodine, J.R., 1984: Debris flow. *In* D. Brunsden and D.B. Prior (eds.) *Slope Instability*. New York, New York: John Wiley & Sons Ltd., Chapter 8.

Jonasson, C., 1988: Slope processes in periglacial environments of Northern Scandinavia. *Geografiska Annaler*, 70A: 247-253.

Kotarba, A., 1992: High-energy geomorphic events in the Polish Tatra mountains. *Geografiska Annaler*, 74A: 123-131.

Kotarba, A., 1997: Formation of high-mountain talus slopes related to debris-flow activity in the High Tatra Mountains. *Permafrost and Periglacial Processes*, 8: 191-204.

Kunze, G.W., 1965: Pretreatment for mineralogical analysis. *In* C.A. Black, D.D. Evans, L.W. Ensminger, J.L. White, and F.E. Clark (eds.) *Methods of Soil Analysis Part I, Physical and Mineralogical Properties, Including Statistics of Measurement and Sampling, Agronomy No. 9.* American Society of Agronomy: Wisconsin, 568-577.

Lamoureux, S., 2000: Five centuries of interannual sediment yield and rainfall-induced erosion in the Canadian High Arctic recorded in lacustrine varves. *Water Resources Research*, 36(1): 309-318.

Lamoureux, S., 2002: Temporal patterns of suspended sediment yield following moderate to extreme hydrological events recorded in varved lacustrine sediments. *Earth Surface Processes and Landforms*, 27: 1107-1124.

Larsson, S., 1982: Geomorphological effects on the slopes of Longyear Valley, Spitsbergen, after a heavy rainstorm in July 1972. *Geografiska Annaler*, 64A: 105-125.

Last, W.M., 2001: Textural analysis of lake sediments. *In* W.M. Last and J.P. Smol (eds.) *Tracking Environmental Change Using Lake Sediments Volume 2: Physical and Geochemical Methods*. Dordrecht, The Netherlands: Kluwer Academic Publishers, 41-81.

Lerbekmo, J.F. and Campbell, F.A., 1969: Distribution, composition, and source of the White River Ash, Yukon Territory. *Canadian Journal of Earth Sciences*, 6: 109-116.

Lewkowicz, A.G. and Hartshorn, J., 1998: Terrestrial record of rapid mass movements in the Sawtooth Range, Ellesmere Island, NT, Canada. *Canadian Journal of Earth Sciences*, 35: 55-64.

Linnick, W., Damon, P.E., Donahue, D.J., and Jull, A.J.T., 1989: Accelerator mass spectrometry: The new revolution in radiocarbon dating. *Quaternary International*, 1: 1-6.

Lowey, G.W., 2002: Sedimentary processes of the Kusawa Lake torrent system, Yukon, Canada, as revealed by the September 16, 1982 flood event. *Sedimentary Geology*. 151(3-4): 293-312.

Miles, M.J. and Kellerhalls, R., 1981: Some engineering aspects of debris torrents. *Fifth Canadian Hydrotechnical Conference*. Fredericton, New Brunswick, Canadian Society for Civil Engineering, 395-413.

Murray, M.R., 2002: Is laser particle size determination possible for carbonate-rich lake sediments? *Journal of Paleolimnology*, 27: 173-183.

Nieuwenhuijzen, M.E. and van Steijn, H., 1990: Alpine debris flows and their sedimentary properties. A case study from the French Alps. *Permafrost and Periglacial Processes*, 1: 111-128.

Nowaczyk, N.R., 2001: Logging of magnetic susceptibility. *In* W.M. Last and J.P. Smol (eds.) *Tracking Environmental Change Using Lake Sediments Volume 1: Basin Analysis, Coring, and Chronological Techniques*. Dordrecht, The Netherlands: Kluwer Academic Publishers, 155-170.

Nyberg, R. and Lindh, L., 1990: Geomorphic features as indicators of climatic fluctuations in a periglacial environment, northern Sweden. *Geografiska Annaler*. 72A: 203-210.

Pyle, D.M., 1989: The thickness, volume, and grain size of tephra fall deposits. *Bulletin of Volcanology*, 51: 1-15.

Rapp, A., 1960. Recent development of mountain slopes in Karkevägge and surroundings, Northern Scandinavia. *Geografiska Annaler*, 42: 65-200.

Rapp, A., 1985: Extreme rainfall and rapid snowmelt as causes of mass movements in high latitude mountains. *In*, M. Church and H.O. Slaymaker, (ed.) *Field and Theory: Lectures in Geocryology*. Vancouver: University of British Columbia Press, 36-56.

Rapp, A. and Nyberg, R., 1981: Alpine debris flows in northern Scandinavia. Morphology and dating by lichenometry. *Geografiska Annaler*, 63A: 183-196.

Rapp, A. and Stromquist, L., 1976: Slope erosion due to extreme rainfall in the Scandinavian mountains. *Geografiska Annaler*, 58A: 193-201.

Rebetez, M., Lugon, R., and Baeriswyl, P.A., 1997: Climatic change and debris flows in high mountain regions: The case study of the Ritigraben torrent (Swiss Alps). *Climatic Change*. 36(3-4): 371-389.

Sandgren, P., and Snowball, I., 2001: Application of mineral magnetic techniques to paleolimnology. *In* W.M. Last and J.P. Smol (eds.) *Tracking Environmental Change Using Lake Sediments Volume 2: Physical and Geochemical Methods*. Dordrecht, The Netherlands: Kluwer Academic Publishers, 217-237.

Selby, M.J., 1993: *Hillslope Materials and Processes 2nd Edition.* New York: Oxford University Press, Inc.

Sparks, R.S.J., Bursik, M.I., Ablay, G.J., Thomas, R.M.E., and Carey, S.N., 1992: Sedimentation of tephra by volcanic plumes, Part 2: Controls on thickness and grain-size variations of tephra fall deposits. *Bulletin of Volcanology*, 54: 685-695.

Swanston, D.N. and Swanson, F.J., 1976: Timber harvesting, mass erosion, and steepland forest geomorphology in the Pacific Northwest. *In* D.R. Coates (ed.) *Geomorphology and Engineering*. Stroudsburg, Pennsylvania: Dowden, Hutchinson & Ross, Inc., 199-221.

Theakstone, W.H., 1982: Sediment fans and sediment flows generated by snowmelt: observations at Austerdalsisen, Norway. *Journal of Geology*, 90: 589-588.

Thompson, R., Bloemendal, J., Dearing, J.A., Oldfield, F., Rummery, T.A., Stober, J.C., and Turner, G.M., 1980: Environmental applications of magnetic measurements. *Science*, 207(4430): 481-486.

Thompson, R. and Oldfield, F., 1986: *Environmental Magnetism.* London: Allen & Unwin Ltd.

Turney, C.S.M. and Lowe, J.J., 2001: Tephrochronology. *In* W.M. Last and J.P. Smol (eds.) *Tracking Environmental Change Using Lake Sediments Volume 1: Basin Analysis, Coring, and Chronological Techniques.* Dordrecht, The Netherlands: Kluwer Academic Publishers, 451-471.

van Steijn, H., de Ruig, J., and Hoozemans, F., 1988: Morphological and mechanical aspects of debris flows in parts of the French Alps. *Zeitschrift fur Geomorphologie*, 32: 143-161.

van Steijn, H., 1996: Debris-flow magnitude-frequency relationships for mountainous regions of Central and Northwest Europe. *Geomorphology*, 15: 259-273.

Varnes, D.J., 1978: Slope movement types and processes. *In* R.L. Schuster and R.J. Krisek (eds.) *Landslides, Analysis and Control.* National Academy of Sciences, Transportation Research Board, Special Report 176: 11-33.

Whiteman, C.D., 2000: *Mountain Meteorology: Fundamentals and Applications.* New York: Oxford University Press, Inc.

Wieczorek, G.F., 1987: Effects of rainfall intensity and duration on debris flows in Central Santa Cruz Mountains, California. *Geological Society of America, Reviews in Engineering*, 7: 93-104.

Zolitschka, B., Mingram, J., Van Der Gaast, S., Jansen, J.H.F., Naumann, R., 2001: Sediment logging techniques. *In* W.M. Last and J.P. Smol (eds.) *Tracking Environmental Change Using Lake Sediments Volume 1: Basin Analysis, Coring, and Chronological Techniques.* Dordrecht, The Netherlands: Kluwer Academic Publishers, 137-153.

APPENDIX A: CORE DATA

Core MA1

Sample Interval (cm)	Magnetic Susceptibility (SI Units)	LOI at 550°C (%DW)
1	-	11.33
2	-	10.58
3	-	15.00
4	-	14.63
5	-	14.86
6	-	13.02
7	-	12.71
8	-	11.15
9	-	15.38
10	-	13.73
11	-	13.66
12	-	13.91
13	-	14.49
14	-	14.02
15	-	12.39
16	-	14.09
17	-	14.80
18	8.96	15.93
19	11.61	14.73
20	13.97	15.03
21	16.57	15.38
22	19.28	15.26
23	21.88	12.36
24	25.49	10.72
25	30.69	16.46
26	39.09	18.82
27	50.50	17.63
28	63.10	15.70
29	82.61	10.05
30	109.91	9.39
31	139.71	6.02
32	151.47	7.41
33	132.07	0.76
34	101.13	3.48
35	79.13	15.30
36	62.79	6.55
37	49.79	16.46
38	40.10	15.75

Sample Interval (cm)	Magnetic Susceptibility (SI Units)	LOI at 550°C (%DW)
39	32.90	15.83
40	26.36	13.79
41	22.86	15.38
42	21.17	15.02
43	20.32	13.71
44	20.02	13.95
45	19.08	10.72
46	16.98	10.64
47	15.34	16.87
48	14.19	16.67
49	13.64	17.11
50	13.30	17.31
51	13.70	16.34
52	14.21	16.53
53	14.91	16.89
54	16.27	17.39
55	17.07	16.95
56	16.48	17.17
57	14.83	17.28
58	13.54	17.00
59	12.34	16.37
60	11.55	18.07
61	10.25	18.72
62	10.85	16.79
63	11.51	17.20
64	11.51	15.87
65	11.22	17.33
66	11.22	18.15
67	11.32	18.10
68	11.48	17.52
69	12.08	12.28
70	12.64	11.86
71	13.84	12.02
72	15.45	11.52
73	16.55	9.43
74	17.51	12.90
75	20.46	12.27
76	25.52	9.41
77	30.22	10.75
78	37.13	10.32
79	48.38	10.18
80	65.03	7.11

Sample Interval (cm)	Magnetic Susceptibility (SI Units)	LOI at 550°C (%DW)
81	73.04	3.95
82	59.19	7.99
83	36.44	13.97
84	24.10	14.22
85	19.10	14.02
86	17.56	13.67
87	17.36	12.98
88	17.92	11.64
89	18.67	13.53
90	18.68	13.73
91	17.83	15.06
92	17.24	15.51
93	17.09	15.32
94	17.35	13.16
95	16.50	14.79
96	14.56	14.60
97	12.66	15.20
98	11.31	14.58
99	10.67	16.74
100	11.17	17.54
101	11.12	17.54
102	10.53	16.55
103	8.33	16.83
Minimum	8.33	0.76
Mean	29.22	13.87
Median	17.29	14.63
Maximum	151.47	18.82
Std. Deviation	29.84	3.44

Core MA2

Sample Interval (cm)	Magnetic Susceptibility (SI Units)	LOI at 550°C (%DW)
1	-	0.00
2	-	21.01
3	-	12.29
4	-	6.38
5	-	9.12
6	-	6.80
7	-	9.47
8	-	17.05
9	-	18.39
10	-	17.31
11	-	17.14
12	-	16.91
13	-	17.07
14	-	15.53
15	-	14.57
16	-	13.74
17	3.96	18.65
18	7.83	19.32
19	10.09	18.47
20	14.46	17.19
21	19.63	13.65
22	24.39	15.87
23	22.76	17.61
24	16.87	18.03
25	12.44	17.56
26	10.90	14.29
27	10.61	17.53
28	9.48	18.25
29	8.34	18.46
30	7.96	17.75
31	8.27	17.11
32	9.23	16.61
33	11.40	15.65
34	14.46	13.93
35	18.53	14.91
36	23.84	8.24
37	30.01	13.83
38	36.82	11.01
39	46.29	5.94
40	63.30	8.87

Sample Interval (cm)	Magnetic Susceptibility (SI Units)	LOI at 550°C (%DW)
41	79.22	8.51
42	86.73	7.91
43	88.50	5.05
44	90.76	2.78
45	89.48	4.28
46	79.54	13.65
47	62.00	16.67
48	40.42	16.49
49	27.08	17.45
50	19.45	17.83
51	16.66	17.84
52	16.23	14.37
53	16.79	17.11
54	17.30	15.86
55	18.02	12.77
56	19.33	10.75
57	21.90	7.36
58	26.96	9.64
59	34.83	15.41
60	39.04	10.69
61	37.31	8.15
62	37.22	4.97
63	42.98	7.49
64	57.10	16.10
65	67.72	17.27
66	60.63	17.52
67	36.90	18.85
68	21.36	17.67
69	14.87	16.16
70	13.04	17.77
71	13.55	16.03
72	14.62	17.15
73	14.73	16.12
74	14.39	15.79
75	14.16	9.98
76	14.32	20.00
77	15.34	19.57
78	15.90	18.99
79	14.02	19.49
80	10.73	18.55
81	8.65	18.96
82	7.61	19.12

Sample Interval (cm)	Magnetic Susceptibility (SI Units)	LOI at 550°C (%DW)
83	7.18	14.88
84	6.79	14.86
85	6.86	14.29
86	6.62	14.83
87	6.14	14.74
88	6.70	13.86
89	6.76	13.25
90	6.63	16.34
91	6.74	17.20
92	7.56	16.25
93	8.62	13.79
94	9.34	9.38
95	10.20	15.79
96	14.21	17.67
97	20.23	17.89
98	26.19	19.38
99	26.26	19.60
100	19.02	18.05
101	13.39	18.32
102	10.70	17.49
103	9.92	17.15
104	9.88	14.53
105	10.75	6.19
106	14.71	19.26
107	21.32	19.72
108	31.59	16.62
109	43.15	16.73
110	45.52	18.92
111	36.48	18.24
112	28.20	16.92
113	18.96	17.55
114	10.73	17.34
Minimum	3.96	0.00
Mean	24.35	14.85
Median	16.06	16.42
Maximum	90.76	21.01
Std. Deviation	21.16	4.35

Core MA3

Sample Interval (cm)	Magnetic Susceptibility (SI Units)	LOI at 550°C (%DW)	LOI at 950°C (%DW)
1	-	18.18	3.90
2	-	16.39	2.10
3	-	15.35	2.33
4	-	9.89	2.20
5	-	10.91	1.09
6	-	8.77	1.17
7	-	15.34	1.59
8	-	17.11	1.60
9	-	16.67	2.15
10	-	6.68	0.77
11	-	17.42	1.29
12	-	15.49	2.11
13	-	14.42	2.40
14	-	13.10	1.75
15	-	14.40	0.00
16	-	16.26	0.00
17	13.23	15.46	0.69
18	8.85	14.29	0.70
19	11.67	13.96	0.65
20	15.29	14.15	0.64
21	18.61	13.49	0.99
22	19.78	12.67	1.03
23	19.50	12.50	1.01
24	19.62	11.39	0.51
25	20.99	10.53	0.66
26	23.21	14.80	0.72
27	25.68	14.89	0.76
28	28.84	14.43	1.37
29	33.21	14.43	1.03
30	37.49	13.99	0.70
31	39.76	14.43	0.69
32	42.22	12.17	0.87
33	49.34	10.21	0.79
34	59.16	10.93	0.80
35	63.33	12.50	1.25
36	56.65	11.14	1.51
37	45.07	5.47	0.77
38	29.84	7.86	0.45
39	19.26	10.01	0.88

Sample Interval (cm)	Magnetic Susceptibility (SI Units)	LOI at 550°C (%DW)	LOI at 950°C (%DW)
40	14.48	14.57	1.12
41	12.40	14.59	1.78
42	11.77	14.79	1.56
43	12.04	14.57	1.57
44	12.31	14.57	2.02
45	12.28	14.24	1.39
46	12.45	12.25	1.42
47	13.27	14.38	1.37
48	15.58	13.33	1.90
49	18.86	13.36	1.81
50	21.13	12.58	1.23
51	18.90	10.80	1.11
52	14.46	6.64	0.92
53	11.43	15.02	2.15
54	10.55	14.61	2.25
55	10.48	14.93	1.87
56	10.44	14.91	2.18
57	9.91	15.08	1.59
58	8.98	14.51	1.57
59	8.60	14.91	2.19
60	8.77	15.09	2.16
61	8.99	14.52	2.49
62	9.31	14.57	2.02
63	9.78	13.36	2.43
64	10.45	14.18	2.18
65	11.07	13.09	2.01
66	12.29	15.79	1.05
67	14.46	15.02	0.68
68	17.23	12.23	0.92
69	23.75	15.30	1.12
70	29.07	13.55	0.97
71	29.69	9.61	0.75
72	22.81	14.90	1.18
73	16.47	16.08	1.18
74	12.99	15.57	1.23
75	14.42	15.66	1.61
76	16.84	15.30	1.07
77	15.65	16.73	1.22
78	14.77	16.93	1.18
79	14.49	15.77	1.66
80	14.91	15.90	1.26

Sample Interval (cm)	Magnetic Susceptibility (SI Units)	LOI at 550°C (%DW)	LOI at 950°C (%DW)
81	16.33	15.62	1.17
82	20.45	15.69	1.18
83	28.47	16.00	0.36
84	43.49	14.53	1.04
85	68.31	3.78	0.53
86	101.38	3.09	0.33
87	130.30	3.03	0.23
88	153.07	2.83	0.24
89	164.64	2.71	0.36
90	166.96	2.56	0.35
91	165.28	2.64	0.33
92	159.30	2.75	0.34
93	145.16	2.79	0.21
94	125.89	12.33	1.37
95	102.61	7.13	0.63
96	77.98	12.53	0.52
97	55.74	15.00	1.54
98	41.01	13.10	1.28
99	36.33	10.70	1.04
100	37.51	8.01	0.52
101	40.37	11.30	1.13
102	45.49	11.17	0.97
103	53.06	8.64	0.76
104	65.08	7.47	0.34
105	72.65	9.08	0.36
106	66.07	16.36	0.74
107	51.59	17.09	0.85
108	30.51	16.18	0.83
109	19.88	15.91	0.38
110	14.40	15.38	0.70
111	13.57	14.33	0.96
112	13.44	14.29	0.95
113	13.86	14.29	0.32
114	14.68	14.07	0.60
115	15.20	12.97	0.63
116	15.42	14.90	0.66
117	15.38	14.88	1.04
118	15.20	14.60	0.62
119	15.22	15.21	1.29
120	15.20	15.60	1.42
121	15.11	16.10	0.68

Sample Interval (cm)	Magnetic Susceptibility (SI Units)	LOI at 550°C (%DW)	LOI at 950°C (%DW)
122	14.78	15.85	0.86
123	13.75	14.24	0.87
Minimum	8.60	2.56	0.00
Mean	35.32	12.87	1.14
Median	18.61	14.38	1.04
Maximum	166.96	18.18	3.90
Std. Deviation	38.58	3.75	0.64

Core MA4

Sample Interval (cm)	Magnetic Susceptibility (SI Units)	LOI at 550°C (%DW)	LOI at 950°C (%DW)	Median Grain Size (μm)
1	-	17.02	4.26	37.14
2	-	14.49	3.62	36.83
3	-	13.47	2.59	36.56
4	-	10.80	2.00	36.20
5	-	11.03	2.57	39.78
6	-	17.48	2.80	41.85
7	-	19.02	2.45	39.67
8	-	18.25	2.92	39.01
9	-	17.28	3.09	39.27
10	-	15.38	3.50	35.69
11	-	14.61	3.37	33.74
12	-	14.43	2.99	36.08
13	-	13.22	2.07	31.26
14	-	14.21	3.05	35.69
15	-	15.23	2.03	41.15
16	-	14.65	3.18	32.90
17	11.77	15.14	1.58	36.36
18	13.88	15.35	2.76	37.06
19	14.94	15.35	2.19	36.59
20	15.59	14.39	1.52	37.40
21	15.45	14.56	1.92	34.90
22	15.06	16.88	2.16	35.68
23	15.47	16.67	2.02	35.92
24	16.58	16.52	1.79	36.18
25	18.03	15.74	2.54	36.42
26	19.55	16.74	1.81	37.21
27	21.85	15.83	1.67	36.53
28	24.21	14.96	1.82	37.54
29	26.82	13.43	1.77	36.29
30	29.53	14.45	1.52	35.89
31	33.44	11.33	1.33	47.32
32	39.94	13.58	1.89	40.47
33	53.40	11.95	1.89	41.51
34	76.91	7.82	1.09	36.59
35	98.67	4.59	0.88	22.65
36	111.13	3.11	0.58	55.80
37	110.88	7.01	0.73	108.10
38	106.60	9.55	0.80	113.10
39	105.75	8.40	0.85	121.30

Sample Interval (cm)	Magnetic Susceptibility (SI Units)	LOI at 550°C (%DW)	LOI at 950°C (%DW)	Median Grain Size (μm)
40	109.76	7.31	0.66	147.00
41	118.27	10.36	0.73	151.30
42	133.12	11.21	0.71	141.90
43	155.84	9.60	0.70	151.40
44	183.34	6.40	0.55	254.40
45	197.00	2.11	0.59	299.80
46	187.26	1.30	0.41	543.70
47	156.12	1.14	0.33	762.60
48	112.88	8.98	1.56	362.50
49	77.68	14.58	2.50	82.18
50	54.64	15.42	2.34	54.02
51	40.05	15.57	2.46	55.32
52	31.81	15.49	1.88	38.70
53	23.77	14.13	1.81	30.25
54	20.62	17.41	0.45	35.81
55	19.39	11.76	1.34	26.85
56	19.14	15.15	2.02	30.43
57	20.15	14.12	1.57	28.52
58	22.81	10.00	1.43	23.37
59	23.77	7.95	0.95	20.24
60	19.88	16.51	2.29	36.12
61	16.43	15.98	2.28	38.26
62	14.34	16.81	1.77	35.56
63	13.50	16.18	2.07	30.17
64	12.86	16.74	1.36	33.69
65	11.87	16.67	2.70	31.69
66	11.42	15.06	2.70	32.46
67	11.28	16.74	1.32	31.16
68	11.39	15.38	0.77	39.82
69	11.90	15.44	0.77	31.92
70	12.81	18.07	1.26	35.38
71	14.06	18.50	1.32	39.06
72	15.33	18.02	0.90	37.62
73	16.68	16.88	0.87	36.10
74	17.29	13.92	1.29	35.39
75	16.80	16.18	1.66	35.97
76	16.26	17.14	1.63	36.07
77	16.07	17.24	0.86	34.79
78	16.72	16.27	1.19	33.42
79	18.13	16.37	1.33	34.18
80	20.39	15.94	1.20	34.18

Sample Interval (cm)	Magnetic Susceptibility (SI Units)	LOI at 550°C (%DW)	LOI at 950°C (%DW)	Median Grain Size (μm)
81	24.15	15.19	1.27	35.61
82	28.06	12.73	1.21	37.90
83	30.16	11.48	0.94	46.49
84	30.33	15.00	1.92	38.73
85	30.78	15.69	0.73	42.08
86	34.19	12.05	0.72	36.64
87	41.10	13.92	0.97	36.64
88	51.75	7.69	0.53	33.25
89	60.32	17.46	1.25	92.61
90	64.17	15.72	0.76	79.58
91	64.13	12.14	0.71	88.85
92	58.94	13.04	0.64	59.34
93	50.60	15.22	0.31	57.67
94	37.66	16.67	1.32	33.86
95	27.91	14.75	0.33	37.48
96	21.77	10.20	0.26	37.23
97	19.48	10.32	0.23	39.37
98	18.94	9.41	0.84	38.35
99	18.75	5.51	0.64	35.05
100	18.10	15.25	0.71	36.56
101	16.97	14.73	0.34	37.27
102	14.62	14.94	0.32	38.30
Minimum	11.28	1.14	0.23	40.60
Mean	43.96	13.52	1.54	65.51
Median	22.33	14.84	1.35	36.74
Maximum	197.00	19.02	4.26	762.60
Std. Deviation	44.97	3.92	0.88	99.65

Core TG1

Sample Interval (cm)	Magnetic Susceptibility (SI Units)
1	-
2	-
3	-
4	-
5	-
6	-
7	-
8	-
9	-
10	-
11	-
12	-
13	-
14	-
15	5.92
16	10.19
17	13.85
18	16.92
19	20.28
20	24.85
21	28.77
22	27.54
23	21.25
24	15.37
25	10.88
26	8.15
27	6.97
28	6.13
29	5.65
30	5.36
31	5.43
32	5.55
33	5.57
34	5.38
35	5.00
36	5.06
37	5.13
38	4.95
39	4.51
40	3.88
41	3.24

Sample Interval (cm)	Magnetic Susceptibility (SI Units)
42	2.71
43	2.43
44	2.40
45	2.66
46	3.23
47	3.64
48	4.06
49	4.68
50	5.34
51	6.56
52	7.57
53	8.84
54	9.56
55	9.98
56	10.49
57	11.21
58	12.07
59	12.14
60	11.51
61	10.57
62	10.14
63	10.00
64	9.92
65	9.29
66	7.71
67	5.47
68	2.69
Minimum	2.40
Mean	8.86
Median	6.76
Maximum	28.77
Std. Deviation	6.17

Core TG2

Sample Interval (cm)	Magnetic Susceptibility (SI Units)
1	-
2	-
3	-
4	-
5	-
6	-
7	-
8	-
9	-
10	-
11	-
12	8.11
13	10.62
14	11.77
15	11.88
16	10.99
17	9.50
18	8.31
19	8.46
20	7.77
21	7.38
22	6.78
23	6.49
24	6.75
25	6.80
26	6.51
27	5.97
28	5.68
29	5.39
30	5.04
31	4.85
32	4.76
33	4.36
34	4.22
35	4.53
36	4.33
37	4.44
38	4.40
39	4.01
40	3.46
41	3.07

Sample Interval (cm)	Magnetic Susceptibility (SI Units)
42	2.83
43	2.74
44	2.99
45	3.40
46	3.66
47	3.67
48	3.72
49	3.53
50	3.39
51	3.24
52	3.10
53	3.06
54	2.92
55	2.77
56	2.48
57	2.39
58	2.20
59	2.40
60	2.76
61	3.82
62	5.22
63	6.58
64	7.69
65	8.40
66	8.90
67	9.11
68	8.62
69	8.18
70	7.88
71	7.59
72	7.55
73	7.85
74	8.31
75	8.52
76	8.12
77	7.38
78	6.69
79	6.40
80	5.96
81	5.86
82	6.27
83	6.98
84	7.23

Sample Interval (cm)	Magnetic Susceptibility (SI Units)
85	6.99
86	6.45
87	6.20
88	6.27
89	6.32
90	6.78
91	5.94
92	3.74
Minimum	2.20
Mean	5.89
Median	6.20
Maximum	11.88
Std. Deviation	2.36

Core TG3

Sample Interval (cm)	Magnetic Susceptibility (SI Units)	LOI at 550°C (%DW)	LOI at 950°C (%DW)	Median Grain Size (μm)
1	-	17.52	3.65	27.62
2	-	16.86	0.00	23.75
3	-	14.50	0.00	26.99
4	-	15.89	0.00	29.01
5	-	14.98	0.00	26.72
6	-	14.38	3.12	26.71
7	-	14.15	0.98	25.99
8	-	12.50	2.40	25.02
9	-	12.28	0.44	25.96
10	-	14.87	0.00	26.49
11	-	14.35	0.00	25.52
12	-	11.96	0.48	25.84
13	-	8.77	1.32	26.97
14	-	10.20	2.35	25.82
15	-	11.54	1.71	27.47
16	-	9.77	2.73	26.79
17	9.56	9.77	0.78	24.71
18	13.31	9.05	0.82	24.84
19	15.77	8.87	1.21	26.58
20	17.73	8.12	1.48	27.02
21	19.08	6.67	0.63	27.00
22	18.84	7.50	0.71	24.67
23	17.34	10.80	0.40	29.89
24	14.80	10.80	0.94	30.54
25	10.85	11.79	1.42	28.91
26	8.81	13.46	0.48	29.81
27	8.01	11.27	1.88	29.48
28	8.27	10.62	1.77	27.78
29	8.67	10.43	1.74	28.26
30	8.98	10.09	1.75	28.44
31	8.74	11.44	1.99	28.18
32	8.19	11.88	1.49	29.84
33	7.95	11.76	2.14	30.74
34	8.01	13.00	1.00	31.31
35	8.21	13.37	0.50	31.31
36	8.57	12.50	1.85	31.30
37	8.82	12.00	1.78	26.17
38	9.07	12.32	0.95	25.66
39	8.73	12.62	2.43	25.43

Sample Interval (cm)	Magnetic Susceptibility (SI Units)	LOI at 550°C (%DW)	LOI at 950°C (%DW)	Median Grain Size (µm)
40	8.68	12.94	1.99	26.04
41	9.04	13.21	0.94	25.84
42	9.50	12.63	2.53	25.23
43	10.15	12.71	2.21	31.87
44	10.71	12.79	1.37	24.63
45	11.37	11.21	1.35	24.23
46	11.92	10.98	1.52	26.73
47	12.18	11.69	0.81	25.53
48	12.33	11.48	1.23	26.50
49	11.94	11.25	0.83	25.49
50	11.09	12.16	1.35	26.64
51	9.55	13.30	1.97	24.68
52	7.85	14.87	2.05	24.05
53	7.16	15.03	0.52	24.75
54	7.07	14.22	1.42	25.51
55	7.52	12.50	2.08	26.39
56	7.63	13.46	1.44	24.30
57	7.63	12.55	1.73	24.65
58	7.99	12.65	1.22	28.97
59	8.29	12.30	1.23	25.61
60	8.65	12.03	1.24	23.84
61	8.60	12.33	1.32	24.17
62	8.31	12.66	0.87	23.56
63	7.71	13.27	1.42	24.74
64	7.27	13.40	0.96	23.72
65	7.13	13.74	0.47	24.62
66	7.08	12.89	0.89	24.30
67	7.49	10.09	1.75	25.12
68	8.25	10.88	1.26	25.11
69	8.90	10.07	0.72	25.39
70	9.66	9.82	1.05	24.02
71	10.31	8.52	0.74	24.45
72	10.62	9.80	1.22	24.50
73	10.67	9.23	1.11	25.19
74	10.33	9.57	1.06	25.12
75	9.08	10.07	1.39	26.78
Minimum	7.07	6.67	0.00	23.56
Mean	9.93	11.96	1.29	26.44
Median	8.82	12.16	1.24	25.84
Maximum	19.08	17.52	3.65	31.87
Std. Deviation	2.92	2.08	0.74	2.11

Core TG4

Sample Interval (cm)	Magnetic Susceptibility (SI Units)
1	-
2	-
3	-
4	-
5	-
6	-
7	-
8	-
9	-
10	-
11	-
12	-
13	-
14	-
15	-
16	-
17	-
18	4.72
19	6.58
20	7.74
21	8.50
22	8.97
23	9.38
24	9.94
25	10.50
26	10.87
27	10.88
28	10.69
29	10.25
30	9.82
31	8.98
32	8.04
33	7.31
34	7.07
35	7.23
36	7.39
37	7.36
38	7.17
39	6.64
40	6.35
41	6.41

Sample Interval (cm)	Magnetic Susceptibility (SI Units)
42	6.57
43	6.79
44	6.80
45	6.86
46	6.83
47	6.89
48	6.90
49	7.06
50	7.08
51	6.99
52	6.80
53	6.66
54	6.38
55	6.29
56	6.05
57	6.11
58	6.13
59	6.24
60	6.40
61	6.77
62	7.48
63	8.09
64	8.35
65	7.72
66	6.68
67	5.84
68	5.50
69	5.47
70	5.33
71	5.24
72	5.11
73	4.97
74	4.83
75	4.69
76	4.61
77	4.72
78	4.73
79	4.65
80	4.21
81	3.92
82	3.54
83	3.30
84	3.46

Sample Interval (cm)	Magnetic Susceptibility (SI Units)
85	3.57
86	3.89
87	4.20
88	4.46
89	4.13
90	4.14
91	4.20
92	4.36
93	4.48
94	4.34
95	4.25
96	3.61
97	2.18
98	0.79
Minimum	0.79
Mean	6.25
Median	6.40
Maximum	10.88
Std. Deviation	2.06

Core TG5

Sample Interval (cm)	Magnetic Susceptibility (SI Units)	LOI at 550°C (%DW)	LOI at 950°C (%DW)
1	-	25.00	0.00
2	-	19.05	0.00
3	-	16.85	0.00
4	-	17.42	0.65
5	-	19.01	0.70
6	-	20.00	0.71
7	-	17.12	0.68
8	-	16.28	1.16
9	-	14.69	0.00
10	-	14.15	0.00
11	-	13.27	0.00
12	-	13.45	0.00
13	-	13.97	0.00
14	-	13.68	0.00
15	-	13.92	0.00
16	-	16.97	0.00
17	3.82	12.76	0.00
18	3.77	14.71	0.00
19	3.48	14.21	0.00
20	3.13	13.68	0.00
21	3.09	11.76	0.00
22	3.10	14.01	0.00
23	2.75	13.43	0.00
24	2.46	14.00	0.00
25	2.37	14.85	0.00
26	2.17	12.30	1.07
27	2.13	14.12	1.69
28	2.23	14.29	0.00
29	2.34	15.82	0.00
30	2.80	13.73	0.00
31	3.16	11.59	0.00
32	3.41	12.03	0.00
33	3.72	12.18	0.42
34	3.92	9.57	0.00
35	4.33	8.95	0.62
36	4.64	11.30	0.42
37	5.14	10.37	0.37
38	5.60	9.90	0.68
39	6.70	10.04	0.40
40	7.46	8.84	0.34

Sample Interval (cm)	Magnetic Susceptibility (SI Units)	LOI at 550°C (%DW)	LOI at 950°C (%DW)
41	8.02	8.71	0.70
42	7.27	8.99	0.58
43	5.88	9.84	0.66
44	4.84	9.06	0.65
45	4.39	10.04	0.37
46	4.05	11.07	0.41
47	4.20	10.48	0.40
48	4.51	9.16	0.40
49	4.52	8.83	0.63
50	4.28	11.89	0.88
51	4.58	12.22	0.90
52	5.29	10.85	0.78
53	5.89	10.76	0.40
54	6.40	9.15	0.70
55	7.66	8.55	0.66
56	8.67	6.71	0.46
57	8.57	7.10	0.55
58	7.12	8.29	0.86
59	5.43	8.89	1.11
60	4.44	9.31	0.34
61	4.10	8.90	0.68
62	4.20	10.00	0.69
63	4.36	7.62	0.59
64	4.41	6.73	0.75
65	4.22	8.36	0.29
66	4.12	8.55	0.66
67	4.58	8.89	0.32
68	5.69	7.94	0.53
69	7.60	6.63	0.51
70	10.15	5.65	0.58
71	13.36	4.55	0.43
72	15.11	3.28	0.36
73	15.37	4.46	0.48
74	13.63	4.45	0.58
75	10.19	5.61	0.58
Minimum	2.13	3.28	0.00
Mean	5.50	11.40	0.41
Median	4.44	10.85	0.41
Maximum	15.37	25.00	1.69
Std. Deviation	3.08	4.00	0.36

APPENDIX B: GRAIN-SIZE DATA FOR CORES TG3 AND MA4

Core MA4

Sample Interval	Mean (phi)	Sorting (phi)	Skewness (phi)	Kurtosis (phi)	Textural Group
1	4.815	1.485	0.111	2.624	Sandy Silt
2	4.815	1.494	0.083	2.604	Sandy Silt
3	4.861	1.374	0.154	2.849	Sandy Silt
4	4.878	1.368	0.156	2.871	Sandy Silt
5	4.719	1.390	0.158	2.806	Sandy Silt
6	4.558	1.352	-0.025	2.859	Sandy Silt
7	4.657	1.318	-0.057	3.009	Sandy Silt
8	4.699	1.295	-0.044	3.100	Sandy Silt
9	4.686	1.385	0.012	2.941	Sandy Silt
10	4.861	1.464	0.045	2.773	Sandy Silt
11	5.007	1.402	0.221	2.701	Sandy Silt
12	4.805	1.630	-0.077	2.747	Sandy Silt
13	5.032	1.622	-0.069	2.832	Sandy Silt
14	4.859	1.537	0.076	2.679	Sandy Silt
15	4.565	1.688	-0.018	2.603	Sandy Silt
16	5.065	1.462	0.288	2.742	Sandy Silt
17	4.865	1.408	0.134	2.778	Sandy Silt
18	4.793	1.405	0.025	2.735	Sandy Silt
19	4.824	1.375	0.040	2.811	Sandy Silt
20	4.801	1.430	0.095	2.778	Sandy Silt
21	4.921	1.493	0.117	2.673	Sandy Silt
22	4.858	1.439	0.050	2.764	Sandy Silt
23	4.818	1.393	-0.053	2.761	Sandy Silt
24	4.814	1.405	0.000	2.707	Sandy Silt
25	4.815	1.441	0.057	2.695	Sandy Silt
26	4.816	1.527	0.140	2.624	Sandy Silt
27	4.847	1.526	0.134	2.626	Sandy Silt
28	4.777	1.499	0.088	2.586	Sandy Silt
29	4.846	1.573	0.115	2.492	Sandy Silt
30	4.885	1.576	0.140	2.455	Sandy Silt
31	4.526	1.551	0.315	2.601	Sandy Silt
32	4.715	1.587	0.208	2.459	Sandy Silt
33	4.676	1.669	0.185	2.392	Sandy Silt
34	4.902	1.691	0.228	2.385	Sandy Silt
35	5.499	1.623	0.079	2.293	Sandy Silt
36	4.316	1.552	0.376	2.723	Sandy Silt
37	3.320	1.187	0.574	3.473	Silty Sand
38	3.275	1.207	0.682	3.766	Silty Sand

Sample Interval	Mean (phi)	Sorting (phi)	Skewness (phi)	Kurtosis (phi)	Textural Group
39	3.210	1.300	0.735	3.762	Silty Sand
40	2.933	1.245	0.738	3.713	Silty Sand
41	2.936	1.390	0.846	3.747	Silty Sand
42	3.053	1.721	0.217	2.905	Silty Sand
43	2.996	1.754	0.439	2.486	Silty Sand
44	2.536	1.822	0.614	2.708	Silty Sand
45	2.164	1.709	0.986	3.584	Silty Sand
46	1.392	1.942	1.015	3.573	Silty Sand
47	0.886	1.897	1.296	4.362	Silty Sand
48	2.217	2.527	0.388	1.923	Silty Sand
49	3.754	1.815	0.304	2.391	Silty Sand
50	4.164	1.742	0.065	2.350	Sandy Silt
51	4.108	1.741	0.057	2.370	Sandy Silt
52	4.700	1.523	0.035	2.592	Sandy Silt
53	5.131	1.437	0.150	2.533	Sandy Silt
54	4.854	1.483	0.082	2.571	Sandy Silt
55	5.258	1.435	0.068	2.506	Sandy Silt
56	5.099	1.383	0.085	2.546	Sandy Silt
57	5.177	1.416	0.067	2.483	Sandy Silt
58	5.419	1.442	-0.034	2.444	Sandy Silt
59	5.618	1.394	-0.091	2.516	Sandy Silt
60	4.868	1.357	0.089	2.811	Sandy Silt
61	4.773	1.394	0.128	2.727	Sandy Silt
62	4.898	1.442	0.121	2.677	Sandy Silt
63	5.172	1.274	0.217	2.814	Sandy Silt
64	4.947	1.427	0.050	2.645	Sandy Silt
65	5.041	1.390	0.100	2.538	Sandy Silt
66	4.987	1.437	0.060	2.540	Sandy Silt
67	5.038	1.406	0.061	2.469	Sandy Silt
68	4.691	1.454	0.095	2.470	Sandy Silt
69	5.007	1.398	0.081	2.481	Sandy Silt
70	4.857	1.523	0.036	2.494	Sandy Silt
71	4.727	1.553	0.107	2.433	Sandy Silt
72	4.784	1.532	0.094	2.481	Sandy Silt
73	4.851	1.485	0.078	2.590	Sandy Silt
74	4.905	1.471	0.139	2.642	Sandy Silt
75	4.857	1.540	0.093	2.516	Sandy Silt
76	4.857	1.559	0.100	2.460	Sandy Silt
77	4.906	1.555	0.081	2.468	Sandy Silt
78	4.943	1.552	0.041	2.463	Sandy Silt
79	4.906	1.485	0.036	2.551	Sandy Silt
80	4.924	1.483	0.071	2.631	Sandy Silt

Sample Interval	Mean (phi)	Sorting (phi)	Skewness (phi)	Kurtosis (phi)	Textural Group
81	4.874	1.502	0.105	2.596	Sandy Silt
82	4.815	1.522	0.196	2.573	Sandy Silt
83	4.519	1.465	0.299	2.779	Sandy Silt
84	4.755	1.594	0.151	2.353	Sandy Silt
85	4.638	1.622	0.167	2.376	Sandy Silt
86	4.851	1.601	0.147	2.368	Sandy Silt
87	4.851	1.601	0.147	2.368	Sandy Silt
88	4.994	1.573	0.105	2.353	Sandy Silt
89	3.493	1.229	0.284	3.096	Silty Sand
90	3.712	1.271	0.284	3.024	Silty Sand
91	3.531	1.253	0.190	2.993	Silty Sand
92	4.079	1.240	0.155	3.200	Sandy Silt
93	4.198	1.397	0.288	2.961	Sandy Silt
94	4.873	1.522	0.009	2.367	Sandy Silt
95	4.749	1.530	0.050	2.375	Sandy Silt
96	4.776	1.516	0.075	2.413	Sandy Silt
97	4.715	1.521	0.140	2.417	Sandy Silt
98	4.777	1.542	0.176	2.481	Sandy Silt
99	4.910	1.561	0.138	2.432	Sandy Silt
100	4.811	1.510	0.087	2.473	Sandy Silt
101	4.787	1.529	0.104	2.442	Sandy Silt
102	4.756	1.581	0.142	2.395	Sandy Silt
103	4.695	1.527	0.178	2.487	Sandy Silt

Core TG3

Sample Interval	Mean (phi)	Sorting (phi)	Skewness (phi)	Kurtosis (phi)	Textural Group
1	5.162	1.580	-0.084	2.285	Sandy Silt
2	5.303	1.697	-0.219	2.231	Sandy Silt
3	5.172	1.630	-0.084	2.214	Sandy Silt
4	5.045	1.676	-0.091	2.194	Sandy Silt
5	5.126	1.736	-0.206	2.304	Sandy Silt
6	5.130	1.739	-0.218	2.362	Sandy Silt
7	5.187	1.745	-0.176	2.414	Sandy Silt
8	5.245	1.758	-0.196	2.406	Sandy Silt
9	5.196	1.737	-0.170	2.429	Sandy Silt
10	5.173	1.671	-0.106	2.338	Sandy Silt
11	5.231	1.685	-0.130	2.343	Sandy Silt
12	5.215	1.684	-0.121	2.353	Sandy Silt
13	5.160	1.699	-0.086	2.311	Sandy Silt
14	5.209	1.740	-0.178	2.428	Sandy Silt
15	5.118	1.711	-0.151	2.450	Sandy Silt
16	5.143	1.685	-0.185	2.515	Sandy Silt
17	5.253	1.631	-0.221	2.357	Sandy Silt
18	5.258	1.663	-0.168	2.393	Sandy Silt
19	5.151	1.631	-0.177	2.356	Sandy Silt
20	5.143	1.615	-0.116	2.455	Sandy Silt
21	5.154	1.629	-0.109	2.360	Sandy Silt
22	5.285	1.701	-0.140	2.306	Sandy Silt
23	4.995	1.606	-0.076	2.375	Sandy Silt
24	4.973	1.585	-0.023	2.465	Sandy Silt
25	5.046	1.597	-0.081	2.384	Sandy Silt
26	4.992	1.529	-0.076	2.507	Sandy Silt
27	4.999	1.551	-0.106	2.438	Sandy Silt
28	5.100	1.615	-0.093	2.397	Sandy Silt
29	5.074	1.641	-0.098	2.313	Sandy Silt
30	5.089	1.661	-0.042	2.331	Sandy Silt
31	5.079	1.614	-0.091	2.354	Sandy Silt
32	4.986	1.582	-0.077	2.395	Sandy Silt
33	4.944	1.581	-0.084	2.368	Sandy Silt
34	4.928	1.584	-0.044	2.394	Sandy Silt
35	4.933	1.574	-0.059	2.371	Sandy Silt
36	4.947	1.599	-0.012	2.364	Sandy Silt
37	5.128	1.579	-0.244	2.443	Sandy Silt
38	5.166	1.579	-0.224	2.478	Sandy Silt
39	5.181	1.556	-0.239	2.496	Sandy Silt
40	5.155	1.622	-0.200	2.378	Sandy Silt

Sample Interval	Mean (phi)	Sorting (phi)	Skewness (phi)	Kurtosis (phi)	Textural Group
41	5.161	1.626	-0.205	2.394	Sandy Silt
42	5.181	1.607	-0.246	2.432	Sandy Silt
43	4.948	1.646	-0.019	2.262	Sandy Silt
44	5.225	1.568	-0.268	2.484	Sandy Silt
45	5.264	1.587	-0.251	2.464	Sandy Silt
46	5.166	1.638	-0.139	2.321	Sandy Silt
47	5.202	1.611	-0.217	2.387	Sandy Silt
48	5.144	1.612	-0.192	2.402	Sandy Silt
49	5.190	1.625	-0.225	2.392	Sandy Silt
50	5.136	1.676	-0.224	2.477	Sandy Silt
51	5.253	1.635	-0.209	2.388	Sandy Silt
52	5.266	1.562	-0.276	2.516	Sandy Silt
53	5.224	1.553	-0.259	2.519	Sandy Silt
54	5.182	1.613	-0.223	2.414	Sandy Silt
55	5.135	1.603	-0.206	2.408	Sandy Silt
56	5.237	1.576	-0.280	2.489	Sandy Silt
57	5.218	1.594	-0.265	2.444	Sandy Silt
58	5.071	1.661	-0.061	2.269	Sandy Silt
59	5.168	1.600	-0.233	2.418	Sandy Silt
60	5.275	1.590	-0.274	2.471	Sandy Silt
61	5.282	1.605	-0.221	2.436	Sandy Silt
62	5.301	1.579	-0.269	2.508	Sandy Silt
63	5.227	1.556	-0.252	2.513	Sandy Silt
64	5.281	1.581	-0.281	2.494	Sandy Silt
65	5.224	1.572	-0.264	2.497	Sandy Silt
66	5.254	1.592	-0.251	2.475	Sandy Silt
67	5.207	1.588	-0.231	2.455	Sandy Silt
68	5.207	1.596	-0.234	2.446	Sandy Silt
69	5.189	1.600	-0.234	2.429	Sandy Silt
70	5.281	1.624	-0.243	2.423	Sandy Silt
71	5.258	1.591	-0.232	2.480	Sandy Silt
72	5.262	1.590	-0.222	2.490	Sandy Silt
73	5.226	1.585	-0.198	2.491	Sandy Silt
74	5.227	1.560	-0.211	2.551	Sandy Silt
75	5.119	1.529	-0.205	2.565	Sandy Silt